Design of efficient catalysts for gasification of biomass-derived waste streams in hot compressed water

Towards industrial applicability

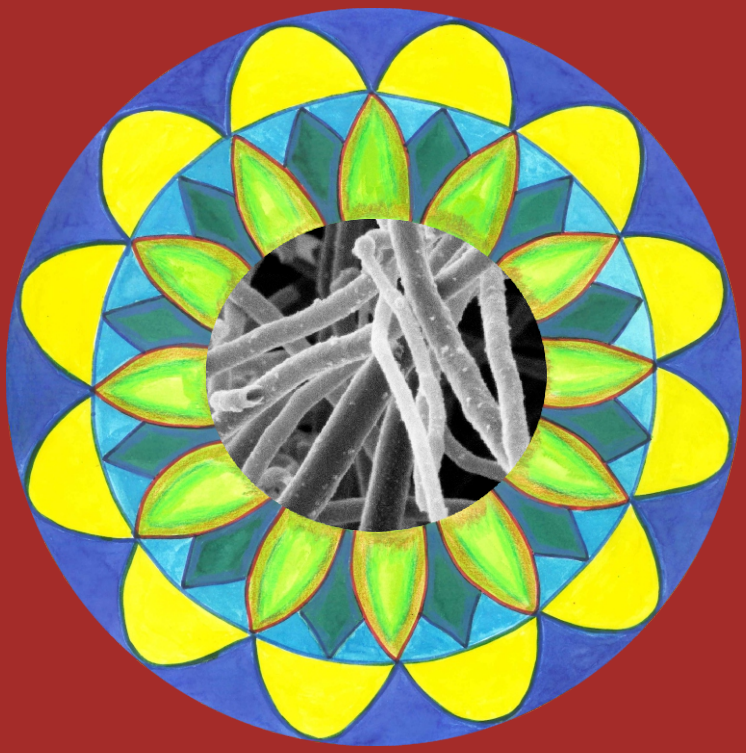

Dionysius Jacobus Maria de Vlieger

DESIGN OF EFFICIENT CATALYSTS FOR GASIFICATION OF BIOMASS-DERIVED WASTE STREAMS IN HOT COMPRESSED WATER

TOWARDS INDUSTRIAL APPLICABILITY

Dionysius Jacobus Maria de Vlieger

Promotion committee

Prof. dr. G. van der Steenhoven	Chairman	University of Twente, The Netherlands
Prof. dr. K. Seshan	Promoter	University of Twente, The Netherlands
Prof. dr. ir. L. Lefferts	Promotor	University of Twente, The Netherlands
Prof. dr. J.A. Lercher		University of Munich, Germany
Prof. dr. J.P. Lange		University of Twente, The Netherlands
Prof. dr. S.R.A. Kersten		University of Twente, The Netherlands
Dr. A. Zwijnenburg		Johnson Matthey, United Kingdom
Dr. B.L. Mojet		University of Twente, The Netherlands

The research described in this thesis was conducted in the *Catalytic Processes and Materials* (CPM) group at the University of Twente in the Netherlands. Financial support was provided by *Advanced Chemical Technologies for Sustainability* (ACTS) under project number 053.61.023.

ISBN: 978–90–365–3492–5

Cover picture: The cover picture is designed by cum–fine artist Wilma Peperkamp and represents a Mandala which symbolizes the background of my PhD study. The core of the Mandala shows a key finding of my research, which is a Ru/CNT catalyst (HRSEM picture by Mark A. Smithers)

Printed by: Gildeprint Drukkerijen – The Netherlands

DESIGN OF EFFICIENT CATALYSTS FOR GASIFICATION OF BIOMASS-DERIVED WASTE STREAMS IN HOT COMPRESSED WATER

TOWARDS INDUSTRIAL APPLICABILITY

PROEFSCHRIFT

ter verkrijging van
de graad van doctor aan de Universiteit Twente,
op gezag van de rector magnificus,
prof. dr. H. Brinksma
volgens besluit van het College voor Promoties
in het openbaar te verdedigen
op vrijdag 8 februari 2013 om 16.45 uur

door

Dionysius Jacobus Maria de Vlieger

geboren op 18 maart 1982

te Hengelo (Ov), Nederland

This dissertation has been approved by the promoters

Prof. dr. K. Seshan

Prof. dr. ir. L. Lefferts

"Ignore the environment. It will go away."
-unknown

Contents

Summary

Mankind is on the eve of the greatest challenge this world has ever faced. The energy required for the globalized living standards of our society depends currently on fossil fuels. The availability and use of fossil fuels were taken for granted during the last century, but depletion of cheap oil and the environmental concerns related to combustion of fossil fuels force us to shift to alternative energy sources. Renewable and sustainable energy carriers must be developed and implemented in the next decades to sustain our energy needs. A failure to complete this challenge will have a disastrous impact on our way of living.

Biomass is believed to be a promising renewable energy source for the future. Conversion of biomass waste to liquid fuels or hydrogen is projected to provide, partly, the required energy demand. The anticipated intensification of biomass conversion processes will result in an increase in biomass derived aqueous waste streams (*e.g.* the aqueous phase of flash pyrolysis oil). Gasification of these wastes to produce high energy value gases (*e.g.* hydrogen) is an interesting way of diminishing waste by making valuable products. Conventional steam reforming of these biomass derived streams is economically unattractive because of their high water contents (>80 wt%) and the energy required to carry out the reactions in gas phase. Aqueous phase reforming (APR) is a recently developed process and shows promising results for gasification of biomass derived aqueous feeds in liquid phase. During APR, water is kept in the liquid phase by applying elevated pressures. The exact reaction conditions of APR have a huge influence on the properties of water, which in turn affect the catalytic reforming reaction. Especially, an enormous change in properties occurs when the water is conditioned beyond the supercritical point (> 374 °C and 221 bars). Earlier work in this field shows the need for stable and active reforming catalysts to make APR of bio/organic aqueous waste streams a commercially feasible process. The study described in this thesis focuses on the development of such a catalyst.

Background to the need for sustainable fuels is discussed in detail in Chapter 1. The role of APR is further discussed in this chapter and the effects of the operating conditions on the reaction are addressed. The chapter concludes with an evaluation of the current challenges in APR.

The experimental setup used to study catalytic APR of oxygenates is described in Chapter 2. The setup is able to perform experiments up to 450 °C and 250 bar in a continuous

mode by using a fixed bed reactor. Furthermore, catalyst preparation and characterization methods, analysis methods, and definitions that are used throughout this thesis, are also described in this chapter.

An initial study to screen promising catalysts for APR of a model bio-oxygenate molecule, ethylene glycol (EG), is described in Chapter 3. Based on a literature survey, alumina supported Ir, Pt and Ni catalysts were selected as possible catalysts for this screening study. These catalysts were tested for catalytic reforming of EG (5 & 15 wt%) in supercritical water (450°C and 250 bar). The Pt/Al_2O_3 catalyst showed the highest hydrogen yields compared to Ir and Ni. Varying the Pt loading between 0.3 and 1.5 wt% showed that the intrinsic reforming activity increased with decreasing Pt loadings. However, a large negative effect on the H_2 selectivity and catalyst stability was observed with decreasing Pt loading. It was found that promoting Pt/Al_2O_3 catalysts with Ni improved H_2 yields and enhanced catalyst stability. $Pt\text{-}Ni/Al_2O_3$ catalysts showed to be very promising for EG reforming in supercritical water and this catalyst was selected for further APR studies.

The deactivation mechanism of Pt/Al_2O_3 during APR of EG and the role of Ni in enhancing catalyst lifetime and H_2 selectivity is discussed in Chapter 4. Methanol, ethanol and acetic acid were identified as the main liquid products during EG reforming over alumina supported Pt and Pt-Ni catalysts. The effect of these products on selectivity and catalyst stability was further studied by APR of these compounds. The high dehydrogenation activity of $Pt\text{-}Ni/Al_2O_3$ increased H_2 yields during EG reforming by (i) suppressing methane formation during methanol reforming (a major by-product in EG reforming) and (ii) suppressing the formation of acetic acid. The latter reason is also found to be the cause for the enhanced lifetime of Ni promoted Pt/Al_2O_3 catalysts. Acetic acid causes hydroxylation and migration of the alumina support, leading to coverage of the catalytic sites and resulting in deactivation of the catalyst. The instability of the alumina support towards acetic acid in hot compressed water is a major problem for the feasibility of this technique because acetic acid will be a major component in many future bio-gasification feed streams (*e.g.* the aqueous fraction of pyrolysis oil), and thus stable catalyst supports must be developed.

In Chapter 5, the potential of CNT as catalyst support in APR is demonstrated. Carbon nanotubes (CNT) are widely recognized for their excellent physical and chemical stability. Furthermore, their open structure is very interesting for catalytic applications with respect to diffusion limitations. The performance of Pt decorated CNT was studied as catalyst in

supercritical water reforming of EG and acetic acid. The remarkable stability of CNT offers great potential for catalysis in supercritical water. The acetic acid reforming activity of Pt/CNT catalyst is rather low and requires improvement for commercial applications.

The study described in Chapter 6 aims at the development of a stable catalyst with commercially relevant catalytic activity for acetic acid gasification in sub- and supercritical water. The catalytic performance of Ru/CNT catalyst was studied for reforming of acetic acid (1-25 wt%) in sub- (195-340 °C, 225 bar) and supercritical water (400 °C, 250 bar). Ru/CNT catalyst showed remarkably stable catalytic performance and commercially relevant reaction rates for reforming of acetic acid in supercritical water. It was found that the high ionic product in high temperature subcritical water (300-340 °C) was responsible for Ru over-oxidation during acetic acid reforming and caused catalyst deactivation. This problem has been overcome by working under low ionic supercritical water conditions (>374 °C and 221 bar). The high stability and activity of Ru/CNT for acetic acid reforming in supercritical water paved the way for studying reforming of real biomass derived waste streams under these conditions.

Supercritical water reforming (400 °C and 250 bar) of a diluted feed stream of the aqueous phase of flash pyrolysis oil is studied over Ru/CNT catalyst in Chapter 7. It was found that the reaction conditions caused significant coke/char formation in the preheater. Blockage of the preheater by coke was prevented by using highly diluted feeds. But even under those conditions, coke was formed in significant quantities and prevented the assessment of the Ru/CNT catalyst. Coke formation is a non-catalytic challenge that should first be addressed before the catalytic performance of Ru/CNT can be assessed. However, the latter is beyond the scope of this thesis.

The thesis is concluded in Chapter 8 with an evaluation of (i) the APR process in general and (ii) the integration of the APR process in a bio-refinery to produce the necessary hydrogen from waste and use it for upgrading of the bio-oil. Current non-catalytic challenges with APR of the aqueous fraction of pyrolysis oil prevent feasible exploitation of this process. However, it is projected that the APR technology developed in this thesis is applicable for reforming of other aqueous bio/organic aqueous waste streams that are produced in large quantities in the paper and food production industry.

The main achievements of the work described in this thesis, involved the development of a stable catalyst support for APR in sub- and supercritical water, which formed the basis

for the design of an efficient APR catalyst for reforming of challenging model compounds. The developed Ru/CNT catalyst not only showed remarkable stability for supercritical water APR of acetic acid but also showed commercially relevant reforming rates. Reforming of real aqueous waste streams revealed that the process is subjected to engineering challenges which should first be overcome before the developed catalyst can be further assessed.

Samenvatting

De mensheid staat aan de vooravond van één van de grootste uitdagingen aller tijden. Onze geglobaliseerde samenleving ligt ten grondslag aan de energie verslaving van onze maatschappij en wordt momenteel gevoed door fossiele brandstoffen. De beschikbaarheid en gebruik van fossiele brandstoffen werd de afgelopen eeuw als vanzelfsprekend beschouwd, maar uitputting van goedkope oliebronnen en de milieu aspecten gerelateerd aan de verbranding van fossiele brandstoffen leiden ertoe dat wij deze energie bronnen in de toekomst niet langer kunnen aanspreken. Hernieuwbare en duurzame energiedragers moeten ontwikkeld worden om te voorzien in onze energievraag. Het niet volbrengen van deze uitdaging zal een enorme impact hebben op onze hedendaagse manier van leven.

Biomassa wordt gezien als een veelbelovende toekomstige bron van duurzame energie. Omzetting van biomassa-afval naar vloeibare brandstoffen of waterstof kan mogelijk (gedeeltelijk) voorzien in onze vraag naar duurzame energie. De geanticipeerde toename in biomassa gerelateerde processen zullen leiden tot een toename van bio-organische waterige afvalstromen (bijv. de waterige fase van flash pyrolyse olie). Een interessante mogelijkheid voor het valorizeren van deze afvalstromen is d.m.v. reforming (vergassing) naar hoog calorische gassen (bijv. H_2). Conventionele stoomreforming van deze afvalstromen is economisch gezien niet uitvoerbaar door de grote hoeveelheid energie die nodig is om deze stromen (>80 gew.% water) in gas fase te brengen. Waterige fase reforming (WFR) is een recent ontwikkeld proces voor vergassing van bio/organische waterige voedingstromen. Tijdens WFR vindt vergassing plaats terwijl de voedingstroom in vloeibare fase gehouden wordt door het toepassen van verhoogde drukken. De WFR procescondities hebben een grote invloed op de eigenschappen van het water, en beinvloeden daarmee de katalytische reforming reactie. Vooral het passeren van het superkritische water punt (> 374 °C en 221 bar) zorgt voor een drastische verandering in water eigenschappen. Reeds uitgevoerde studies op het gebied van WFR hebben de noodzaak voor een stabiele en actieve vergassings katalysator aangetoond om vergassing van bio-organische afvalstromen commerciel mogelijk te maken. Het onderzoek, zoals beschreven in dit proefschrift, is gericht op de ontwikkeling van een dergelijke katalysator.

Argumenten voor de ontwikkeling en implementatie van duurzame brandstoffen worden behandeld in Hoofdstuk 1. Verder wordt in dit hoofdstuk de rol van WFR in deze ontwikkeling besproken en worden de effecten van de reactieconditions op dit proces

uitgelegd. Dit hoofdstuk sluit af met een evaluatie van de huidige uitdagingen op het gebied van katalytische WFR.

In Hoofdstuk 2 wordt de experimentele opstelling die gebruikt is voor dit onderzoek beschreven. De opstelling maakt het mogelijk om WFR te bestuderen tot maximaal 450 °C en 250 bar in een continue modus door gebruik te maken van een fixed-bed reactor. Verder worden de katalysator bereiding en karakterisatie methoden, analyse methoden, en definities die in het proefschrift gebruikt zijn, in dit hoofdstuk beschreven.

In Hoofdstuk 3 wordt een initieel katalysator screening onderzoek beschreven, dat als doel heeft geschikte katalysatoren te identificeren voor WFR van de modelstof ethyleen glycol (EG) voor de productie van waterstof. Gebaseerd op een literatuur onderzoek zijn Ir, Pt en Ni op alumina drager geselecteerd als veelbelovende katalysatoren voor dit proces. De eigenschappen van deze katalysatoren zijn onderzocht voor WFR van EG (5 en 15 gew.%) in superkritisch water (450 °C en 250 bar). Uit dit onderzoek bleek dat γ-alumina onder deze omstandigheden omgezet wordt naar boehmiet. Verder gaf de Pt/Al_2O_3 katalysator de hoogste waterstof opbrengst in vergelijking met Ir en Ni. Het varieren van de Pt belading tussen 0.3 en 1.5 % toonde aan dat de intrinsieke reforming activiteit toenam met lagere Pt beladingen. Echter vertoonde een lagere Pt belading een negatief effect op de waterstof selectiviteit en op de stabiliteit van de katalysator. Promotie van de Pt/Al_2O_3 katalysator met Ni leidde tot verhoogde waterstof opbrengsten en stabiliteit. Deze bevindingen tonen aan dat $Pt\text{-}Ni/Al_2O_3$ een veelbelovende katalysator is voor WFR van EG in superkritisch water en daarom is deze katalysator geselecteerd voor vervolg onderzoek.

Deactivatie van Pt/Al_2O_3 tijdens WFR van EG, en de rol van Ni in het verhogen van de katalysator levensduur en H_2 selectiviteit, is bestudeerd en beschreven in Hoofdstuk 4. Het is gebleken dat de vorming van vloeibare bij-producten tijdens WFR van EG een grote invloed hebben op de catalytische eigenschappen. Methanol, ethanol en azijnzuur zijn geidentificeerd als bij-producten tijdens WFR van EG over Pt/Al_2O_3 en $Pt\text{-}Ni/Al_2O_3$ katalysatoren. Het effect van deze bij-producten op katalysator gedrag is verder onderzocht. WFR van deze producten leidde tot de vorming van alkanen. De hoge dehydrogenatie activiteit van $Pt\text{-}Ni/Al_2O_3$ zorgde voor hoge waterstof opbrengsten tijdens EG WFR door (1) het onderdrukken van methaan vorming tijdens methanol reforming (voornaamste bij-product tijdens EG reforming) en (2) door het onderdrukken van azijnzuur vorming. De laatste reden ligt ook ten grondslag aan de langere levensduur van Ni bevorderde Pt/Al_2O_3. Azijnzuur bleek

verantwoordelijk te zijn voor hydroxylatie en migratie van de alumina drager. Dit leidde tot bedekking van de katalytische actieve sites met een laagje alumina en had deactivatie van de katalysator tot gevolg. De instabiliteit van de alumina drager in de aanwezigheid van azijnzuur is een groot probleem voor de toepasbaarheid van deze techniek, doordat azijnzuur een belangrijk bestanddeel (10-20 gew.%) zal zijn in toekomstige industriele voedingstromen (bijv. de waterige fase van flash pyrolyse olie).

In Hoofdstuk 5 wordt de potentie van koolstof nanobuizen (KNB) als katalytisch drager materiaal voor WFR gedemonstreerd. KNB zijn wereldwijd erkend voor hun grote fysische en chemische stabiliteit. Verder is de open structuur van KNB zeer interessant voor katalytische toepassingen vanuit het oogpunt van diffusie limitaties en het afvoeren van gevormde coke. De katalytische eigenschappen van Pt op KNB zijn onderzocht voor WFR van EG en azijnzuur in superkritisch water (450 °C en 250 bar). De Pt/KNB katalysator bleek een opmerkelijk goede stabiliteit te hebben voor deze reacties. Echter, de WFR activiteit van Pt/KNB is relatief laag en moet verbeterd worden om commerciele toepassingen mogelijk te maken.

Het werk beschreven in Hoofstuk 6 richt zich op de ontwikkeling van een stabiele katalysator met commercieel aantrekkelijke activiteit voor WFR van azijnzuur. De katalytische eigenschappen van Ru/KNB zijn bestudeerd voor WFR van azijnzuur (1-25 gew.%) in sub- (195-340 °C, 225 bar) en superkritisch water (400 °C, 250 bar). Ru/KNB vertoonde stabiele katalytische eigenschappen tijdens WFR van azijnzuur in superkritisch water. Het hoge ion product van hoog temperatuur subkritisch water (300-340 °C, 225 bar) veroorzaakte Ru over-oxidatie tijdens azijnzuur WFR en leidde tot deactivatie van de katalysator. De goede stabiliteit en activiteit van Ru/KNB voor azijnzuur reforming in superkritisch water heeft het fundament gelegd voor WFR van echte bio-organische afvalstromen onder deze condities.

WFR van de waterige phase van flash pyrolyse olie over Ru/KNB is bestudeerd en beschreven in Hoofdstuk 7. Vorming van significante hoeveelheden coke vond plaats in de preheater. Zeer verdunde voedingstromen waren noodzakelijk om verstopping van de voorverwarmer door coke te voorkomen. Maar coke werd zelfs onder deze condities in significante hoeveelheden gevormd en zorgde ervoor dat de katalytische eigenschappen van Ru/KNB niet goed beoordeeld kon worden. Coke vorming is een procestechnologisch probleem en ligt buiten het bereik van dit onderzoek.

Dit proefschrift wordt afgesloten in Hoofdstuk 8 met een evaluatie van (i) het WFR proces in zijn algemeenheid en (ii) de integratie van het WFR proces in een bio-raffinaderij voor het produceren van noodzakelijk waterstof voor het opwaarderen van bio-olie. Non-katalytische problemen met betrekking tot WFR van de waterige fase van flash pyrolyse olie staan een commerciele exploitatie van dit proces in de weg. Maar het is voorzien dat de technologie, die ontwikkelt is zoals beschreven in dit proefschrift, toepasbaar is voor de reforming van andere waterige bio-organische afvalstromen die in grote hoeveelheden geproduceerd worden in de papier en voedingsindustrie.

Het belangrijkste resultaat van dit onderzoek is de ontwikkeling van een stabiele katalysator met commercieel aantrekkelijke activiteit voor reforming van bio-organische voedingstromen in superkritisch water. Verder is aangetoond dat hoog temperatuur subkritisch water ontzien moet worden voor reforming reacties. Reforming van de waterige fase van flash pyrolysis olie is onderheving aan non-katalytische uitdagingen die eerst opgelost dienen te worden voordat dit proces verder bestudeerd kan worden.

Chapter 1

Hydrogen production from biomass derived waste streams

Currently, hydrogen is mostly produced by steam reforming of natural gas and other fossil feed stocks. Hydrogen is widely used in oil refineries, fertilizer and food industry. In future, hydrogen based fuel cell will become very important as a source of power. It is foreseen, that the demand for hydrogen will also increase in the future for bio-refinery applications. Furthermore, sustainable hydrogen is expected to (partly) replace peaking fossil fuels and mitigate the environmental concerns associated with their use. Hydrogen from bio-renewable organic sources is an elegant solution to meet the projected hydrogen demands in a sustainable way. Converting aqueous bio/organic waste (>80% water) to hydrogen by catalytic Aqueous Phase Reforming is an attractive way to simultaneously diminish waste and produce the highly desired hydrogen sustainably.

1.1 Towards renewable fuels

Currently, 97% of global liquid fuels are derived from crude-oil [1] and almost 87 million barrels of crude oil have to be produced every day to support these energy needs [2]. Future energy needs will increase as a result of the rapid growth in worldwide population, industrialization and globalization. British Petroleum (BP) calculated world proven oil reserves to be around 1400 billion barrels. Proven oil reserves are based on known oil reservoirs that are feasible to exploit from technological and geological point of view. It is predicted that, at current consumption rates, proven crude-oil reserves will be depleted within 50 years from now [2]. In addition to the proven reserves, there are also unproven reserves that equal 7 trillion barrels of oil which are subjected currently to technological, economical or geopolitical challenges that prevent a feasible exploitation [3]. It is predicted by the IEA (International Energy Agency) that 20-40% of the unproven oil reserves will be technological feasible to be exploited in the future [4], however from economical viewpoint the feasibility is questionable.

The future (proven) crude oil will also evolve to a heavier and more sour oil with higher viscosity and of lower quality [5, 6]. The increase in viscosity makes it more difficult and costly to extract, transport and process the oil. Furthermore, the heavier molecular composition of heavy crude oil requires more costly cracking reactions to produce the desired liquid fuels [5, 6]. In addition, the sulfur content of todays oil is < 2% but is expected to increase by an average of 0.1 % by the year 2020 [7]. This increase seems small on paper but has a huge influence on the refining process. Increase of the sulfur content makes the oil more sour leading to corrosion problems in pipelines. An increase of sulfur is also an environmental concern. Sulfur in oil derived fuels is responsible for the majority of SO_x emissions. SO_x is toxic, causes the formation of acid rain and is responsible for deactivation of automotive catalytic converters. The Environmental Protection Agency (EPA) has therefore set stringent SO_x exhaust limits of less than 30 ppm. In the near future, this limit is expected to be tightened to <10 ppm, forcing a better and more costly desulfurization process in refineries [8]. Desulphurisation requires hydrogen to remove sulphur as hydrogen sulphide.

In the near future, the major concern is not the depletion of global oil reserves, but the depletion of easy accessible and high quality oil. Oil extraction and processing become increasingly more difficult and hence more energy intensive. This will cause a dramatic decrease in the net energy gained for crude oil extraction, making this form of energy

production less attractive. The energy efficiency of oil extraction is usually discussed in terms of *Energy Return over Energy Invested* (EROEI) and is defined as the (barrel) units of energy retrieved per unit of energy invested. Around 1930, oil extraction was cheap in energy with an EROEI of 100. This number declined to 30 around the year 1970 and is currently around 11 and decreasing rapidly [9]. It is just a matter of time until oil extraction is not profitable anymore from energy perspective. The same reasons that are responsible for a decreasingly EROEI also lead to an increase in costs. It is expected that these costs will escalate in such a way that the consequent high price of crude oil derived fuels will lead to a decline in demand because consumers can simply not afford these fuels anymore.

The decreasing EROEI and increasing costs of crude oil extraction is expected to result in a terminally decreasing oil production. The point at which this transition occurs is called Peak Oil. A lower demand for crude oil derived fuels after the Peak Oil point does not mean a decreasing demand for energy. Our society is strongly dependent on global economics which are dictated by global trade of products. Crude-oil derived fuels, which are taken for granted in our current society, enable transportation of goods globally and hence are the backbone of globalization. Peak Oil is believed to lead to a reverse globalization because it is simply too expensive to transport goods. Localization of economics can have a huge impact on a local society in terms of wealth, living standards and availability of products. Therefore, the Peak Oil moment is reported by many to be a very crucial point for our society as we know it today [9-14]. The energy demand that cannot be fulfilled anymore by crude oil derived fuels has to be replaced by other fuels to keep our society "running" [10]. Many studies were performed to predict the Peak Oil moment. Some researchers reported that we passed the Peak Oil moment already, while others say that it is happening around the time of writing of this thesis (2012) [15, 16] and more positive studies report 2020-2030 to be the transition point [17, 18]. These studies show that the exact point of Peak Oil is unclear but that it will likely happen within the next decades. On the other hand, there are reports that Peak Oil will never happen or at least not in the near future [3] but in general the occurrence of a Peak Oil event is accepted.

Peak oil is not the only concern involved with crude oil derived fuels. The combustion of fossil fuels is a major contributor to the accumulation of greenhouse gases in the atmosphere (*e.g.* CO_2, NO_x and SO_x) [19, 20]. Global warming (attributed to exhausted greenhouse gases) was reported to have caused a temperature rise of 0.8 °C in the year 2000 compared to pre-industrial time. A study to assess global warming predicted that another

temperature rise of more than 1 °C compared to the year 2000 will invoke an irreversible dangerous effect on the Earth's climate system. Modeling studies predict that this limit is reached when the CO_2 levels in air will be around 450 ppm, which is projected to happen by the year 2050 [21]. The role of emitted greenhouse gases in global warming is discussed intensively and the luring danger of global warming on our civilization is widely accepted [22-26].

Based on the studies above, the next decades will be very important for the society as we know it today with respect to the depletion of cheap oil and the irreversible environmental impact associated with the combustion of fossil fuels. It is imperative that a global transition from fossil fuels to sustainable and renewable energy carriers is realized as soon as possible. The clock is ticking to ensure a livable planet for future generations!

1.2 Biomass as sustainable energy carrier

Biomass is expected to become one of the major global sustainable energy sources of the future that will (partly) replace crude oil derived fuels [27-29]. Emissions of CO_2 due to combustion of biomass derived fuels contribute much less to global warming as the exhausted carbon originated from the atmosphere (Figure 1.1). Plants and trees convert CO_2 and H_2O under influence of sunlight to sugars which form the basis of the biomass material. Biomass can be considered as a storage material for solar energy. Combustion of biomass material releases the contained solar energy.

The most interesting way to use biomass as an energy carrier is to convert it to liquid bio-fuels [27, 30, 31]. Liquid bio-fuels have similar properties as conventional liquid fuels and can therefore be introduced in our society without the need for major adjustments to the infrastructure or automotive engines. The conversion of biomass to liquid fuels (BTL-fuels) is already being studied for decades. The largest advantages of BTL fuels are (i) up to 90% lower CO_2 emissions, (ii) no emissions of fine dust and (iii) very low NO_x emissions [27].

The 1st generation of bio-fuels involved the conversion of relatively simple molecules such as sugars and vegetable oils to produce liquid biofuels [32, 33]. From the viewpoint of process technology, these biomass components are relatively easy to convert to bio-fuels due to their simple chemical structure. Examples of such processes are (i) the production of bio-

ethanol from corn by fermentation and (ii) the production of biodiesel from transesterification of plant oils [31]. The feed stocks of interest for the 1st generation of biofuels are usually extracted from the edible parts of biomass [32]. 1st generation bio-fuels clearly illustrate the potential of biomass as an energy carrier. However, it is ethically incorrect to use food for fuel production in a world where almost 15% of the global population is starving [31, 34, 35]. In addition, the edible parts of biomass only account for a minor part of the biomass and therefore only a small percentage of the total energy in biomass is obtained [36].

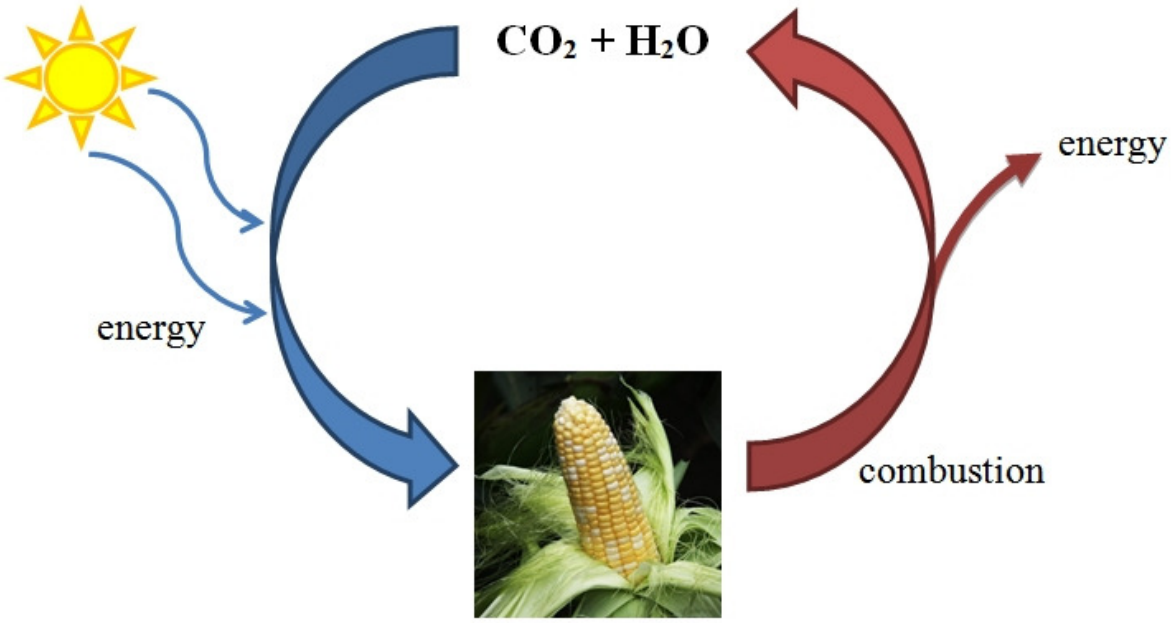

Figure 1.1: Carbon neutral use of biomass as energy carrier.

The non-edible parts of biomass (waste) account for the majority of the energy content of biomass and are therefore much more interesting for bio-fuel production in terms of ethics and efficiency. Liquid bio-fuels from biomass waste are therefore considered as a 2nd generation of sustainable energy carriers. Biomass waste (*e.g.* the stock and leaves of corn) consists mainly of (ligno)cellulosic and lignin material and are technologically challenging to reform [31, 32]. Different processes can be used to convert lignocellulosic material to valuable products [32, 37, 38]. A scheme (Figure 1.2) was published by Bridgwater [37] and shows products from thermal biomass conversion processes. Simple combustion of biomass can be applied to generate heat but also more technologically advanced processes can be used

to get more valuable products such as liquid biofuels or other bio-chemicals. One widely studied multistage process is gasification of the biomass to produce syngas which is converted to liquid fuels by the Fischer Tropsch process [27, 28]. The biggest advantage of this process is that properties of the fuel can be controlled very well and tuned to specific requirements. The thermal efficiency of this process is relatively low as the process is energy intensive. In addition, the cost of producing biodiesel by BTL is higher than for fossil diesel [39].

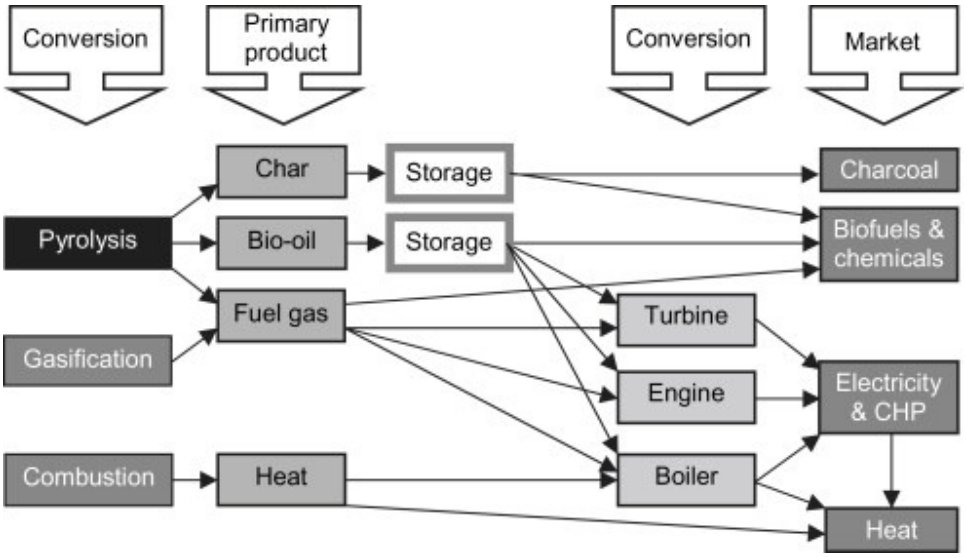

Figure 1.2: Products from thermal biomass conversion as reported by Bridgwater [37].

A more economically feasible approach than Fischer-Tropsch coupled gasification is the direct conversion of biomass to pyrolysis-oil *via* flash pyrolysis [40, 41]. Biomass is heated in a few seconds to a temperature of ±500 °C in an oxygen-free reactor [37]. During this process, the lignocellulosic structure of biomass disintegrates to smaller molecules due to the heat but is not combusted due to the lack of oxygen. Gas, liquid and solid products are formed during the pyrolysis process. The gas products consist of gases such as CO_x, CH_4 and H_2 and can be combusted to generate heat for the pyrolysis reactor. The solid product consists mainly of salt which can be used as a fertilizer and char which can be burned to generate heat for the process. The liquid product formed during pyrolysis is commonly referred to as pyrolysis oil and consists of a complex mixture of organic compounds with different polarities and up to 30 wt% of water [37, 42, 43]. The compounds in pyrolysis-oil are usually distinguished in an organic and an aqueous fraction. Pyrolysis-oil has a few disadvantages that makes it a low grade fuel compared to fossil fuel; (i) the high oxygen and water content

of bio-oil is responsible for a low heating value, (ii) the low pH caused by the high concentration of organic acids leads to a corrosive nature of the oil, (iii) chemical and thermal instability, (iv) immiscible with conventional fuels and (v) high viscosity and surface tension compromises its applicability [43]. Further processing of pyrolysis oil is necessary to upgrade the properties to commercially attractive levels [40, 44]. One way to achieve this is to remove the aqueous fraction from the pyrolysis-oil. The aqueous fraction consists of soluble oxygenated components such as alcohols, ketones, aldehydes and organic acids. These components are by definition rich in oxygen -partly oxidized already- and therefore contribute in a great extent to the low heating value of the pyrolysis oil [45]. In addition, carboxylic acids such as acetic acid removed by water extraction reduce the corrosive properties of the oil [43]. The organic fraction of the oil (or in this thesis referred to as bio-oil) can be further processed to liquid fuels. However, the organic fraction is still rich in oxygen [37] and therefore has a lower heating value compared to crude oil. Removal of oxygen from bio-oil is therefore required to increase the energy content. Hydro-de-oxygenation is a process that can be applied to remove this oxygen in the form of water by treating the bio-oil with expensive hydrogen [44]. The amount of hydrogen needed for de-oxygenation of the bio-oil is dependent on the degree of oxidation and the complexity of the molecules in the bio oil. It was reported by Bridgwater that ± 62 gram of H_2 is necessary to achieve full deoxygenation of 1 kg of bio-oil with an initial 50% oxygen content [46]. An elegant way to (partly) obtain the necessary hydrogen for upgrading of the oil fraction is to produce hydrogen from the extracted aqueous fraction [47, 48]. The integration of the bio-oil refinery with hydrogen production from the aqueous fraction is a promising route to sustainable liquid bio-fuels as shown in Figure 1.3.

In the future, hydrogen from renewable resources is also projected to partly replace conventional fuels to reduce anthropogenic CO_2 emissions [49]. Hydrogen is expensive and is sold on the market for >$2200 per ton. The future technology developed for hydrogen production from the aqueous phase of bio oil is also expected to be applicable for the production of hydrogen from other bio-organic aqueous waste streams. Production of hydrogen by eliminating bio-organic waste streams is very attractive from both economic and environmental viewpoint.

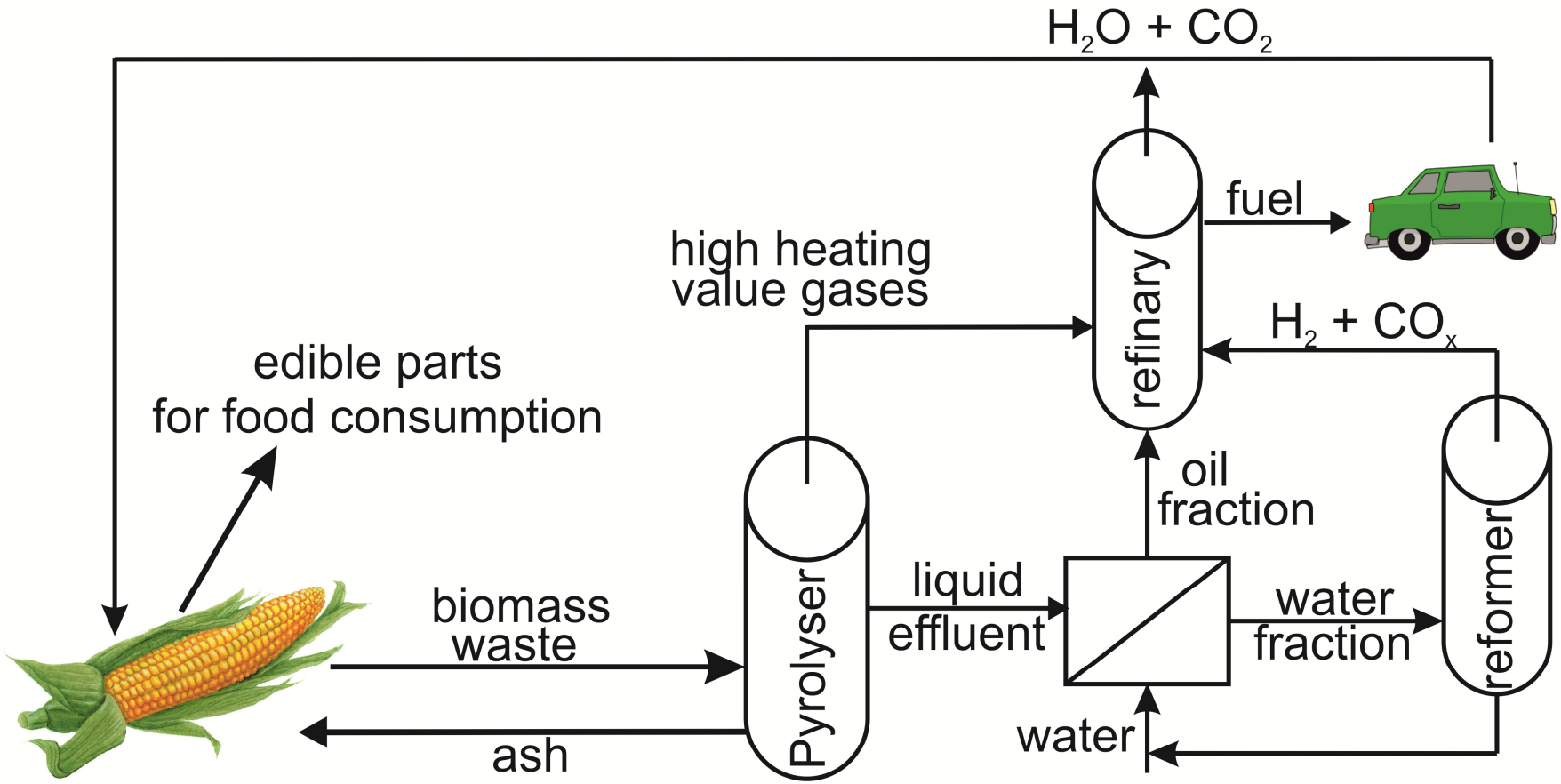

Figure 1.3: Integration of hydrogen production from aqueous waste stream with the bio-oil reformer.

1.3 Aqueous phase reforming of oxygenates

Biomass derived aqueous waste-streams usually contain a variety of water soluble organic compounds. For instance, the aqueous fraction of flash pyrolysis oil commonly consist of 80 wt% water and 20 wt% of a complex mixture of different oxygenates such as aldehydes, ketones, alcohols, acids and sugars [50]. The conversion of aqueous bio/organic wastes (>80% water) into high heating value products such as hydrogen, syngas (CO/H_2) and methane using conventional reforming processes at lower pressures is energy intensive due to the need for the evaporation of water. Dumesic and co-workers tackled this problem by developing the so called "aqueous phase reforming" (APR) process [47, 51, 52], in which the water is kept in the liquid phase by applying elevated pressures. The concept was demonstrated for reforming of diluted oxygenate feeds at mild temperatures in pressurized liquid water (225 – 265 °C, 29 – 56 bar) over supported metal catalysts. The phase diagram of water is shown in Figure 1.4 and shows the pressures required to keep hot water in the liquid phase.

Catalytic APR studies with model compounds are carried out to simplify the process and gain fundamental understanding of catalytic reforming. The knowledge gained from these fundamental studies can be exploited to improve and design catalysts to favor certain pathways and products and prevent the formation of others. Important reactions during reforming are C-H, C-C and C-O bond cleavage. To prevent alkane formation, it is preferred that every carbon atom is connected to one oxygen atom to enable reforming of the molecule to CO and H_2. Ethylene glycol (EG) is chosen as a model compound to study fundamental catalytic behavior because it is the smallest molecule (hence avoiding the occurrence of complicated side reactions) with all carbon atoms bonded to oxygen (preventing intrinsic methane formation) where both desired and undesired pathways (C-C, C-O and C-H cleavage) can occur.

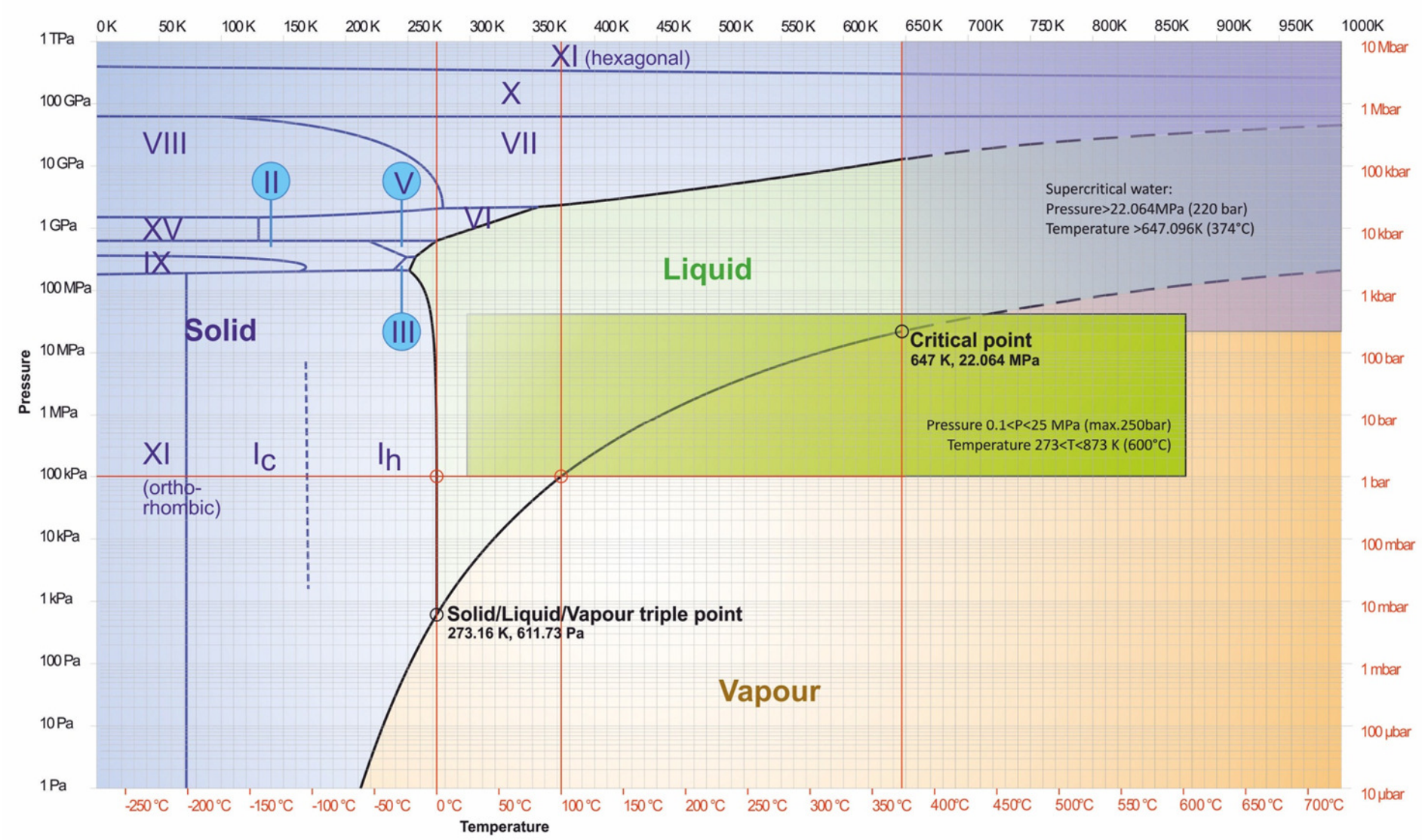

Figure 1.4: Phase diagram of water.

The reforming of ethylene glycol has been studied intensively by Dumesic and colleagues [53] and a reforming mechanism has been proposed by them as shown in Figure 1.5. EG first undergoes dehydrogenation and adsorption on the catalyst surface. The formed intermediate can further react through two pathways. The desired pathway to form hydrogen involves C-C cleavage which results in H_2 gas and adsorbed CO. Hydrogen yields can be further increased by the water gas shift reaction ($CO + H_2O \rightarrow CO_2 + H_2$). The undesired pathway involves cleavage of the C-O bond leading to species such as acids and alcohols that can further undergo sequential reforming to produce alkanes. Other pathways leading to undesired products include dehydration of ethylene glycol to produce vinyl alcohol. Sequential hydrogenation of vinyl alcohol results in the formation of ethanol. Direct hydrogenation of CO_x can also lead to the formation of CH_4 or even higher alkanes through the Fischer-Tropsch process.

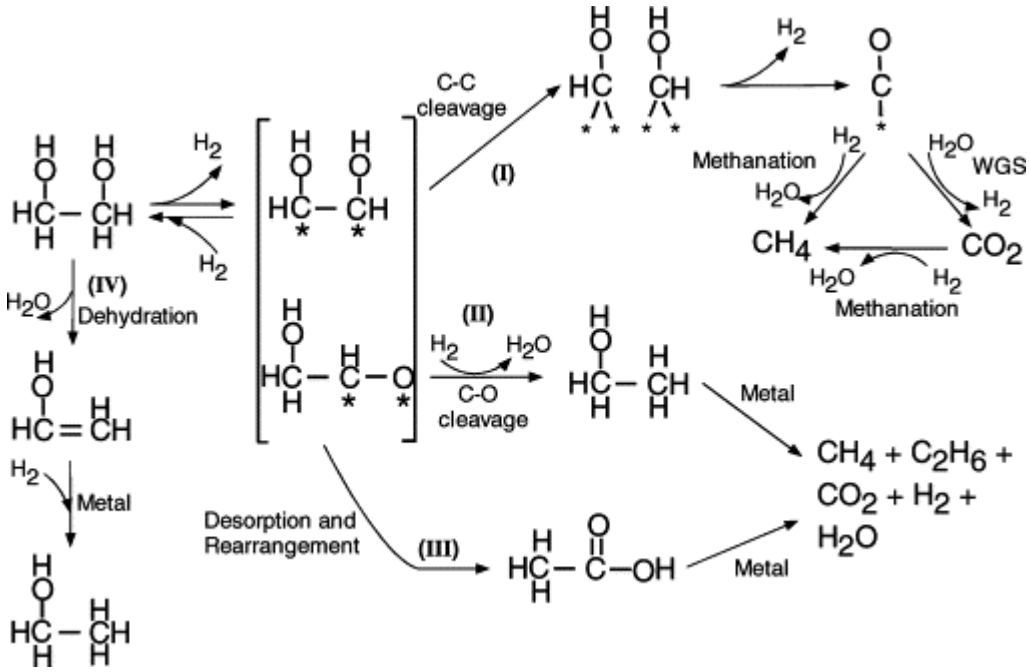

Figure 1.5: Ethylene glycol reforming pathway as suggested by Dumesic *et al.* [53].

Dumesic *et al.* [53] reported the thermal dependence of the standard Gibbs free energy for water gas shift and EG reforming reactions in liquid and vapor phase as shown in Figure 1.6. A negative value for the standard Gibbs free energy ($\Delta G/RT<0$) indicates that the process is spontaneous. The Gibbs free energy of the water gas shift reaction in liquid phase was

reported to be negative and temperature independent in the range 300 – 650 K (27-375 °C). In case of vapor phase water gas shift reaction, the reaction becomes less favorable at higher temperatures. The reforming of ethylene glycol in liquid phase compared to vapor phase becomes more favorable beyond 450 K (175 °C). The advantages of aqueous phase reforming are (i) no need for evaporation of the water and (ii) the water gas shift activity and reforming are more favored in liquid phase than in vapor phase at temperatures above 175 °C.

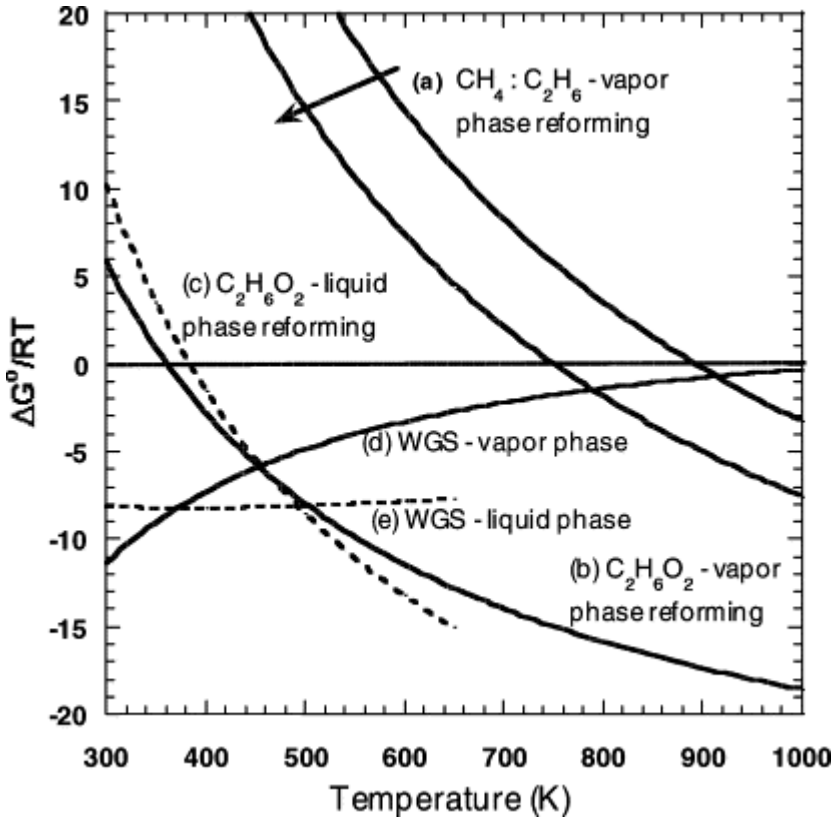

Figure 1.6: Thermodynamic calculations for the reforming of ethylene glycol [53].

Shabaker *et al.* [51] studied the reaction order of EG reforming at 225 °C and 29 bars. They found that the reaction order was dependent on the EG feed concentrations. The order was reported to be 0.5 for 1-4 wt% feed streams and decreased to 0.3 for 10 wt% feed streams. Furthermore, it was shown that the order for hydrogen production was -0.5 which indicates that the presence of hydrogen had a weak inhibiting effect on the reaction. An Activation energy of 100 KJ/mol was calculated for EG reforming at those reaction conditions.

Typical temperatures for fundamental APR studies of model components (*e.g.* ethylene glycol, methanol and sorbitol) are usually performed in the temperature range of 200-265 °C [51, 54]. The reforming of more concentrated feed streams or more complex oxygenates, that are of more commercial relevance, require higher temperatures to obtain the reaction rates which are necessary for industrial application [48]. Properties of hot compressed water are strongly dependent on the exact temperature and pressure of the water and show a significant influence on the reaction. Increasing the temperature of liquid water above 374 °C (and 221 bar pressure) brings the water into the supercritical state. A dramatic change in properties occurs when water becomes supercritical and these offer some other advantages for the reforming of biomass derived waste streams into gaseous products [48, 55-57]. Sub- and supercritical water are considered different reaction regimes due to the extreme differences in properties. Sub- and supercritical water are discussed in more detail in the next section (section 1.4)

1.4 Reaction in sub- and supercritical water

Aqueous Phase Reforming can be divided in a sub- and a supercritical regime. The transition from sub- to supercritical water occurs at 374 °C and 221 bars. Properties of sub- and supercritical water (SCW) vary significantly and will be reflected in reforming reactions. Kritzer [58, 59] reported the effect of temperature on density, dielectric constant and ionic product of liquid water as shown in Figure 1.7. It can be seen that density of water decreases gradually with increasing temperature. However, a drastic decrease in density occurs crossing the supercritical point. The density beyond the supercritical point is around ± 100 kg / m^3. A further increase in temperature does not affect the density significantly anymore. The properties of liquid water and compressed gas converge around the supercritical point, resulting in complete mixture of both phases and the removal of the liquid/gas phase boundary. The latter is very beneficial for fast rates of heat and mass transfer [48].

Another very important parameter for reactions in hot compressed water is the ionic product. The dissociation of water is an endothermic process and therefore an increase in temperature results in a higher ion product. However, at the same time, an increase in temperature results in lower density which causes a lower ionic solvability [58, 59]. These two competing phenomena determine the ionic product of hot compressed water. The

behavior of the ionic product can be seen from Figure 1.7 [59]. Initially, the ion product increases with temperature and reaches a maximum around 300 °C. Under those conditions, the ion product is ±1000 times higher than under ambient conditions. A further increase in temperature results in a gradual decrease in ionic product because the decrease in water density becomes more pronounced. On passing the supercritical point, ionic product decreases strongly due to the collapse of the water density value. The ionic product of supercritical water is about a billion times less than under ambient conditions. The high ionic product in subcritical water can be exploited for acid/based catalyzed reactions. The ionic product can significantly influence reaction rates and selectivities. On the other hand, the high ionic product of subcritical water causes a lot of stress on (reactor) materials because the high amounts of protons and ions are reported to propagate material leaching/corrosion [58, 60]. The low ionic product of supercritical water reduces the corrosive properties of water under those conditions. However, severe corrosion in SCW is frequently reported (especially at high temperatures and high densities) and is usually related to the presence of oxidizing species (*e.g.* oxygen or halogens) in the feed stream [60].

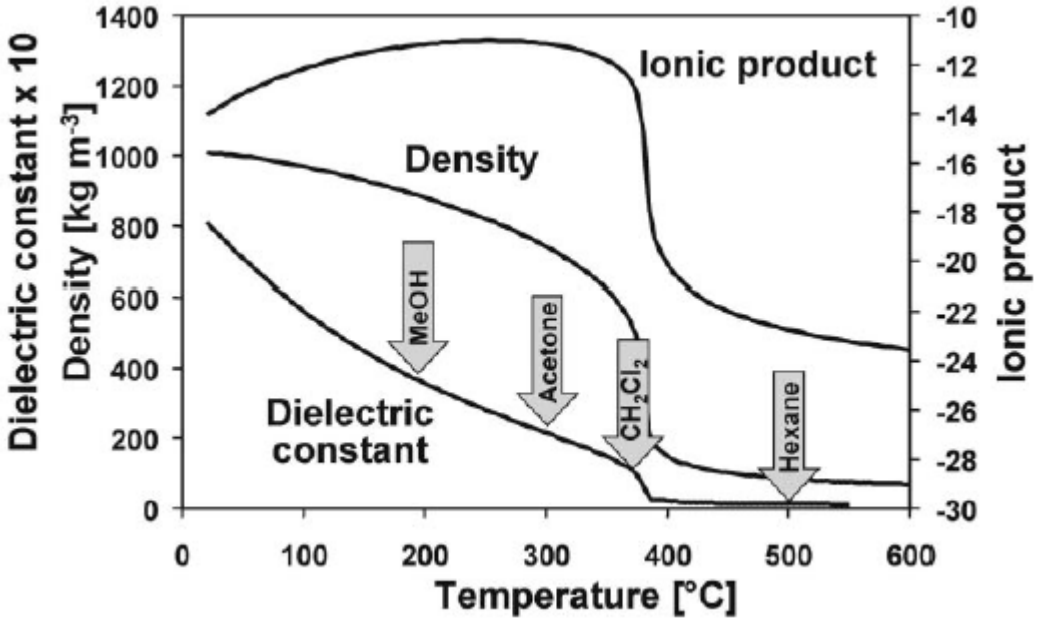

Figure 1.7: The effect of temperature on the physical properties of liquid water (240 bar) [59].

The polarity of a liquid is a very important factor that determines its salvation properties. Polarity is strongly dependent on the dielectric constant of water which is again influenced by the temperature. The effect of temperature on the dielectric constant of water can be seen in Figure 1.7 and includes a comparison with organic solvents [59]. Under ambient conditions, water has a high dielectric constant of ± 80 and has therefore a polar character. Polar compounds such as salts (e.g. NaCl) and polar gases (*e.g.* NH_3, SO_2) have a high solvability in ambient water. An increase in temperature disrupts the hydrogen-bond network, resulting in a lower dielectric constant and hence polarity. The dielectric constant just before the supercritical point is 20 and decreases rapidly to less than 5 beyond this point. The low dielectric constant of supercritical water causes water to behave as a non-polar solvent. Therefore, organic components (*e.g.* Lignin and other biomass derived compounds) and non-polar gases dissolve easily in supercritical water while salts do not. The non-polar character of supercritical water can be exploited for catalytic reactions to prevent coke deposition on the catalyst [61].

1.5 Challenges

Many APR studies [47, 62-65] were already undertaken by different research groups to study the reforming of model compounds under mild subcritical water conditions (175-265 ^{o}C and 32-56 bar). APR conditions are ideal for fundamental reforming studies; however reaction rates are relatively slow at these low temperatures and therefore studies are limited to low concentrated feed solutions or long residence times.

The ultimate goal is to develop a commercial and technologically feasible (catalytic) process for the production of hydrogen by APR of industrial biomass derived aqueous streams that contain complex mixtures (15-25 wt%) of oxygenates. Therefore, much higher reaction rates are required compared to low temperature APR to achieve this goal. Achieving high H_2 yields by reforming of high concentrated feeds is not only a matter of increasing the catalytic reaction rate. Thermodynamics predict an increase in alkane formation for reforming reactions with higher feed concentrations [66]. Production of alkanes should be avoided as it competes with the hydrogen yields. Furthermore, low temperature APR is also reported to be subject to mass transfer limitations which can severely hinder the catalytic reaction for high feed concentrations. As an example, it was shown by Shabaker and colleagues [51] that APR

of ethylene glycol (225 °C and 29.3 bar) with a 3.4 wt% Pt/Al_2O_3 (63 – 125 μm particle size) catalyst was affected by intra-particle mass transfer limitations when an EG feed concentration of 10 wt% was used.

Catalytic supercritical water reforming is promising for achieving high reforming rates and overcome mass transfer limitations. Tang *et al.* [48] published a nice overview of catalytic supercritical water reforming studies of biomass derived compounds. High reaction rates for the reforming of concentrated oxygenate streams were reported. However, stability and selectivity issues with the studied catalysts are serious drawbacks for industrial exploitation of this process [48]. Catalyst stability issues in hot compressed water are mainly related to sintering of the supported metal particles [48] or instability of conventional metal oxides catalyst supports (*e.g.* Al_2O_3, TiO_2 and ZrO_2) [67, 68]. Issues with metal oxide supports are already experienced at low temperature APR conditions [69].

The challenge to make sub- or supercritical water reforming of biomass derived waste streams commercially feasible involves the development of catalysts that (i) show high stability in hot compressed water, (ii) are able to convert high concentrated feed streams under industrial relevant residence times, and (iii) produce high H_2 yields. Fundamental understanding of the reforming pathways and deactivation mechanisms help in the development of such catalysts.

1.6 Scope and outline of the thesis

The main objective of this thesis is to develop an efficient catalyst for hydrogen production by reforming of industrial biomass derived waste streams and in parallel gain more understanding about reaction pathways and catalyst deactivation mechanisms.

Initial experiments were performed with the model compound Ethylene Glycol (EG) because of the reasons discussed earlier in section 1.3. Industrial waste streams commonly have oxygenate concentrations of ±15 wt% and therefore this concentration was chosen as target for the initial EG reforming experiments.

From literature, it was also clear that long residence times were necessary for reforming of high concentrated feeds under temperate APR conditions. Residence times in the catalytic bed should be industrially applicable and this would generally mean that it should be

in the order of seconds. Furthermore, mass transfer was expected to be a problem for reforming of high concentrated feed streams under mild APR conditions. Therefore, it was decided to start studying APR under supercritical water conditions to achieve high reaction rates and overcome mass transfer limitations.

An initial catalyst screening experiment is described in Chapter 3. Potential catalysts were selected based on a literature study and were studied for reforming of high concentration EG solutions in SCW (450 °C and 250 bar). The most promising catalyst (Pt/Al_2O_3) was further optimized by promoting it with a second metal (Ni). The developed Pt-based catalyst was found to be very promising for EG reforming at those conditions and is selected for further studies. This chapter is published in the following manuscript:

D.J.M. de Vlieger, A.G. Chakinala, L. Lefferts, S.R.A. Kersten, K. Seshan and D.W.F. Brilman, Appl. Catal. B 111-112 (2012) 536-544

The effect of side reactions during catalytic reforming of EG in SCW on the catalytic performance of the developed alumina supported Pt based catalyst is discussed in Chapter 4. The effect on H_2 yields and catalyst stability of sequential reforming of the identified byproducts methanol, ethanol and acetic acid is discussed. The reason for catalyst deactivation in the presence of acetic acid is addressed. This chapter led to the publication of the following manuscript:

D.J.M. de Vlieger, B.L. Mojet, L. Lefferts and K. Seshan, J. Catal. 292 (2012) 239-245

Chapter 5 addresses the need for new catalytic support materials for acidic feed streams. The performance of carbon nanotubes (CNT) supported Pt catalysts for SCW reforming ethylene glycol and acetic acid is discussed. CNT showed to be very stable catalyst support material for reforming in SCW. Furthermore, it became evident that acetic acid is an important model compound for which Pt does not show good activity. This chapter resulted in publication of the subsequent article:

D.J.M. de Vlieger, D.B. Thakur, L. Lefferts and K. Seshan, ChemCatChem 4 (2012) 2068-2074

In Chapter 6, stability and efficiency of Ru-CNT for the catalytic reforming of acetic acid in sub- and supercritical water was studied. Ru/CNT deactivated in high temperature subcritical water and the reason for deactivation is discussed. Ru/CNT showed high stability

and commercial attractive activity for the reforming of acetic acid in supercritical water. This work is submitted for publication and is currently being reviewed.

The high stability and good reforming activity of Ru/CNT catalyst opened the door to move away from model compounds and study the reforming of real aqueous phase of flash pyrolysis oil as discussed in Chapter 7. Non-catalytic issues were observed during this study and prevent a feasible exploitation of APR of certain feed streams at the moment. Conclusions, concept evaluations and outlook of this study are discussed in Chapter 8.

References

[1] International Energy Agency, *World energy outlook* (2008)

[2] British Petroleum, *Statistical Review of World Energy* (2011)

[3] J. Kjarstad, F. Johnsson, Energ. Policy 37 (2009) 441-464.

[4] International Energy Agency, *From Resources to reserves* (2005)

[5] R. Martninez-Palou, M. Mosqueira, B. Zapata-Rendón, E. Mar-Juárez, C. Bernal-Huicochea, J. de la Cruz Clavel-López, J. Aburto, J. Pet. Sci. Eng. 75 (2011) 274-282.

[6] D.K. Olsen, E.B. Ramzel, Fuel 71 (1992) 1391-1401.

[7] G. Houlton, *Global Crude oil supply and quality trends*, COQA San Antonio (2011)

[8] H.R. Mortaheb, F. Ghaemmaghami, B. Mokhtarani, Chem. Eng. Res. Des. 90 (2012) 409-432.

[9] L. Hughes, J. Rudolph, Curr. Opin. Environ. Sustainability 3 (2011) 225-234.

[10] F. Curtis, Ecol. Econ. 69 (2009) 427-434.

[11] W.P. Nel, C.J. Cooper, Energ. Policy 36 (2008) 1096-1106.

[12] P. Hanlon, G. McGartney, Public Health 122 (2008) 647-652.

[13] C. Lutz, U. Lehr, K.S. Wiebe, Energ. Policy In Press (10.1016/j.enpol.2012.05.017)

[14] G. Bridge, Geoforum 41 (2010) 523-530.

[15] G. Maggio, G. Cacciola, Fuel 98 (2012) 111-123.

[16] K. Aleklett, M. Höök, K. Jakobsson, M. Lardelli, S. Snowden, B. Söderbergh, Energ. Policy 38 (2010) 1398-1414.

[17] D.L. Greene, J.L. Hopson, J. Li, Energ. Policy 34 (2006) 515-531.

[18] S. Sorrell, J. Speirs, R. Bentley, A. Brandt, R. Miller, Energ. Policy 38 (2010) 5290-5295.

[19] C. Anastasi, R. Hudson, V.J. Simpson, Energ. Policy 18 (1990) 936-944.

[20] J. Dignon, Atmos. Environ. A-Gen. 26 (1992) 1157-1163.

[21] L. Chiari, A. Zecca, Energ. Policy 39 (2011) 5026-5034.

[22] M.F. Akorede, H. Hizam, M.Z.A. Ab Kadir, I. Aris, S.D. Buba, Renew. Sust. Energ. Rev. 16 (2012) 2747-2761.

[23] G.R. Walther, E. Post, P. Convey, A. Menzel, C. Parmesan, T.J.C. Beebee, J.M. Fromentin, O. Hoegh-Guldberg, F. Bairlein, Nature 416 (2002) 389-395.

[24] T. Abbasi, M. Premalatha, S.A. Abbasi, Renew. Sust. Energ. Rev. 15 (2011) 891-894.

[25] D.G. Kessel, J. Pet. Sci. Eng. 26 (2000) 157-168.

[26] K. Sipila, A. Johansson, K. Saviharju, Bioresource Technol. 43 (1993) 7-12.

[27] P.K. Swain, L.M. Das, S.N. Naik, Renew. Sust. Energ. Rev. 15 (2011) 4917-4933

[28] D.O. Hall, J.I. House, Sol. Energ. Mat. Sol. C. 38 (1995) 521-542.

[29] T. Gul, S. Kypreos, H. Turton, L. Barreto, Energ. 34 (2009) 1423-1437.

[30] M. Grahn, C. Azar, K. Lindgren, G. Berndes, D. Gielen, Biomass Bioenerg. 31 (2007) 747-758.

[31] P.S. Nigam, A. Singh, Prog. Energ. Combus. 37 (2011) 52-68.

[32] S.N. Naik, V.V. Goud, P.K. Rout, A.K. Dalai, Renew. Sust. Energ. Rev. 14 (2010) 578-597.

[33] A. Demirbas, App. Energ. 86 (2009) s108-s117.

[34] G.R. Timilsina, A. Shrestha, Energy 36 (2011) 2055-2069.

[35] H.N. Lazarides, Procedia Food Sci. 1 (2011) 1854-1860.

[36] L.O. Pordesimo, B.R. Hames, S. Sokhansanj, W.C. Edens, Biomass Bioenerg. 28 (2005) 366-374.

[37] A.V. Bridgwater, D. Meier, D. Radlein, Org. Geochem. 30 (1999) 1479-1493.

[38] T. Damartzis, A. Zabaniotou, Renew. Sust. Energ. Rev. 15 (2011) 366-378.

[39] K. Sunde, A. Brekke, B. Solberg, Forest Pol. Econ. 13 (2011) 591-602.

[40] A.V. Bridgwater, Biomass Bioenerg. 38 (2012) 68-94.

[41] M.M. Wright, D.E. Daugaard, J.A. Satrio, R.C. Brown, Fuel 89 (2010) S2-S10.

[42] J. Xie, D. Su, X. Yin, C. Wu, J. Zhu, Int. J. Hydrogen Energ. 36 (2011) 15561-15572.

[43] Q. Lu, W.Z. Li, X.F. Zhu, Energ. Convers. Manage. 50 (2009) 1376-1383.

[44] P.M. Mortensen, J. D. Grunwaldt, P.A. Jensen, K.G. Knudsen, A.D. Jensen, Appl. Catal. A 407 (2011) 1-19.

[45] S. Zhang, Y. Yan, T. Li, Z. Ren, Bioresource Tech. 96 (2005) 545-550.

[46] A.V. Bridgwater, Catal. Today 29 (1996) 285 – 295.

[47] R.D. Cortright, R.R. Davda, J.A. Dumesic, Nature 418 (2002) 964-967.

[48] Y. Guo, S.Z. Wang, D.H. Xu, Y.M. Gong, H.H. Ma, X.Y. Tang, Renew. Sust. Energ. Rev. 14 (2010) 334-343.

[49] A. Tanksale, J.N. Beltramini, G.M. Lu, Renew. Sust. Energ. Rev. 14 (2010) 166-182.

[50] J.A. Medrano, M. Oliva, J. Ruiz, L. Garcia, J. Arauzo, J. Anal. Appl. Pyrol. 85 (2009) 214-225.

[51] J.W. Shabaker, R.R. Davda, G.W. Huber, R.D. Cortright, J.A. Dumesic, J. Catal. 215 (2003) 344-352.

[52] G.W. Huber, J.W. Shabaker, S.T. Evans, J.A. Dumesic, Appl. Catal. B 62 (2006) 226-235.

[53] R.R. Davda, J.W. Shabaker, G.W. Huber, R.D. Cortright, J.A. Dumesic, Appl. Catal. B 43 (2003) 13-26.

[54] R.R. Davda, J.W. Shabaker, G.W. Huber, R.D. Cortright, J.A. Dumesic, Appl. Catal. B 56 (2005) 171-186.

[55] Y. Matsumura, T. Minowa, B. Potic, S.R.A. Kersten, W. Prins, W.P.M. van Swaaij, B. van de Beld, D.C. Elliott, G.G. Neuenschwander, A. Kruse, M.J. Antal jr., Biomass Bioenerg. 29 (2005) 269-292.

[56] A. Yamaguchi, N. Hiyoshi, O. Sato, K.K. Bando, M. Osada, M. Shirai, Catal. Today 146 (2009) 192-195.

[57] M.H. Waldner, F. Krumeich, F. Vogel, J. Supercrit. Fluid. 43 (2007) 91-105.

[58] P. Kritzer, J. Supercrit. Fluid. 29 (2004) 1-29.

[59] P. Kritzer, E. Dinjus, Chem. Eng. J. 83 (2001) 207-214.

[60] P.A. Marrone, G.T. Hong, J. Supercrit. Fluid. 51 (2009) 83-103.

[61] J.B. Muller, F. Vogel, J. Supercrit. Fluid. 70 (2012) 126-136.

[62] F.Z. Xie, X.W. Chu, H.R. Hu, M.H. Qiao, S. R. Yan, Y. L. Zhu, H.Y. He, K.N. Fan, H.X. Li, B.N. Zong, X.X. Zhang, J. Catal. 241 (2006) 211-220.

[63] A.V. Tokarev, A.V. Kirilin, E. V. Murzina, K. Eränen, L.M. Kustov, D.Y. Murzin, J.P. Mikkola, Int. J. Hydrogen Energ. 35 (2010) 12642-12649.

[64] R.L. Manfro, A.F. da Costa, N.F.P. Ribeiro, M.M.V.M. Souza, Fuel Process. Technol. 92 (2011) 330-335.

[65] A.O. Menezes, M.T. Rodrigues, A. Zimmaro, L.E.P. Borges, M.A. Frago, Renew. Energ. 36 (2011) 595-599.

[66] R.R. Davda, J.A. Dumesix, Angew. Chem. Int. Edit. 42 (2003) 4068-4071.

[67] A.J. Byrd, R.B. Gupta, Appl. Catal. A 381 (2010) 177-182.

[68] P. Azadi, R. Farnood, Int. J. Hydrogen Energ. 36 (2011) 9529-9541.

[69] R.M. Ravenelle, J.R. Copeland, W.G. Kim, J.C. Crittenden, C. Sievers, ACS Catal. 1 (2011) 552-561.

Chapter 2

Experimental

The experimental setup used for this study is described in detail in this Chapter. Catalyst preparation and characterization, and methods used for analysis of feed and product streams, are discussed. Furthermore, the definitions and calculations used for this study are explained.

2.1 Experimental setup

Two similar experimental setups were used for the study that is discussed in this thesis. Initial experiments (used for Chapter 3) were performed on a reforming setup which was available in the TCCB group (University of Twente). Follow-up studies were performed on a setup that was built for our research group CPM. The design of this setup was a direct copy from the setup used at the TCCB group and dimensions were therefore similar. However a few differences exist between the two setups, which are related to external apparatus and discussed below.

Figure 2.1 shows the schematic diagram of the continuous flow aqueous phase reformer used for the experiments in Chapter 3. Feed streams of oxygenates (typical concentrations in the range of 1 - 30 wt% were used depending on the experiment) were preheated to reaction conditions. After preheating, the solution entered a 63 cm long reactor (ID = 7 mm) in which the catalyst was placed. The reactor effluent was cooled down to room temperature with a counter-current heat exchanger and pressure was reduced by a back pressure regulator to atmospheric pressure. A glass bottle was used to allow the separation of gas and liquid products. The flow rate of the liquid reactor effluent was monitored using a balance under the glass vessel. The amount of gas produced was measured with an Actaris Gallus 2000 gas meter. Products in gas phase were determined by a Varian CP-4900 Micro GC using MS5 and PPQ columns. Argon was used as carrier gas for both columns and this configuration enabled us to detect CO levels above 0.1 v/v%. Gas analysis was subject to a relative error of 1% per component. Carbon content analysis of the feed solution and the liquid product was conducted using an Interscience Flash 2000 Organic Elemental Analyzer. The total liquid effluent was analyzed after the reaction by a Shimadzu HPLC to identify the liquid products formed during the reforming reaction. The HPLC was equipped with a RID-10A detector and an Aminex HPX-87H (300x7.8mm) column. The latter was operated at 35 °C. An aqueous solution of 0.005 M H_2SO_4 was used as elutant phase and was flown at a rate of 0.600 mL. min^{-1}. Sample volumes of 20 µl were injected into the column.

The experiments performed after Chapter 3 were conducted on the cloned setup at CPM. The only differences between the experimental setups were that (i) gas production was measured by a Brooks SLA-5860S gas meter which was calibrated for N_2. Gas phase analysis was used in combination with theoretical gas response conversion factors (H_2 = 1.01, O_2= 0.993, CO = 1.00, CO_2= 0.70, CH_4= 0.72, C_2H_6 = 0.50, C_2H_4 = 0.60) to correct for the actual

gas production, (ii) High pressure ISCO pumps (model 500D) were used to feed reactants and, (iii) carbon concentrations in the feed solution and the liquid effluent were determined by an online Shimadzu TOC-V_{CSH} analyzer (rel. error of 1% was applicable per TOC analysis).

2.2 Catalyst preparation

2.2.1 Catalyst preparation of metal oxide supported catalysts

Extrudates of γ-alumina (BASF AL-3992) were crushed and sieved to obtain particles within a size range of 300-600 μm and were used as catalyst support. H_2PtCl_6•$6H_2O$, $IrCl_4$ and $Ni(NO_3)_2$•$6H_2O$ precursors (analytical grade > 99.9%) were obtained from Alfa Aesar. Mono- and bi-metallic catalysts were prepared by wet (co) impregnation. The desired amount of precursor(s) was dissolved in water and added to the γ-alumina support (weight ratio H_2O/alumina = 1.8). The water was evacuated under vacuum at 100 °C. Catalysts made with Cl containing precursors were treated at 100 °C for 5 h (10 °C min^{-1}) under hydrogen (100 mL. min^{-1} H_2 and 100 mL. min^{-1} N_2) to remove any residual Cl [1]. Materials were finally calcined at 500°C for 15 h (10 °C min^{-1}) under air (200 mL. min^{-1}).

2.2.2 Catalyst preparation of carbon nanotubes supported catalysts

Carbon nanotubes were obtained from 'carbon NT&F 21®' and used as catalyst support without further purification. The properties of this material were provided by the manufacturer and are given in Table 2.1. Pt and Ru decorated CNT were prepared by impregnation. The metal precursors H_2PtCl_6•$6H_2O$ and $Ru(NO)(NO_3)_3$ (analytical grade > 99.9%) were obtained from Alfa Aesar. The desired amount of precursor was dissolved in acetone and added to the CNT support (10 mL. of acetone per 1.0 gram of CNT). The acetone was removed by evaporation in a vacuum oven. The temperature of the oven was increased at a rate of 5 °C min^{-1} to a temperature of 100 °C under atmospheric pressure and subsequently dried overnight at this temperature in reduced pressure (0.2 bar). Synthesized CNT supported catalysts were further treated at 500 °C for 15 h (10 °C min^{-1}) in hydrogen (100 mL min^{-1}, 50 v/v% H_2 in N_2, 1 bar).

Table 2.1 Properties of CNT

Purity (%)	> 90
Diameter (nm)	~ 80-150
Length (μm)	~ 30
Amorphous carbon (%)	< 5
Special surface area (m^2/g)	~ 20
Thermal conductivity	< 2000

2.3 Catalyst characterization

The following analysis methods were used to characterize fresh and used catalyst:

XRF analysis: Metal loadings on catalysts supports were determined using a Philips X-ray fluorescence spectrometer (PW 1480).

BET analysis: Surface areas of the catalysts were measured applying the BET method on an ASAP 2400 (Micromeritics).

TEM imaging: TEM images were taken on a JEOL 2010F equipped with EDX.

SEM imaging: SEM images were taken on a Zeiss 1550 HR-SEM.

CO-Chemisorption: Metal dispersions were determined with pulse CO chemisorption at room temperature on 100 mg of alumina catalyst using a Micromeritics Chemisorb 2750. CO/Metal stoichiometric ratios of 1 were assumed for all the catalysts. Before pulsing, the catalyst was reduced in H_2 at 400°C for 1 h and cooled down in helium to room temperature subsequently. Average metal particle sizes for monometallic catalysts were calculated based on dispersion values, assuming hemispherical particle shape.

TGA-MS analysis: Spent catalysts were analyzed by TGA-MS to determine any coke deposits on the surface. Argon with 1 v/v% O_2 was flown over the catalyst while the temperature was increased from 25 to 800°C. The weight of the catalyst was monitored by TGA and the composition of the gas output was analyzed by MS.

Raman Spectroscopy: Raman spectroscopy of catalysts were recorded at ambient conditions on a Bruker Senterra in a frequency range of 65 – 4000 cm^{-1} with a resolution of 9 – 13 cm^{-1}. A laser wavelength of 532 cm^{-1} with 10 mW and 5 mW power was used for alumina and CNT supported catalysts, respectively.

XRD analysis: X-ray diffraction (XRD) patterns were collected over the range $2\theta = 20 – 90°$ on a Brooker D2 Phaser using Cu Kα1 radiation source.

TPR analysis: Catalysts (100mg) studied by TPR were first heated up to 500°C in oxygen (5% O_2 / 95% He) and then cooled down to room temperature in argon to remove any moisture from the surface. TPR experiments were carried out in a 10 ml/min hydrogen flow (5% H_2 / 95% Ar) and the temperature was increased to 10°C min^{-1}. Consumption of hydrogen was taken as measure of reduction and plotted as function of temperature.

FT-IR spectroscopy: FT-IR spectra of alumina supported catalysts were taken on a Bruker Tensor 27 with 4 cm^{-1} resolution and using a 5 mm aperture. Spectra were taken in the range of 600 to 4000 cm^{-1} and averaged over 64 scan.

XPS spectroscopy: XPS spectra of the catalysts were obtained on a Quantera SXM from Physical Electronics with an Al Kα X-Ray source (monochromatic at 1486.6 eV).

2.4 Definitions and calculations

Definitions and calculations used for this study are discussed in this section. The catalyst performance is presented in terms of (i) carbon to gas conversion (sometimes referred to as gasification efficiency), (ii) selectivities to gas phase products (gas purity), and (iii) catalyst stability. The exposure time of feed stream on the catalyst is reported in terms of weight hourly space velocities (WHSV). The catalyst activity is also discussed in terms of Turn over Frequency (TOF, min^{-1}).

Carbon to gas conversion: Carbon to gas conversion can be determined directly from the GC and gas production results, however the many assumptions (*e.g.* ideal gas law) and parameters involved in this method compromises the accuracy of this direct approach. Therefore, it was decided to use an indirect approach with better accuracy. In this method, carbon to gas conversion is defined as the percentage of carbon in the feed that is transformed to carbon in gaseous products (CO_x, hydrocarbons) and is calculated according to

$\frac{"moles\ carbon"_{Feed} - "moles\ carbon"_{Reactor\ liquid\ effluent}}{"moles\ carbon"_{Feed}} \times 100\%$. Carbon removed from the feed can either go to gas phase products or to coke. This method assumes that the amount of carbon transformed to coke is negligible compared to the amount of carbon in gas phase. In selected cases this was corrected for by estimating the amount of carbon deposited in solid phase. Carbon contents in liquid streams were determined with a Shimadzu TOC–V_{csh} analyzer. A relative error of 1% was applicable per TOC analysis, resulting in a 2% error (relatively) in the conversion number. The target of this study is to produce high heating value gases and therefore conversion of gasified carbon is reported only and transformation to other liquid products is not taken into account in the conversion.

Gas phase selectivities: Selectivity to carbon containing gas phase products (i = CO_x, CH_4 and C_2+) were calculated according $selec.i\ \% = \frac{"C"\ in\ species\ i}{"C"\ in\ gas\ phase} \times 100\%$. The selectivity to carbon containing gas phase products indicates the purity of the produced gas and is calculated based on the distribution of carbon in these molecules. Side-reactions leading to carbon containing molecules in the liquid phase were not taken into account for selectivity calculations.

Selectivity to hydrogen is defined as the percentage of the maximal theoretical amount of hydrogen formed based on the gasified carbon and is expressed as $selec.H_2\ \% = \frac{H_2 moles\ produced}{C\ atoms\ in\ gas\ phase} \times \frac{1}{RR} \times 100\%$. The reforming ratio (RR) is the maximum amount of H_2 (incl. water gas shift reaction) that can be produced per gasified carbon atom (H_2/CO_2). The RR for ethylene glycol and acetic acid reforming is 2.5 and 2.0, respectively, as shown below.

RR for ethylene glycol is 5/2

$C_2H_6O_2$	→	3 H_2 + 2 CO (optimal reforming)
2 CO + 2 H_2O	→	2 H_2 + 2 CO_2 (WGS)
$C_2H_6O_2$	→	5 H_2 + 2 CO_2 (overall optimal reaction)

RR for acetic acid is 4/2

CH_3-COOH	→	2 H_2 + 2 CO (optimal reforming)
2 CO + 2 H_2O	→	2 H_2 + 2 CO_2 (WGS)
CH_3-COOH + 2H_2O	→	4 H_2 + 2 CO_2 (overall optimal reaction)

Weight hourly space velocities: Weight hourly space velocities (WHSV) indicate the grams of oxygenates fed to the reactor per gram of catalyst per hour.

Turn over frequencies: Turn over frequencies (TOF) were calculated for the monometallic catalysts based on the metal dispersions and is defined as the number of respective molecules produced/reacted per active catalytic site per minute.

References

[1] D. Radivojevic, K. Seshan, L. Lefferts, Appl. Catal. A 301 (2006) 51-58.

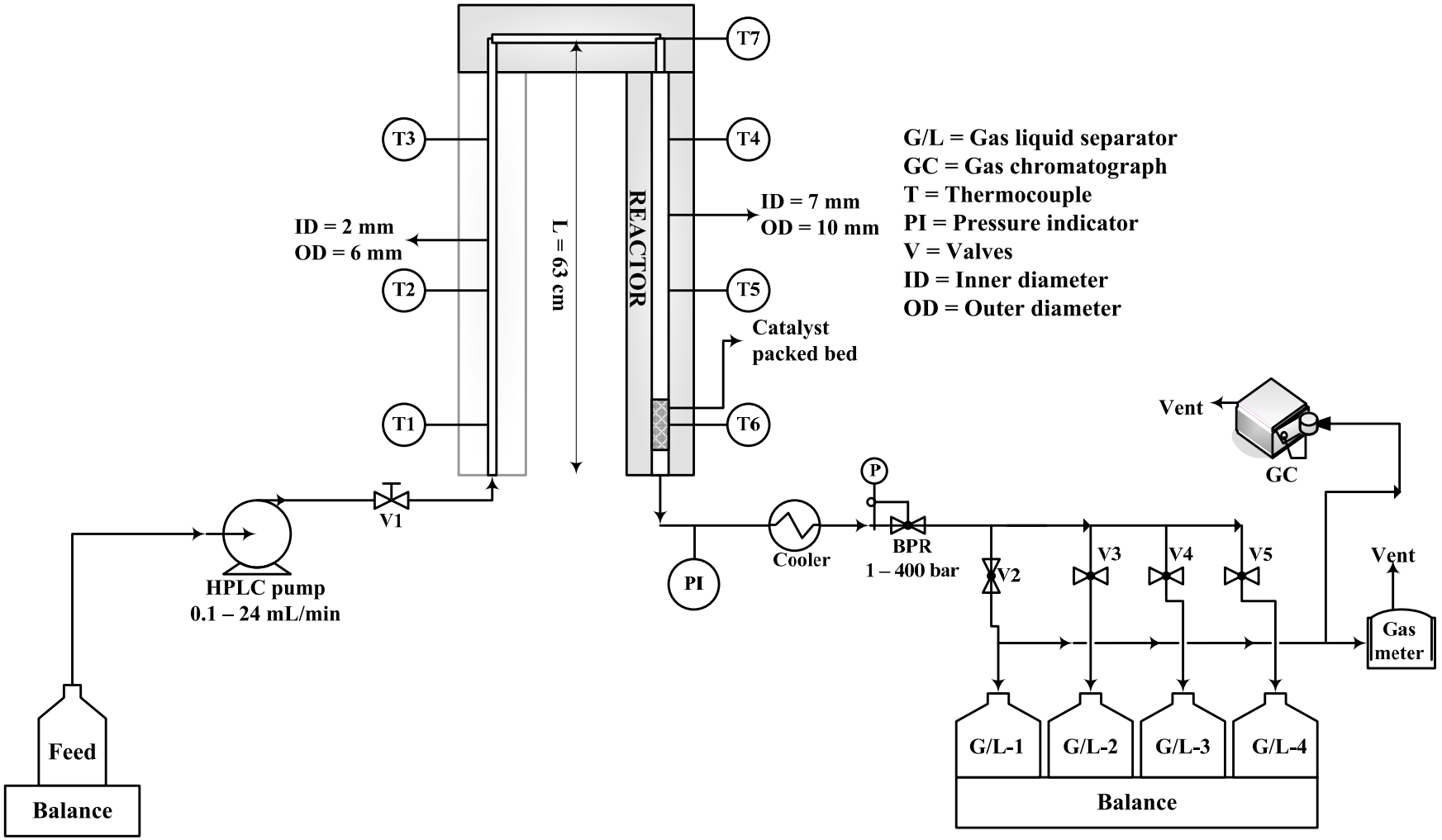

Figure 2.1: Schematical drawing of the experimental setup

Chapter 3

Development of an efficient catalyst for the reforming of ethylene glycol in supercritical water

D.J.M. de Vlieger, A.G. Chakinala, L. Lefferts, S.R.A. Kersten, K. Seshan, D.W.F. Brilman, Appl. Catal. B 111 (2012) 536

Catalytic reforming of ethylene glycol (5 & 15 wt%) in supercritical water (450°C and 250 bar) in the presence of alumina supported mono- and bi-metallic catalysts based on Ir, Pt and Ni was studied. Pt catalyst showed the highest hydrogen yields compared to Ir and Ni. Varying the Pt loading (0.3 - 1.5 wt%) showed that the intrinsic reforming activities improved with decreasing Pt loadings. However, a lower Pt loading had a large negative effect on the H_2 selectivity and catalyst stability. It was found that the presence of Ni in a Pt-Ni bimetallic catalyst improved hydrogen yields by suppressing methane formation. Moreover, the presence of Ni also enhanced catalyst stability. Results reported here were obtained at WHSV of 18 h^{-1}. The Pt-Ni/Al_2O_3 having a total metal loading of 1.5 wt% (molar ratio Pt:Ni=1), is identified as a promising catalyst for the reforming of ethylene glycol in supercritical water.

3.1 Introduction

As discussed in Chapter 1, aqueous phase reforming (APR) of bio/organic feeds is a promising technique for the production of renewable hydrogen. Commercially interesting feeds, such as the aqueous phase of flash pyrolysis oil, typically contain oxygenate concentrations in the range of 15 - 20 wt%. Nakamura *et al.* [1] reported that complete conversion of feeds containing at least 15 wt% oxygenates is required to be economically viable under supercritical APR conditions.

Under low temperature APR conditions, thermodynamics favor selectivity towards alkanes in preference to hydrogen [2]. Increasing the temperature shifts the thermodynamic equilibrium towards hydrogen at the expense of methane. However, large amounts (~ 50%) of alkanes are still favored up to temperatures of 400 °C [2]. Hydrogen and alkanes are formed through different pathways (section 1.3) and therefore catalysts are required to control the reforming reaction kinetically to obtain higher hydrogen yields. The target of this study is the development of such a catalyst for the production of hydrogen from bio/organic feeds, taking into account commercially relevant parameters such as feed concentrations and residence times. The initial study described in this chapter is focused on the reforming of the model compound, ethylene glycol, due to the reasons discussed in section 1.3. Catalyst design should take into account (i) high gasification rates, and (ii) minimization of alkane formation. Further, minimizing coke formation and catalyst deactivation is of importance for practical applications.

It was shown earlier in section 1.3, that catalysts for APR should be active for C-C bond cleavage in order to be able to decompose the organic molecules and they should further enhance the Water Gas Shift (WGS) reaction (Eq. 1) to maximize hydrogen yields. Methanation (Eq. 2) and Fischer Tropsch (Eq. 3) are undesired side reactions, as they consume the desired product, H_2. In order to suppress these reactions, catalysts should not be active for C-O bond breaking [3]. Lower alkane selectivities are therefore expected for catalysts with low affinity towards C-O bond dissociation.

Water-Gas-Shift:	$CO + H_2O \rightarrow CO_2 + H_2$	Eq. 1
Methanation:	$CO_x + (2+x)\ H_2 \rightarrow CH_4 + xH_2O$	Eq. 2
Fischer-Tropsch:	$CO + 2H_2 \rightarrow -CH_2- + H_2O$	Eq. 3

In 2003, Davda *et al.* [3] reported the relative activities of different metals for C-C, C-O bond dissociation, and for WGS reaction. They reported high C-C bond breaking activities for Ir, Ru and Ni. Therefore, these metals might be promising catalysts for breaking down oxygenates. Adsorbed oxygenate fractions on the catalyst surface resulting from C-C bond dissociation undergo dehydrogenation, yielding H_2 and CO [3]. Follow-up reactions, such as methanation and WGS, strongly control the final hydrogen yield. Ir showed very low methanation activity but in contrast to Ru and Ni, almost no WGS activity was reported. Furthermore, Ru and Ni were reported to have high activities for methane formation [3].

Many APR studies with Ru-based catalysts confirm the tendency of Ru to form alkanes. For instance, silica supported Ru catalyst was reported to be an active catalyst for APR of ethylene glycol but the gas formed was very rich in methane [4]. Byrd *et al.* [5] reported complete conversion of a 40 wt% glycerol solution during APR (750 - 800°C) over Ru/Al_2O_3 catalyst, but also observed the formation of considerable amounts of undesired methane. Kersten *et al.* [6] observed full conversion for reforming of a 17 wt% glucose solution to methane rich product gas at 600 °C using a 3 wt% Ru/TiO_2 catalyst. The high tendency of Ru to form alkanes makes it an unsuitable catalyst candidate to achieve high H_2 yields during APR of ethylene glycol.

Ni based catalysts have been explored frequently for gasification of oxygenates (*e.g.* glucose, phenol, methanol) under supercritical water conditions [7-10]. Ni based catalysts are generally active for gasification, but often tend to deactivate due to sintering and or coke formation [7-8]. Selectivities to hydrogen and methane vary significantly in the studies reported and the choice of support seems to have a strong influence [11]. An unsupported Ni metal wire gave high hydrogen selectivities when methanol was used as reactant [8]. Ni is relatively cheap compared to other (noble) metals and is therefore also a very interesting option from an economical viewpoint.

Another very promising catalytically active metal for APR is Pt. Stable catalytic performance with high activity and selectivity towards hydrogen has been reported over Pt/γ-Al_2O_3 catalyst for APR of different model oxygenates, namely methanol, ethylene glycol, glycerol and sorbitol [12-14]. Based on the activity for C-C bond breaking [3], Pt is not expected to be a good candidate to decompose oxygenates during APR. However, Pt does show a relatively high activity for WGS [3], indicating that the rate determining step in APR

of ethylene glycol might be related to the water-gas-shift reaction. Furthermore, methanation is reported to be very low on Pt [3].

Based on the information available for APR, and discussed above in terms of H_2/CH_4 selectivities and maximizing hydrogen yields, three monometallic catalyst systems Ir, Ni and Pt were chosen for the reforming of the model compound ethylene glycol in supercritical water. Alumina is chosen as catalyst support material due to (i) its relatively high thermo-physical stability and (ii) its ability to activate water, which is required for the bi-functional APR mechanism. Development of a bimetallic Pt-Ni catalyst for the efficient production of hydrogen from ethylene glycol is discussed.

3.2 Experimental

3.2.1 Catalyst preparation and characterization

Alumina supported Ir, Ni, Pt and Pt-Ni (molar ratio 1:1) catalysts were prepared as described in section 2.2.1. Fresh and used catalysts were characterized by XRF, BET, CO-chemisorption, XRD, TGA-MS, TPR and TEM imaging. These techniques are further described in detail in section 2.3.

3.2.2 Catalytic testing

The supercritical water reformer, analysis techniques and definitions used for this study are described in detail in Chapter 2. A 2 mL. min^{-1} flow of ethylene glycol (≥99% Sigma Aldrich) solution was preheated to 450°C at a pressure of 250 bar. After preheating, the solution entered the reactor in which 1.0 g of catalyst was placed. The reaction was performed at 450 °C and 250 bars. Under these conditions water is in the supercritical regime. Weight hourly space velocities of EG for reforming of 5 and 15 wt% ethylene glycol solutions were 5.9 and 17.8 h^{-1}, respectively. The residence time in the catalytic bed was 1.3 seconds [density of water at reaction conditions (here: T=450 °C and P=250 bars) is 109 kg/m^3].

3.3 Results and discussion

3.3.1 Catalyst characterization results

Characteristics of the catalysts studied are given in Table 3.1. All fresh catalysts had surface areas of ±200 m^2/g, similar to that for the alumina used. All catalysts showed a decrease in surface areas to ±20 m^2/g when subjected to supercritical water. This decrease was found to happen during the initial stage of the reaction (within the first 15 minutes) and is caused by the collapse of mesopores (± 50-200 Å) as can be seen from the pore volume distribution plots of the fresh and used 1.15-0.35 wt% Pt-Ni/γ-Al_2O_3 catalysts (Figure 3.1 and 3.2).

The collapse of pores (and the consequent decrease in surface area) can be attributed to a phase change of the γ-Al_2O_3 to boehmite $AlO(OH)_x$ as can be seen from the XRD patterns of the fresh and used 1.15-0.35 wt% Pt-Ni/γ-Al_2O_3 catalysts as shown in Figure 3.3. For the fresh catalyst, diffraction peaks located at 2θ = 45.8° and 66.8° are attributed to γ-Al_2O_3. Multiple peaks emerged for the catalyst after exposure to supercritical water and these correspond to the dominant phase of Boehmite, indicating hydrolysis of the support. Weaker reflections of alpha phase were also noticed. Similar observations regarding the phase change of γ-Al_2O_3 in hot compressed water were reported by many authors [5, 15-17]. The phase change occurred during start-up of the reaction and therefore the reactions were performed in the presence of catalysts after stabilization of alumina. It was reported earlier by Wawrzetz *et al.* [18] that the phase change from γ-Al_2O_3 to Boehmite did not cause blocking or deactivation of the catalytic sites.

Table 3.1: Catalyst characterization results for fresh catalysts.

Catalyst supported on γ-alumina	Loading (%)	Dispersion (%)*	Average Particle Size (nm)	Surface area (m^2/g)
Ni	1.31	1	78	196
Ir	1.41	15	7.2	195
Pt	1.45	68	1.6	196
Pt	0.60	85	1.3	199
Pt	0.30	87	1.2	197
Pt-Ni	1.17-0.33	n.d.	n.d.	198
Pt-Ni	0.60-0.20	n.d.	n.d.	197
Pt-Ni	0.30-0.10	n.d.	n.d.	200

* Determined by CO chemisorption; n.d – Not determined

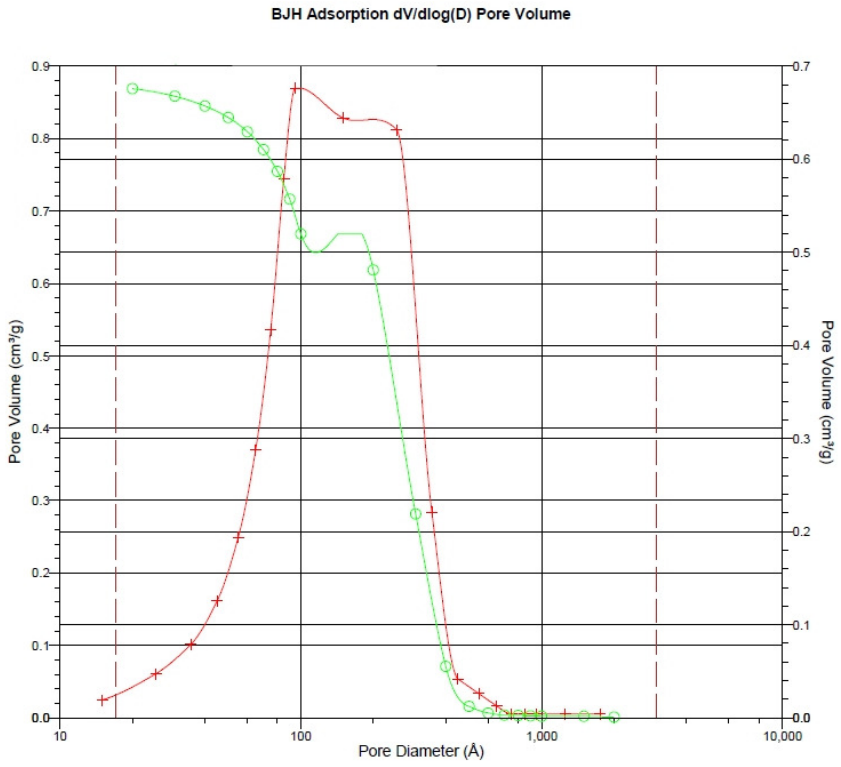

Figure 3.1: Pore size distribution (red line) and cumulative pore volume (green line) of fresh Pt/Al_2O_3 catalyst.

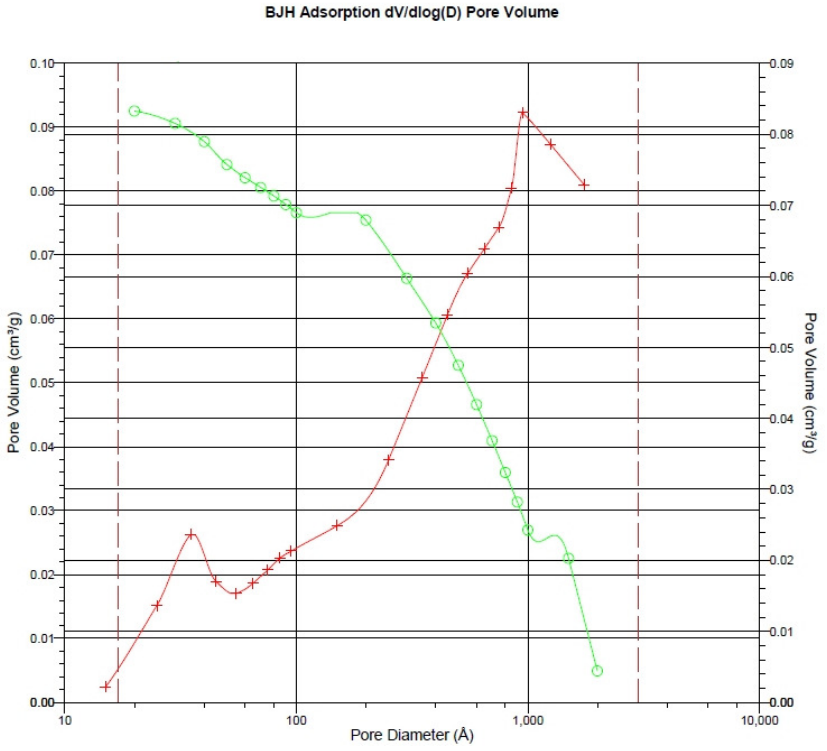

Figure 3.2: Pore size distribution (red line) and cumulative pore volume (green line) of Pt/Al_2O_3 catalyst that was subjected to supercritical water (450 °C and 250 bar).

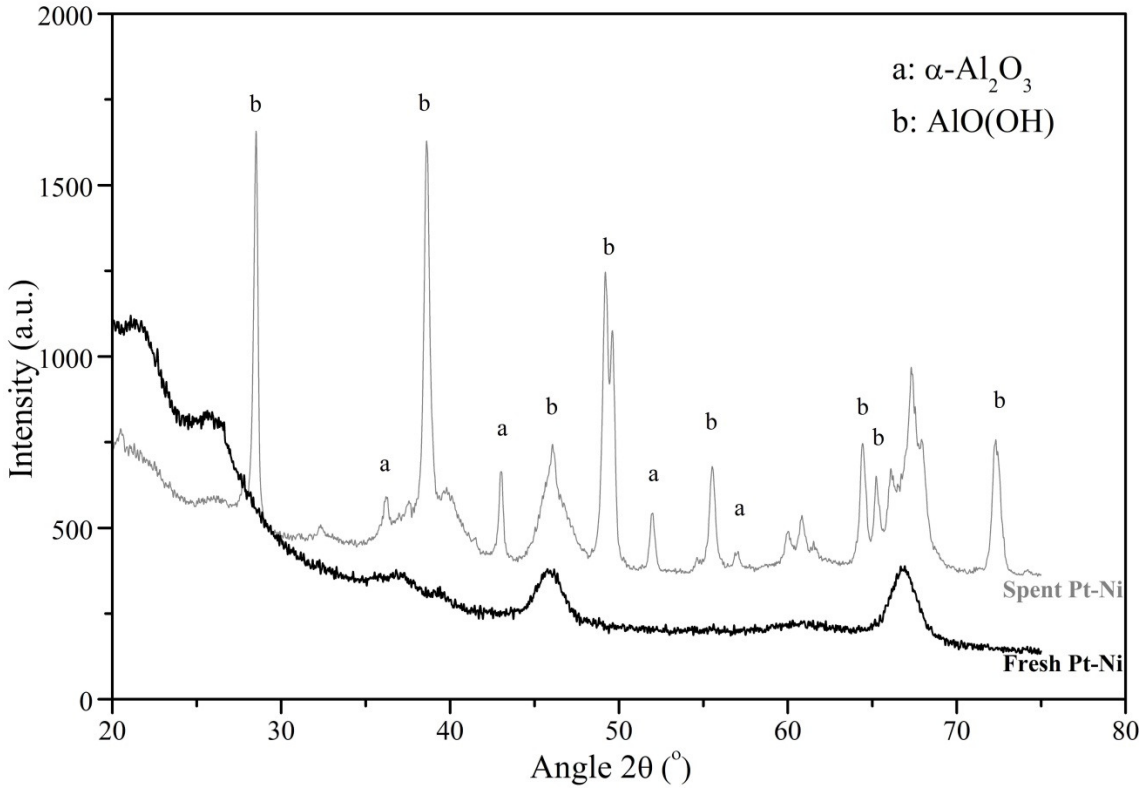

Figure 3.3: XRD spectra of fresh Pt-Ni (Pt-1.15% and Ni-0.35%) bimetallic catalyst (below) vs. spent Pt-Ni catalyst.

Metal dispersions measured by CO chemisorption (Table 3.1) were low for the Ir and Ni catalysts implying large particle sizes of 7.2 nm and 78 nm, respectively. TPR experiment showed that the most dominant Ni species in Ni/γ-Al_2O_3 was $NiAl_2O_4$. A temperature of around 800-1000 °C was necessary to reduce this species under hydrogen at atmospheric pressure. These high reduction temperatures can be the reason for the low Ni dispersions measured, as the $NiAl_2O_4$ could not be reduced under the conditions used for the chemisorption experiment.

The monometallic Pt catalysts showed comparatively higher metal dispersions measured by CO chemisorption (Table 3.1). A lower dispersion was found for the highest Pt loading, indicating larger particles (±1.5 nm) for the highest Pt loading. A TEM image of the fresh 1.5 wt% Pt/Al_2O_3 catalyst is shown in Figure 3.4a. Dark spots with a sub-nanometer diameter can be seen and EDX confirmed the presence of Pt in these regions. These dark spots were not visible in areas were Pt was not indicated by EDX and are therefore attributed to the mass induced contrast between Pt and Alumina.

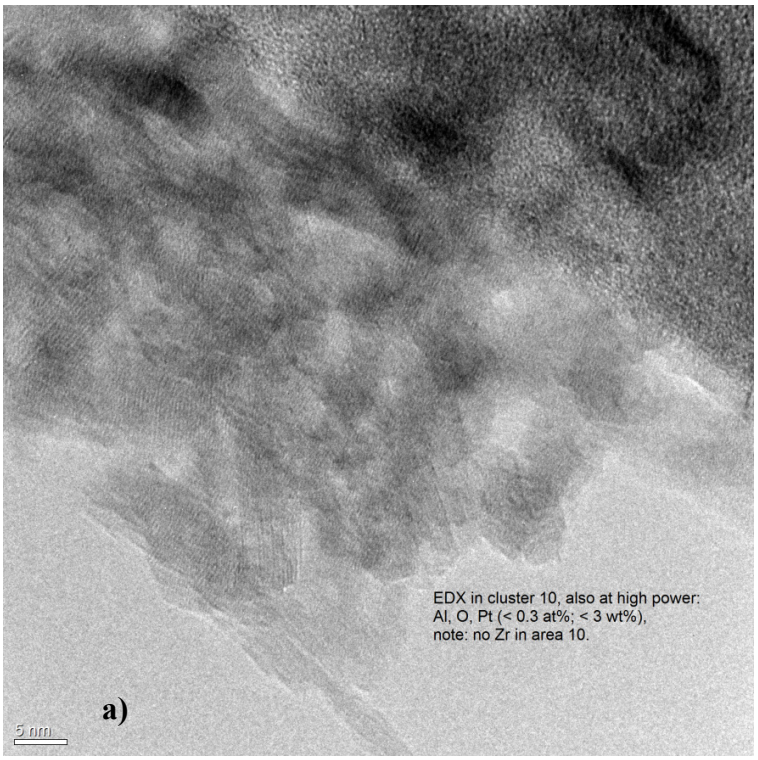

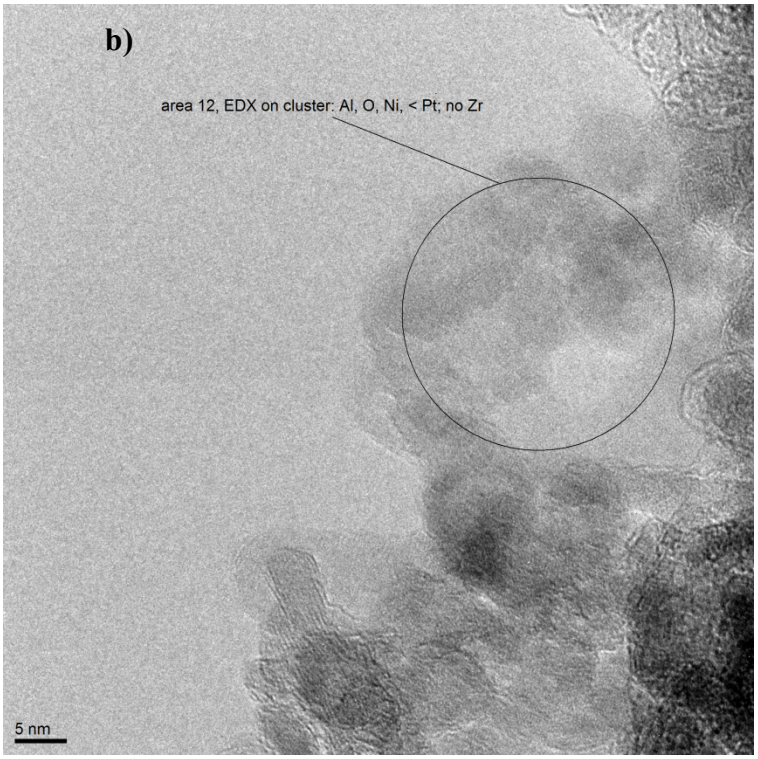

Figure 3.4: TEM images (5 nm scale) of fresh alumina supported **a**) 1.5 wt% Pt/γ-Al_2O_3 and **b)** 1.15-0.35 wt% Pt-Ni catalysts.

In the case of bimetallic catalysts, determining dispersions separately for Pt and Ni is not straight forward and were not determined. A TEM image of the fresh 1.5 wt% Pt-Ni containing catalyst is shown in Figure 3.4B. Again dark spots were observed on the alumina support. The size of these spots was also sub-nanometer in diameter and is also attributed to Pt or Pt-Ni particles. The presence of only Pt was observed in some areas but Ni was always found together with Pt and shows that Ni deposits in the neighborhood of Pt, indicating interactions between Pt and Ni. TEM imaging indicates that the metal particles (Pt and Pt-Ni) on both catalysts are sub-nanometer in diameter.

The nature of the interactions between Pt and Ni on the bimetallic Pt-Ni catalysts was studied by TPR. Mutual influences between Pt and Ni can vary from:

1. no interactions, *Pt and Ni are not situated near each other*
2. weak interactions, *Pt and Ni are close together*
3. strong interaction, *Pt-Ni alloy formation*

The TPR profiles of 0.3 wt% Pt/Al_2O_3, 0.3 wt% Ni/Al_2O_3 and 0.3-0.1 wt% $Pt\text{-}Ni/Al_2O_3$ are shown in Figure 3.5. Pt/Al_2O_3 showed only one reduction peak at 227°C which can be attributed to the reduction of $Pt^{IV}(OH)_xCl_y$ to metallic Pt [19]. Ni/Al_2O_3 showed a large reduction peak between 800 °C and 1000 °C which can be attributed to $NiAl_2O_4$ [20]. In the case of the Pt-Ni catalyst, reduction temperatures of 235, 326, 405, 516 and 809°C were observed. The reduction peak at 809°C is attributed to $NiAl_2O_4$ [20], indicating that some of the added Ni was inactive during the reaction due to strong interaction with the alumina support. Reduction peaks at 405 and 516°C indicate large and smaller NiO particles, respectively [21]. The Pt reduction is shifted to a higher temperature of 235°C when Ni was present on the catalyst. This shift is assigned to interactions between Pt and Ni. However, the strength of this interaction is unknown. Also a reduction peak around 326°C was observed and this is assigned to Ni that is strongly interacting with Pt as Pt is reported to lower the reduction temperature of NiO by facilitating hydrogen which is necessary for the reduction of Ni [22]. Based on the TPR results, it can be concluded that various degrees of interaction between Pt and Ni exist on the Pt-Ni catalysts, varying from no interaction to strong interaction.

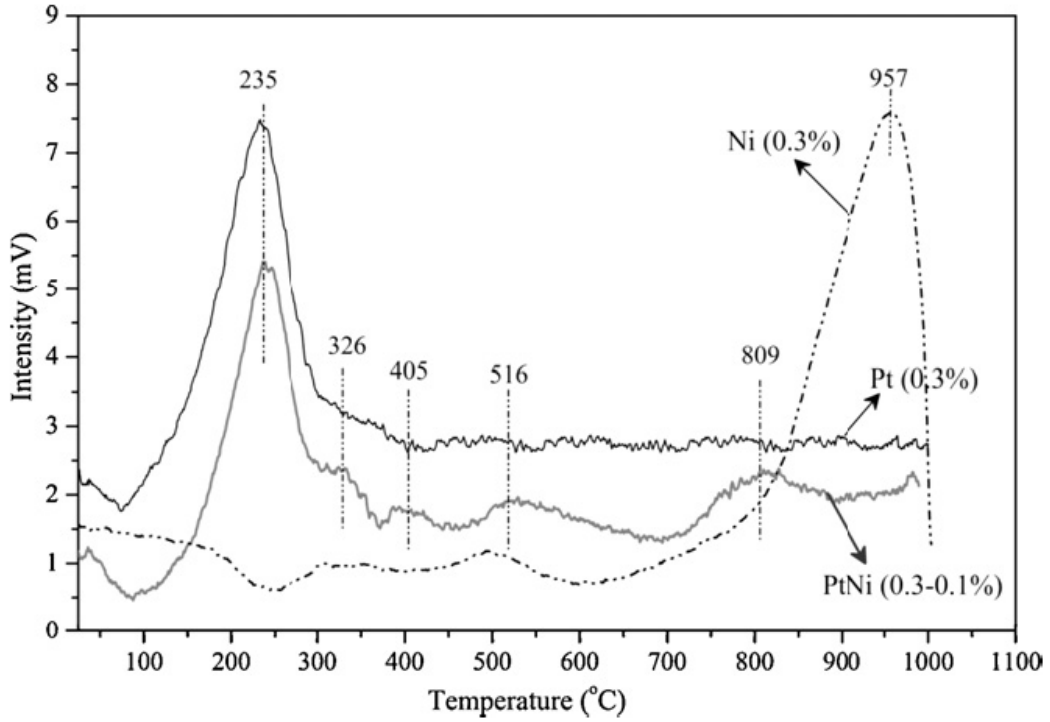

Figure 3.5: TPR profiles of fresh alumina supported Pt(0.3 wt%), Ni(0.3 wt%) and Pt-Ni(0.3–0.1 wt%) catalysts.

3.3.2 Catalytic reforming results

The thermodynamic gas composition equilibrium [23] for different ethylene glycol feed concentrations (5 - 30 wt%) at 450 °C and 250 bar is shown in Figure 3.6. Under the reaction conditions used in this study, CH_4 is the favored product with a selectivity of 54% for 5 wt% EG and increased slightly at the expense of hydrogen with increasing feed concentration.

Results of the catalytic experiments with 5 wt% EG for the alumina supported Ni, Ir, and Pt catalysts, are shown in Table 3.2. Carbon to gas conversion is taken as measure for the gasification activity. Remaining carbon from the feed is either in coke or in the liquid product (EG, plus other carbon containing species). No significant gasification activity for EG was observed in a blank experiment (no catalyst) or with the alumina support only. For the catalytic experiments, it can be seen from Table 3.2 that the sum of carbon to gas conversion and carbon remaining in liquid indicate good carbon balances for the Ni and Pt –based catalyst (102% and 106%, respectively). However, the carbon balance of the Ir-based catalyst was only accounted for ~70%. The missing ±30% was likely carbon deposited on the catalyst as coke.

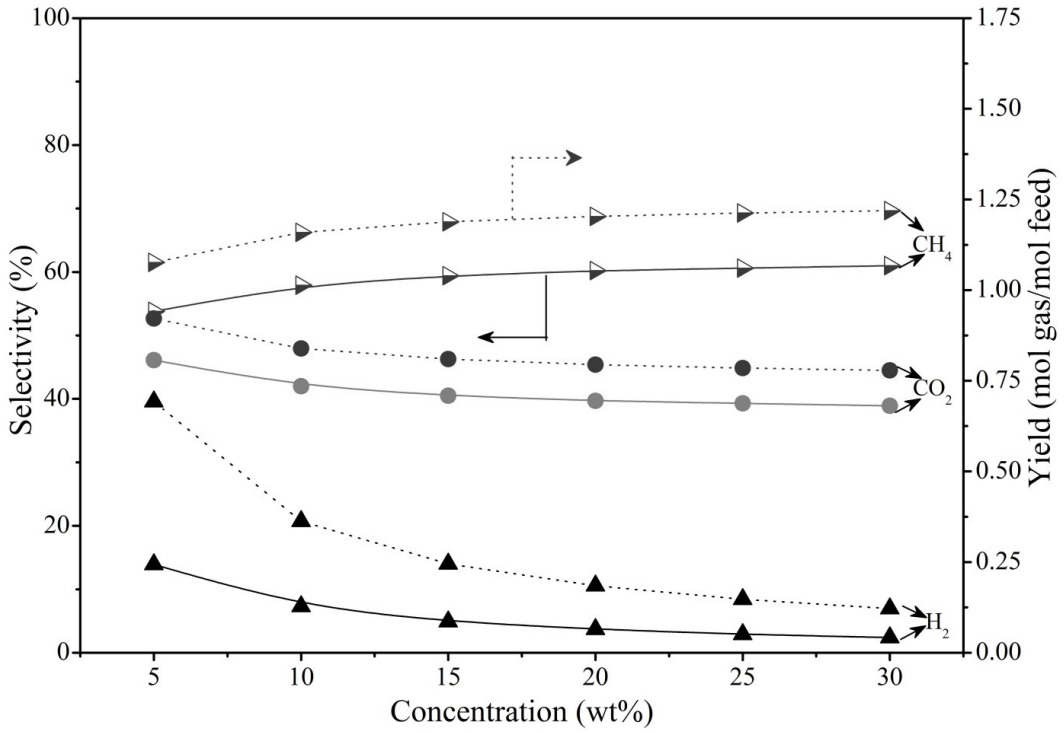

Figure 3.6: Thermodynamic chemical equilibrium composition for different feed concentrations ranging from 5 – 30 wt% of ethylene glycol reformed in supercritical water at 450 °C and 250 bar (symbols with solid trend lines represent selectivity and dotted trend lines represent yield).

The catalytic reforming experiments show that at comparable metal loadings Pt was the most active. The Ni based catalyst showed the lowest carbon to gas conversion of 6%. Ir catalyst gave a conversion of 27%. Pt catalyst showed near complete conversion of EG to gas phase products. These results are in line with Davda *et al.* [14], who also found Pt to be more active than Ir.

In the case of Ni catalyst, we have used a low loading of 1.5 wt% for comparison with the other catalysts in the study. Other studies report usually much higher Ni loadings (~20 wt%). These catalysts were initially very active but underwent rapid catalyst deactivation. It is therefore difficult to compare our results with these studies [7, 14]. Furthermore, NiO clusters formed during calcination can undergo strong interaction with the alumina support, leading to the formation of stable $NiAl_2O_4$. Steam reforming and water gas shift activity is related to the presence of reduced Ni metal particles. The $NiAl_2O_4$ phase is stable under most reforming conditions and does not contribute to catalyst activity. The previously reported TPR experiment showed that the most dominant Ni species on the support was $NiAl_2O_4$. Since the Ni concentration is low in the studied catalyst, this is the only species to be expected.

Catalysts containing larger amounts of Ni usually show both NiO and $NiAl_2O_4$ phases [20]. A temperature in the range of 800-1000°C was necessary to reduce $NiAl_2O_4$ under hydrogen. Thus, the low activity of the studied Ni catalyst compared to Ir and Pt catalysts is due to the presence of Ni as inactive $NiAl_2O_4$.

Table 3.2: Experimental data for the reforming of 5 wt% ethylene glycol (WHSV 5.9 h^{-1}) at 450°C and 250 bar using 1.5 wt% Ni, Ir and Pt supported on γ-alumina.

	1.5 wt% Ni	**1.5 wt% Ir**	**1.5 wt% Pt**
Carbon to gas (%)	6	27	100
Carbon in liquid (%)	96	45	6
Selectivity (%)			
H_2	26	35	87
CO_2	31	30	94
CO	55	40	1
CH_4	1	24	4
C2+	13	6	1
Yield (mol gas / mol feed)			
H_2	0.08	0.61	4.24
CO_2	0.04	0.20	1.78
CO	0.06	0.29	0.01
CH_4	0.00	0.18	0.07
C2+	0.00	0.01	0.01

N.B. C2+ gases include C_2H_4, C_2H_6, C_3H_6 and C_3H_8.

Table 3.2 also gives selectivities to the various gas products observed. The target in this study is to achieve a high selectivity towards hydrogen by (i) maximizing water gas shift and (ii) minimizing methane formation. Both the Ni and Pt catalysts showed low selectivities for methane formation (<4%). Low methanation activity (CH_4 <4%) and high WGS activity (CO/CO_2 = 0.01) (see Table 3.2) resulted in the high selectivity for hydrogen (87%) as observed for the Pt catalyst. From Table 3.1 it is seen that metal dispersions for Pt is about 4 times higher than Ir and this is also reflected in EG conversion. This implies similar intrinsic activities (TOF) for both Ir and Pt for EG gasification. However, Ir catalyst showed the highest selectivity towards methane (24%) and also showed high amounts of carbonaceous deposits. Based on the results so far Pt/Al_2O_3 showed the best activity, highest selectivity to H_2, -and minimal methane formation.

Optimizing the Pt loading without compromising the EG conversion is interesting from an environmental point of view and from the point of cost of Pt. Table 3.3 shows the result of the influence of Pt loading on the catalyst performance for the reforming of 5 wt% EG. Characterization results of these catalysts are summarized in Table 3.1. It can be seen from Table 3.3 that even the use of the catalyst with lowest Pt loading (0.3 wt%) resulted in near complete conversion of EG. Additional experiments with higher EG concentrations (15 wt%) and at higher space velocities (17.8 h^{-1}) were carried out. The results of these experiments are given in Table 3.4. As expected, a lower overall conversion for the reforming of 15 wt% EG solution to carbon containing gaseous products was obtained, under comparable reaction conditions. Interestingly, EG conversion levels were found to be in the same range (42 – 48 mol%) for all the three Pt catalysts.

Table 3.3: Experimental data for the reforming of 5 wt% ethylene glycol (WHSV 5.9 h^{-1}) at 450°C and 250 bar using 0.3, 0.6 and 1.5 wt% Pt supported on γ-alumina.

	0.3wt% Pt	**0.6wt% Pt**	**1.5wt% Pt**
Carbon to gas (%)	95	99	100
Carbon in liquid (%)	4	2	6
Selectivity (%)			
H_2	76	85	87
CO_2	84	87	94
CO	1	1	1
Alkanes (C_xH_y)	15	12	5

Table 3.4: Experimental data for the reforming of 15 wt% ethylene glycol (WHSV 17.8 h^{-1}) at 450°C and 250 bar using 0.3, 0.6 and 1.5 wt% Pt supported on γ-alumina.

	0.3wt% Pt	**0.6wt% Pt**	**1.5wt% Pt**
Carbon to gas (%)	48	48	42
Carbon in liquid (%)	58	59	61
Selectivity (%)			
H_2	42	51	80
CO_2	50	60	79
CO	20	14	14
Alkanes (C_xH_y)	30	26	7

Hydrogen selectivities were lower in the case of experiments with higher EG concentrations (15 wt%). Davda *et al.* [3-4, 14] also reported that a shift towards CO and CH_4 occurs with increasing ethylene glycol concentrations. Lower oxygenate concentrations in the feed favor the formation of higher yields of hydrogen, while at higher concentrations, increased levels of CO_x and H_2 cause consecutive (hydrogen consuming) methane formation. Increased methane formation was observed for all the three Pt catalysts, but was more pronounced for the catalysts with lowest Pt loading. During 15 wt% EG reforming, the two catalysts with lowest Pt loading (0.3 and 0.6 wt%) showed hydrogen selectivities that were almost half of that observed for the experiments with lower EG (5 wt%) concentration. Interestingly, in the case of the 1.5 wt% Pt catalyst, the selectivity towards methane and hydrogen changes only marginally in favor of methane during reforming of higher EG concentration feeds.

The high CO selectivities observed during reforming of high concentrated EG feeds, suggest that hydrogen yields can be further increased by increasing WGS activity of the catalyst. The HPLC analysis of the liquid reactor effluent from the reforming reaction with 0.3 wt% Pt catalyst, indicated the presence of ethylene glycol and other intermediate compounds such as aldehydes, carboxylic acids and alcohols.

The intrinsic rates for reforming and hydrogen formation, in the case of experiments with 15 wt% EG, were calculated for the three monometallic Pt catalysts and are summarized in Table 3.5. Apparent TOF for EG reforming was found to be more than four times higher for the catalyst with 0.3 wt% Pt loading, compared to the catalyst with 1.5 wt% Pt loading. The higher activity (TOF) of the former can be a consequence of (i) the Pt particle structure effect (smaller particles are more active) or (ii) the higher Pt dispersion brings more Pt sites in the vicinity of the support as required in bi-functional catalysts, as explained below. It has been reported earlier [11] that the boundary between alumina and Pt is thought to be the active catalytic area for reforming since alumina also plays a role in the reforming reaction. Reforming and WGS reactions involve oxidation with oxygen from water molecules. This mechanism should involve splitting/activation of water molecules [24]. Pt is normally inert for water activation under typical gasification conditions [25]. On the other hand, alumina is able to activate water by forming hydroxyl groups, which are necessary for the reforming reactions. Therefore reactive Pt sites should be in close proximity of alumina. Decreasing the particle size will increase the amount of Pt sites neighboring alumina and therefore increasing the overall reforming activity [24].

Table 3.5: TOF's for the reforming of 15 wt% ethylene glycol (WHSV 17.8 h^{-1}) and hydrogen production at 450°C and 250 bar using 0.3, 0.6 and 1.5 wt% Pt supported on γ-alumina.

Pt Loading (%)	Dispersion (%)	Average Particle Size (nm)	TOF EG 15wt% EG (min^{-1})	TOF H_2 15 wt% EG (min^{-1})
0.30	87	1.2	173	359
0.60	85	1.3	87	219
1.45	68	1.6	41	163

However, the increase in EG TOF is not proportional with the increase in H_2 TOF, (4 *vs* 2). Results in Table 3.5 seem to indicate that lower Pt loadings (with smaller Pt particles) tend to favor methane formation. Lehnert *et al.* [16] showed that aqueous phase reforming of glycerol was structure sensitive over Pt/Al_2O_3 catalysts. They observed that the selectivity towards CO and CH_4 increased with decreasing Pt particle size. They suggested that smaller particle sizes have more steps in the structure and these favor CO and CH_4 formation. C-C cleavage is suggested to occur on the face atoms while C-O cleavage is favored on steps and edges [16]. Thus, in full agreement with the former, smaller Pt particle size can be responsible for the increase in methane formation.

Conditions during APR in hot compressed water are corrosive and aggressive. Catalyst deactivation is a serious issue and lifetimes can be short due to leaching, sintering (Ostwald ripening) of metal particles and coking. The stability of the catalyst is therefore very critical for practical applications. The EG conversions to gas phase products and selectivities for the three monometallic Pt catalysts during a 9 h life test are shown in Table 3.6 for the reforming of 15 wt% EG. The Pt catalyst with the highest Pt loading (1.5 wt%) showed stable performances with respect to activity (42%) and selectivities (H_2 selectivity of 80%) during 9 h time-on-stream. Lower Pt loadings were less stable. The catalyst with lowest Pt loading (0.3 wt%) showed an initial conversion of 48%. However, the conversion gradually dropped to 31% after 9 h time-on-stream. In parallel to the deactivation, hydrogen selectivity improved at the expense of lower CH_4 formation.

One reason for deactivation can be the loss of metal from the catalyst by leaching. XRF analysis of the liquid products showed, however, no presence of metals. In addition, metal loadings for the fresh and used catalysts were found to be the same, verifying that leaching of Pt and alumina support during the reaction was insignificant.

Table 3.6: Stabilities of Pt catalysts for the reforming of 15 wt% ethylene glycol (WHSV 17.8 h^{-1}) at 450°C and 250 bar using 0.3, 0.6 and 1.5 wt% Pt supported on γ-alumina.

Pt loading (%)	Time (h)	Conversion (%)	Selectivity (%)				
			H_2	CO_2	CO	CH_4	C+
0.3	0.5	48	42	50	20	22	8
	9.0	31	72	57	36	5	3
0.6	0.5	48	51	60	14	19	7
	9.0	36	73	66	22	8	4
1.5	0.5	42	80	79	14	4	3
	9.0	42	82	80	15	2	3

Catalyst deactivation by coking was studied by attempting regeneration of a used 0.3 wt% Pt/Al_2O_3 catalyst by burning off any possible coke deposits. The catalyst was taken out of the reactor after being used for 9 h for the reforming of 15 wt% EG. The used catalyst was re-oxidized in air at 500 °C for 5 h to burn off any coke species. After this treatment the catalyst was again used for the reforming of 15 wt% EG and no changes in activity or selectivities were observed compared to the properties before the regeneration attempt. This indicates that deactivation was not induced by coking. Furthermore, presence of coke on the catalysts was studied by TGA-MS. Spent Pt catalysts used for the reforming of 15 wt% EG all showed 12 ± 1 % weight loss at 513 ± 3°C. The MS results showed that the weight loss was due to the release of H_2O. For all catalysts, release of comparable quantities of water was observed. H_2O is formed during dehydration *via* recombination of hydroxyl groups on the alumina support. Presence of coke on the catalysts was also not indicated by the TGA-MS technique.

An indication for deactivation can be inferred from the selectivity data presented in Table 3.6. With deactivation the selectivity towards hydrogen improved and methane formation decreased. As discussed earlier [16], the Pt particle size is believed to influence the reforming activity and selectivity towards hydrogen and methane. Larger Pt particles tend to favor the formation of hydrogen, but are less active for EG reforming in contrast to smaller Pt particles that are very active for EG reforming but favor the formation of methane. In line with these arguments, we suggest that the dominant deactivation mechanism is related to the increase of the average size of active Pt particles during the reaction. Pt particle growth during the reaction is a likely cause of deactivation. Initially, the catalyst showed a high activity and a higher selectivity towards methane. During the reaction the average size of active Pt

particles are believed to grow, resulting in a lower reforming activity and increased selectivity towards H_2. We can only suggest that the relatively large Pt particle size in the catalyst with the highest Pt loading is the reason for the stability with time. The deactivation mechanism will be studied in more detail in Chapter 4.

From the results discussed so far we have shown that full conversion of a 5 wt% ethylene glycol solution to gas phase products could be achieved with high selectivity towards hydrogen using alumina supported Pt catalysts. For higher EG concentration (15 wt%) feeds, loss of hydrogen was observed at the expense of more methane formation. Using lower Pt loadings showed a negative effect on the hydrogen selectivity for the reforming of 15 wt% ethylene glycol solution. In addition the catalyst with lower Pt loadings deactivated during the reaction. The 1.5 wt% Pt/Al_2O_3 showed to be the best catalyst in terms of stability and hydrogen selectivity for the reforming of a 15 wt% ethylene glycol solution. However, the intrinsic activity of the Pt active sites was still low.

Reforming of solutions with higher EG concentrations to give high hydrogen selectivities are commercially interesting but this requires modification of the Pt catalysts as seen above. In case of the catalysts with lower Pt loadings the hydrogen selectivity and stability should be addressed. For the catalyst with the highest Pt loading the intrinsic activity should be improved. Ni/Al_2O_3 was not a very interesting catalyst with respect to EG conversions and H_2 yields, although Ni/Al_2O_3 showed the lowest CH_4 formation rate. Thus, Ni addition to monometallic Pt catalysts can be expected to improve hydrogen yields. Huber *et al.* [13] already reported that addition of Ni to a Pt/Al_2O_3 catalyst significantly increased the H_2 selectivity by suppressing CH_4 formation and at the same time also enhanced EG reforming activity. Furthermore, Ni is also an active metal for steam reforming and for the water gas shift reaction (necessary to enhance hydrogen yields) and is a cheaper substitute for Pt [26, 27]. Possible synergetic effects of Ni addition to Pt catalysts were investigated for the reforming of ethylene glycol in supercritical water.

Details of the Pt catalysts modified with Ni are given in Table 3.1. The conversions and selectivities for the three Pt-Ni bi-metallic catalysts are shown in Table 3.7 for the reforming of 15 wt% ethylene glycol. Addition of Ni induced a significant improvement on the performance of the catalyst. All Pt-Ni catalysts showed stable conversions and selectivities for the reforming of 15 wt% EG during 9 h time-on-stream. In contrast to the 0.3

wt% Pt catalyst (Table 3.6) no deactivation was observed with the 0.3-0.1 wt% Pt-Ni catalyst during 9 h time-on-stream.

Table 3.7: Stabilities of Pt-Ni catalysts for the reforming of 15 wt% ethylene glycol (WHSV 17.8 h^{-1}) at 450°C and 250 bar using 0.3, 0.6 and 1.5 wt% Pt supported on γ-alumina.

Catalyst loading (%)	Time (h)	Conversion (%)	Selectivity (%)				
			H_2	CO_2	CO	CH_4	C+
0.3 - 0.1 Pt-Ni	0.5	50	77	77	18	4	1
	9.0	50	79	78	17	3	1
0.6 - 0.2 Pt-Ni	0.5	63	84	88	8	3	1
	9.0	60	85	88	8	3	1
1.15 - 0.35 Pt-Ni	0.5	79	83	91	3	4	1
	9.0	77	86	90	5	4	1

Another positive effect was observed on the hydrogen selectivity by addition of Ni. All tested Pt-Ni catalysts showed high H_2 selectivities with remarkably low CH_4 selectivities (maximum 3 - 4%). Addition of Ni to the catalyst with lowest Pt loading (0.3 - 0.1 Pt-Ni) almost doubled the hydrogen selectivity as a result of suppressing methane formation. In the case of Pt and Pt-Ni catalysts comparable initial concentrations of CO were observed. In case of Pt-Ni catalyst the CO_2 concentrations are much higher compared to the mono-metallic Pt catalyst. This is an indication that in presence of Ni, CO underwent a water gas shift reaction instead of a methanation reaction. The role of Ni in that case is to prevent hydrogenation of CO_x due to the intrinsic water gas shift activity of Ni.

Noble metals such as Pt are not capable of activating water for the water gas shift reaction and therefore require an active support material (in this case alumina) that provides the water activation. Ni however is capable of both activating water and CO in the water gas shift reaction without the need for a support. This occurs *via* NiO formation with water [28]. This intrinsic water gas shift activity of Ni can be the reason for the synergetic effect observed in bi-metallic Pt-Ni catalysts.

Remarkably, from Table 3.7, it can be seen that 1.15-0.35 wt% Pt-Ni catalyst is two times as active as the monometallic counterpart (1.5 wt% Pt) with very high selectivity towards hydrogen (86%). The catalyst is also very stable. Based on calculations, Huber *et al.* [13] speculated that Pt-Ni catalysts have lower heats of H_2 and CO adsorption compared to pure Pt catalysts, causing lower surface coverage of adsorbed H_2 and CO and therefore

minimize methanation of CO and allowing more sites to be accessible for the reactant to undergo reforming.

The carbon to gas conversion of 15 wt% EG and the hydrogen selectivities for the three monometallic Pt catalysts and three bi-metallic Pt-Ni catalysts with different metal loadings during a 9 h reaction time are shown in Figure 3.7. It is evident from the figure that the bi-metallic catalysts showed higher conversions and stable hydrogen selectivities than the monometallic catalysts. Furthermore, the higher activities of Pt-Ni catalysts show that the reactions with the mono-metallic Pt catalysts were not affected by mass diffusion limitations.

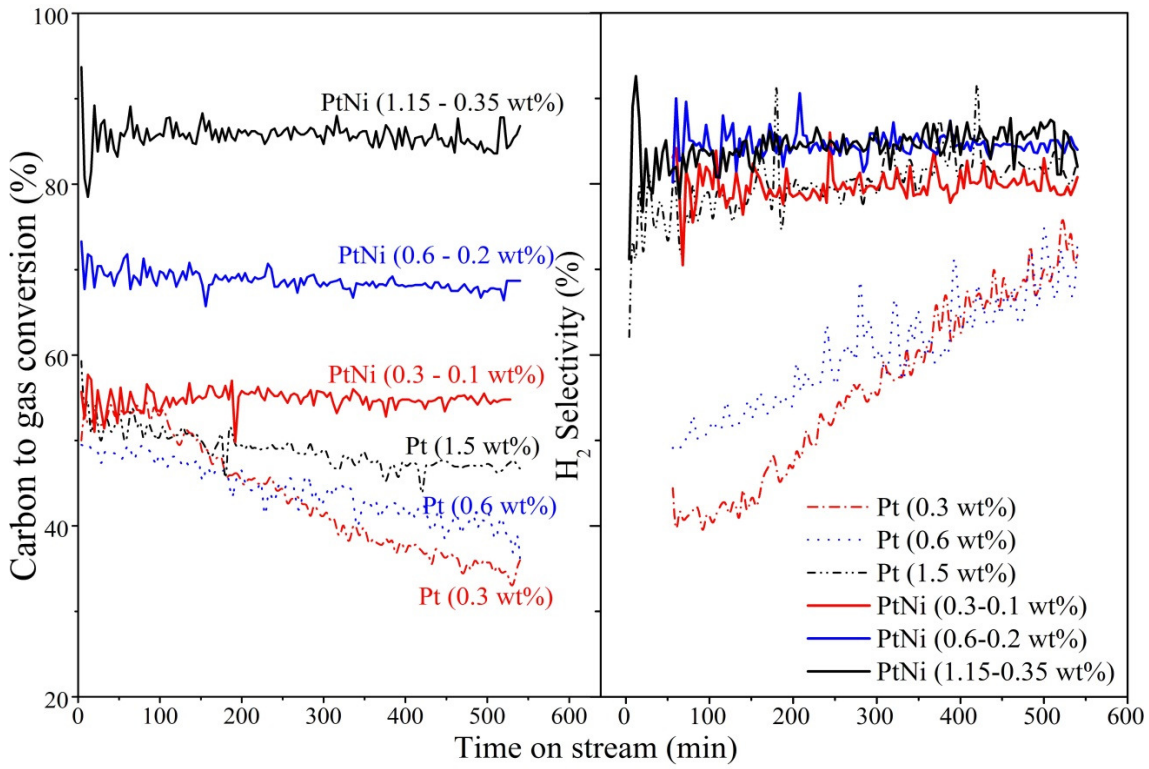

Figure 3.7: Activity and stability of monometallic Pt and bi-metallic Pt-Ni catalysts for the reforming of 15 wt% EG at 450˚C and 250 bar.

The influence of EG concentration ranging from 5 – 30 wt% on the product gas selectivity and gasification efficiency with Pt-Ni (Pt – 1.15 wt% and Ni – 0.35 wt%) is shown in Figure 3.8. The carbon to gas conversion decreased from 100 to 60% with increasing concentration from 5 to 30 wt%. This indicates that under the conditions studied maximum reforming capacity is reached. Decreasing the space velocity (either by increasing the amount of catalyst or decreasing the feed flow) should give complete conversion of high EG

concentrations. The H_2 and CO_2 selectivities decreased while the CO, CH_4 and C2+ selectivities increased with the EG concentration. However, with 30 wt% EG concentration, the carbon to gas conversions remained constant during 3 h experimental run but the CO selectivity increased marginally indicating a decrease in water gas shift activity (Figure 3.9).

The bimetallic Pt-Ni/Al_2O_3 catalyst studied here, shows extremely good activity, is stable and very selective to hydrogen. This catalyst shows promise for practical applications. The role of intermediates formed in the catalytic performance of the alumina supported Pt and Pt-Ni catalysts, is studied in the next chapter.

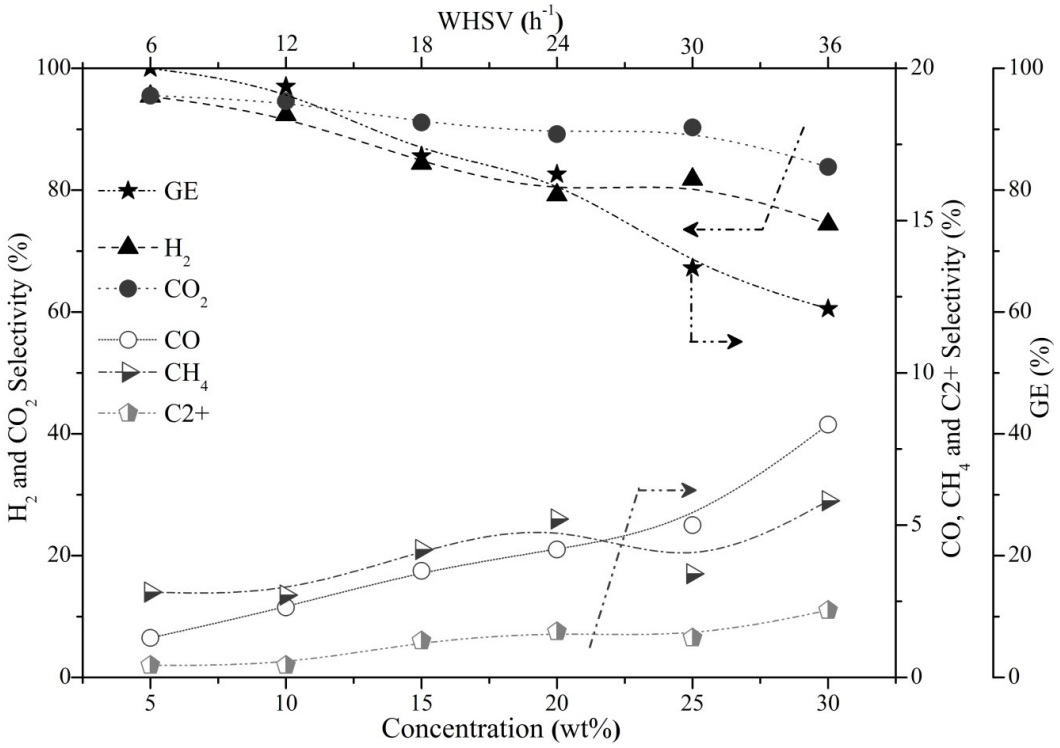

Figure 3.8: The influence of ethylene glycol concentration and its corresponding space velocities on the product gas selectivity and gasification efficiency in the presence of alumina supported Pt-Ni (1.15 wt% Pt, 0.35% Ni) catalyst at 450°C and 250 bar (arrows indicate axis direction).

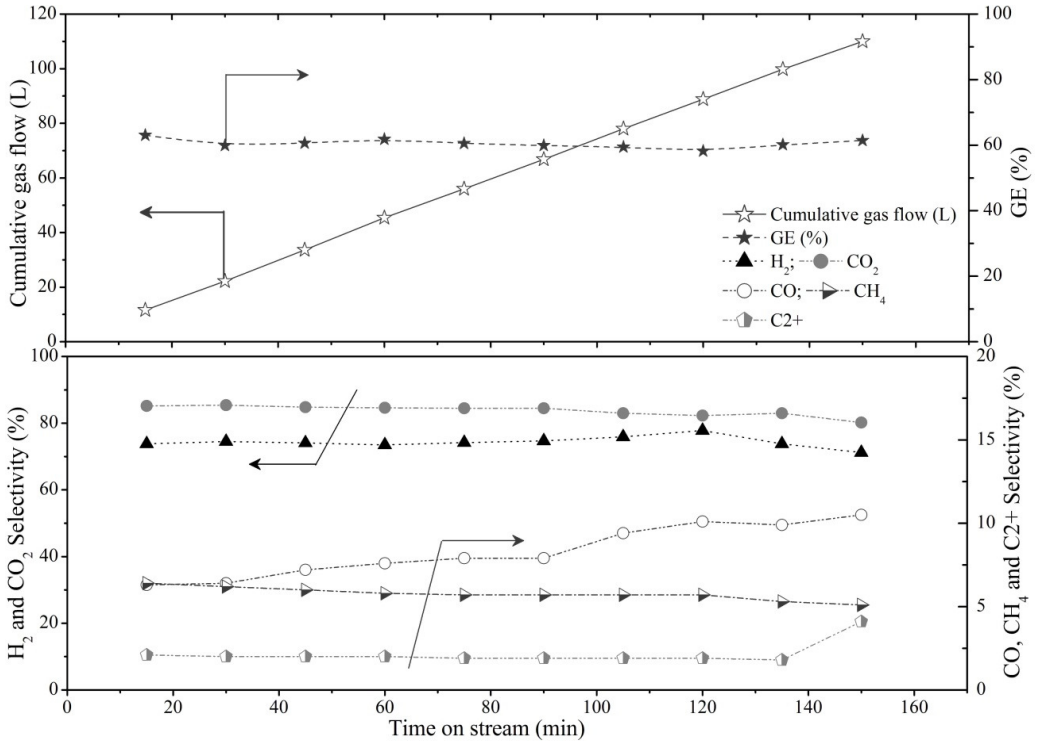

Figure 3.9: The gasification efficiency and the product gas selectivity as function of time, during reforming of 30 wt% ethylene glycol with alumina supported Pt-Ni (1.15 wt% Pt, 0.35% Ni) catalyst at 450°C and 250 bar (arrows point towards axis direction).

3.4 Conclusions

In this chapter, the catalytic properties of alumina supported Pt, Ir and Ni catalysts were studied for the reforming of ethylene glycol in supercritical water. Pt catalyst showed the highest hydrogen yields compared to Ir and Ni. The bi-functional reforming mechanism involved with APR over alumina supported Pt catalysts requires water activation. Water activation happens on the alumina support through the formation of hydroxyl groups. Smaller Pt particles were found to give higher intrinsic reforming activities due to a larger interfacial (metal/support) area, which enabled better interaction between the reforming fragments on the Pt and the hydroxyl groups on alumina support. On the other hand, smaller Pt particles were found to be responsible for lower hydrogen selectivities due to increased methane formation. Methane can be formed by either dehydration of EG, and/or by the hydrogenation of CO_x. A new developed Pt-Ni bimetallic catalyst shows enhanced hydrogen yields by suppressing methane formation. The new Pt-Ni catalyst also shows two times more activity compared to a monometallic Pt catalyst due to supposed lower CO coverage caused by the presence of Ni and an enhanced accessibility to Pt sites for reforming. Moreover, the addition of Ni also

enhanced catalyst lifetime and stable catalytic performances were observed for the reforming of ethylene glycol under supercritical water conditions.

References

[1] A. Nakamura, E. Kiyonaga, Y. Yamamura, Y. Shimizu, T. Minowa, Y. Noda, Y. Matsumura, J. Chem. Eng. Jpn. 41 (2008) 1-12.

[2] J. Xie, D. Su, X. Yin, C. Wu, J. Zhu, Int. J. Hydrogen Energ. 36 (2011) 15561-15572.

[3] R.R. Davda, J.W. Shabaker, G.W. Huber, R.D. Cortright, J.A. Dumesic, Appl. Catal. B 43 (2003) 13-26.

[4] R.R. Davda, J.W. Shabaker, G.W. Huber, R.D. Cortright, J.A. Dumesic, Appl. Catal. B 56 (2005) 171-186.

[5] A.J. Byrd, K.K. Pant, R.B. Gupta, Fuel 87 (2008) 2956-2960.

[6] S.R.A. Kersten, B. Potic, W. Prins, W.P.M. van Swaaij, Ind. Eng. Chem. Res. 45 (2006) 4169-4177.

[7] Y. Guo, S.Z. Wang, D.H. Xu, Y.M. Gong, H.H. Ma, X.Y. Tang, Renew. Sust. Energ. Rev. 14 (2010) 334-343.

[8] G.J. DiLeo, P.E. Savage, J. Supercrit. Fluids 39 (2006) 228-232.

[9] T. Furusawa, T. Sato, H. Sugito, Y. Miura, Y. Ishiyama, M. Sato, N. Itoh, N. Suzuki, Int. J. Hydrogen Energ. 32 (2007) 699-704.

[10] I.G. Lee, S.K. Ihm, Ind. Eng. Chem. Res. 48 (2008) 1435-1442.

[11] J.W. Shabaker, G.W. Huber, R.R. Davda, R.D. Cortright, J.A. Dumesic, Catal. Lett. 88 (2003) 1-8.

[12] R.D. Cortright, R.R. Davda, J.A. Dumesic, Nature 418 (2002) 964-967.

[13] G.W. Huber, J. W. Shabaker, S.T. Evans, J.A. Dumesic, Appl. Catal. B 62 (2006) 226-235.

[14] R.R. Davda, J.A. Dumesic, Angew. Chem. Int. Ed. 42 (2003) 4068-4071.

[15] N. Luo, X. Fu, F. Cao, T. Xiao, P. Edwards, Fuel 87 (2008) 3483-3489.

[16] K. Lehnert, P. Claus, Catal. Commun. 9 (2008) 2543-2546.

[17] R.M. Ravenelle, J.R. Copeland, W-G. Kim, J.C. Crittenden, C. Sievers, ACS Catal. 1 (2011) 552-561.

[18] A. Wawrzetz, B. Peng, A. Hrabar, A. Jentys, A.A. Lemonidou, J.A. Lercher, J. Catal. 269 (2010) 411-420.

[19] H. Lieske, G. Lietz, H. Spindler, J. Volter, J. Catal. 81 (1983) 8-16.

[20] C. Li, Y.W. Chen, Thermochim. Acta 256 (1995) 457-465.

[21] J. Zielinski, J. Catal. 76 (1982) 157-163.

[22] J. Arenas-Alatorre, A. Gomez-Cortes, M. Avalos-Borja, G. Diaz, J. Phys. Chem. B. 109 (2004) 2371-2376.

[23] A.G. Chakinala, D.W.F Brilman, W.P.M. van Swaaij, S.R.A. Kersten, Ind. Eng. Chem. Res. 49 (2009) 1113-1122.

[24] K. Takanabe, K. Aika, K. Inazu, T. Baba, K. Seshan, L. Lefferts, J. Catal. 243 (2006) 263-269.

[25] D.C. Grenoble, M.M. Estadt, D.F. Ollis, J. Catal. 67 (1981) 90-102.

[26] B. Matas Guell, I.V. Babich, L. Lefferts, K. Seshan, Appl. Catal. B 106 (2011) 280-286.

[27] J.H. Lin, P. Biswas, V.V. Guliants, S. Misture, Appl. Catal. A 387 (2010) 87-94.

[28] J.R. Rostrup-Nielsen, Catalytic Steam Reforming. ISBN: 3-540-12665-1 Springer-Verlag Berlin Heidelberg New York Tokyo, 1984.

Chapter 4

Aqueous Phase Reforming of Ethylene Glycol – Role of intermediates on catalyst performance

D.J.M. de Vlieger, B.L. Mojet, L. Lefferts and K. Seshan, J. Catal. 292 (2012) 239

Liquid product formation during the aqueous catalytic reforming of ethylene glycol (EG) was studied up to 450 ºC and 250 bar pressure. Methanol, ethanol and acetic acid were the main liquid by-products during EG reforming in the presence of alumina supported Pt and Pt-Ni catalysts. The effects of these by-products on selectivity and catalyst stability were further investigated by studying reforming of these components. Reforming of these products was shown to be responsible for the formation of alkanes. The high dehydrogenation activity of Pt-Ni catalysts lead to high H_2 yields during EG reforming by (i) suppressing the formation of methane during methanol reforming (a major by-product of EG reforming) and (ii) suppressing the formation of acetic acid. In addition, the decrease in acetic acid formation showed a positive effect on catalyst lifetime. Acetic acid was found to be responsible for hydroxylation of the Al_2O_3 support, leading to migration and coverage of the metal particles by $Al(OH)_x$ and resulting in deactivation of the Pt-based catalysts.

4.1 Introduction

Many studies on the catalytic reforming of model oxygenates under APR conditions have been reported recently [1-5]; ethanol, ethylene glycol, glycerol are typical examples. Information on mechanistic sequences that take place during APR is limited, and in the case of ethylene glycol (EG), Dumesic *et al.* [5] suggested that reforming is initiated *via* dehydrogenation and formation of an adsorbed oxygenate (acetylinic, dialcohol type) intermediate. In a desired sequence, C-C bond cleavage and subsequent water gas shift leads to CO_2 and H_2. However, rearrangement/desorption of the oxygenate intermediate leads to acids and/or one C-O bond scission to formation of alcohols. Sequential reforming of acids and alcohols often cause formation of alkanes as by-products. In addition, direct hydrogenation of CO_x formed also give CH_4 or higher alkanes through the Fischer-Tropsch reaction [5]. These parallel routes lower the hydrogen yield during APR, which is a serious drawback.

Deactivation and instability of the catalyst are other issues during APR. Activity loss during APR is often associated with loss of catalytic sites (leaching, sintering) or blockage by carbonaceous species but specific details are not available in literature. However, in the case of high temperature gas-phase steam reforming of oxygenates, reasons for catalyst deactivation were identified [6-12]. For example, coke deposition caused by oligomerization of olefins formed was reported to be an issue during steam reforming of ethanol [6, 7]. Formation of unsaturated C_xH_y species *via* dehydrogenation reactions is often proposed as a precursor to coke [8-10]. Our group has shown earlier that acetic acid is converted to acetone during steam reforming, which further reacts to form coke precursors such as di-acetonealcohol, mesityl oxide or mesitylene [11]. The product CO can also disproportionate exothermically to form carbon through the Boudouard reaction ($2CO \rightarrow CO_2+C$) [12].

As discussed in Chapter 3, Pt/Al_2O_3 catalyst showed reforming rates for APR of ethylene glycol that are very attractive for commercial application. However, this catalyst was found to deactivate during the reaction. Pt/Al_2O_3 also gave lower H_2 selectivity due to the formation of alkanes. Furthermore, it was shown in Chapter 3 that presence of Ni in the Pt/Al_2O_3 catalyst suppressed the above problems such as catalyst deactivation and high amounts of alkane formation and provided the basis for the development an efficient catalyst.

In this study, the role of intermediates that are formed during APR of ethylene glycol on the formation of alkanes is studied. Further, the reason for the loss of activity is investigated in relation to intermediates formed during reactions. Correlations thus drawn are discussed in relation to the promotion of Pt/Al_2O_3 with Ni. Improving catalyst stability and at the same time enhancing hydrogen selectivity at the expense of alkanes for the reforming of ethylene glycol is essential in the design of an efficient APR catalyst.

4.2 Experimental

4.2.1 Catalyst preparation and characterization

Alumina supported Pt and Pt-Ni (molar ratio 1:1) catalysts were prepared as described in section 2.2.1. Catalysts were characterized by XRF, BET, CO-chemisorption, TEM imaging, FT-IR and Raman spectroscopy. Further details regarding catalyst characterization are discussed in section 2.3. Details of the catalysts used for this study are summarized in Table 4.1.

Table 4.1: Characteristics of the catalysts studied

Catalyst	Metal Loading by XRF (wt %)	Average metal particle Size (nm)	BET Surface area (m^2/g)
γ-Al_2O_3	-	-	200
Pt/γ-Al_2O_3	1.45	$\leq$ 1 (TEM) 1.6 (CO-chemisorption)	198
Pt-Ni/γ-Al_2O_3	1.15 Pt - 0.35 Ni	$\leq$ 1 (TEM)	198

4.2.2 Catalytic testing

The experimental setup and applied definitions are described in detail in Chapter 2. A 2 mL. min^{-1} flow of 1 wt% oxygenate solution (ethylene glycol ($\geq$ 99.9%, Sigma-Aldrich), acetic acid ($\geq$ 99.9%, Merck), methanol ($\geq$ 99.9%, Merck), or ethanol ($\geq$ 99.9%, Merck)) was first preconditioned to the operating conditions (275 °C and 200 bars) before it entered the reactor in which 1.0 g of catalyst was placed. The reforming reactions were studied during 5h time-on-stream. Products in the liquid reactor effluent were determined by HPLC.

4.3 Results and discussion

4.3.1 AP reforming of ethylene glycol

Reforming of aqueous bio-organic streams is only interesting for commercial applications when feeds with high oxygenate concentrations (> 15 wt%) can be used. However, larger concentrations of intermediates and products formed under these conditions can lead to extensive secondary reactions. Thus, two sets of reforming experiments were carried out with 1.5 wt% Pt/Al_2O_3 catalyst; (1) 20 wt% ethylene glycol (EG) solution was studied in supercritical water (450 ^{0}C and 250 bar) and (2) a 1 wt% EG solution was studied at similar conversions obtained by using milder reaction conditions (275 ^{0}C and 200bar). The obtained results are shown in Table 4.2.

Table 4.2: Conversions and alkane selectivities for ethylene glycol reforming under different conditions in the presence of 1.5 wt% Pt/Al_2O_3.

[EG] wt%	Reaction Temp. (°C)	Reaction Press. (bar)	WHSV (h^{-1})	Conversion to gas (%)	Conversion to liquid (%)	Alkanes in gas (%)
20	450	250	24	74	15.4	16.9
1	275	200	1.2	78	11.7	0.3

Conversion to gas and liquid phase products are mentioned separately in Table 4.2 to allow a good comparison of the gasification efficiency. Total EG conversion to liquid and gas products was ±90% for both reactions with the remaining carbon being unconverted EG. Carbon balances were complete within an error margin of 5%. It can be seen that at the higher EG concentration and higher temperature, the amount of carbon containing products in liquid phase increased. Alkane formation is also higher under these conditions. The alkane formation was much lower in the experiment with 1 wt% EG. In both cases, componential HPLC analysis of the liquid reactor effluent showed that (in addition to unconverted EG) three other main components were present in the reactor effluent. These were acetic acid, methanol and ethanol.

As discussed previously, components such as acids and alcohols are often suggested as precursors for the formation of alkanes. Further, we also stated (Chapter 3) that addition of Ni to Pt/Al_2O_3 suppressed formation of alkanes during reforming of EG. In order to probe the role for Ni, a detailed componential HPLC analysis of the liquid reactor effluents of 1 wt%

EG reforming (275 ^{0}C and 200 bar) in the presence of Pt or Pt-Ni catalysts was carried out. The results are shown in Figure 4.1.

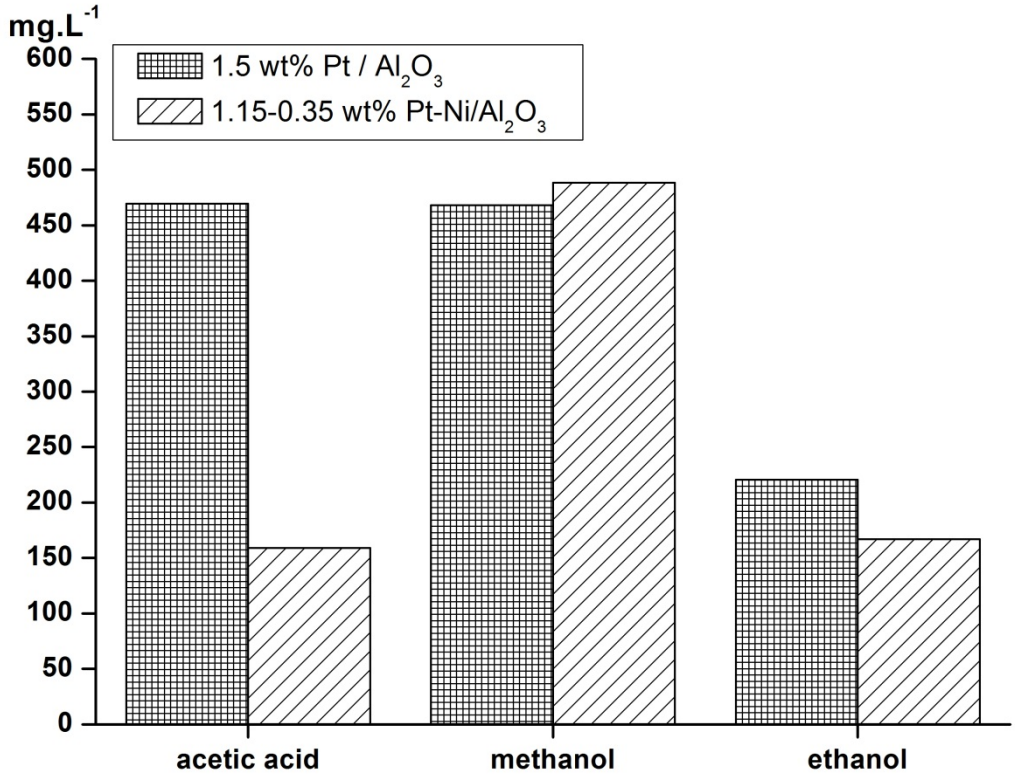

Figure 4.1: Liquid by products during catalytic reforming of 1 wt% ethylene glycol at 375 ^{0}C and 200 bar (WHSV = 1.2 h^{-1}). Results for alumina supported Pt and Pt-Ni catalysts showed conversions to gas phase of 78 and 88%, respectively.

It is seen from Figure 4.1 that the reactor effluent in presence of the Ni-promoted catalyst showed the same by-products (acetic acid, methanol and ethanol). The concentrations of methanol and ethanol in the reactor effluent were not influenced significantly by the presence of Ni. However, the concentration of acetic acid was found to be three times lower for the Ni-promoted catalyst.

At this point, it is useful to recall the mechanistic sequences proposed in the literature for APR of EG by Dumesic *et al.* [5]. It is suggested, without experimental evidence, that dehydrogenation of EG over Pt is the first step in the reforming pathway. During this step the hydrogen atoms from the hydroxyl groups are removed by O-H cleavage on the Pt surface

[13]. In an optimal situation, the resulting adsorbed •O-CH_2-CH_2-O• species is further dehydrogenated and undergoes C-C cleavage to form adsorbed CO [13]. The adsorbed intermediate species •O-CH_2-CH_2-O• can also undergo rearrangement over the acidic γ-Al_2O_3 support to form acetic acid [5]. However, in another study (Chapter 5), we also observed the formation of acetic acid during APR of EG using a carbon-supported Pt catalyst. The chemical inertness of this type of support material excludes the rearrangement of •O-CH_2-CH_2-O• over the support to form acetic acid. The ionic nature of hot compressed water is reported to catalyze organic reactions in the aqueous phase, such as the Cannizzaro reaction [14] and isomerization reactions [15]. As discussed later in this chapter, the Cannizzaro-derived reaction is not a dominant contributor to acetic acid formation. The isomerization reaction (either catalyzed by the support or by the ions from the liquid water) of adsorbed •O-CH_2-CH_2-O• is suggested to be responsible for the majority of acetic acid formed. Competition between dehydrogenation and isomerization of adsorbed •O-CH_2-CH_2-O• dictates the relative formation of hydrogen and acetic acid. Dehydrogenation will be catalyzed by metals (Pt, Ni) and and isomerization would be assisted by an acidic oxide (in this case γ-Al_2O_3 support).

The role of Ni in the suppression of acetic acid formation (Figure 4.1) can be inferred from DFT calculations by Skoplyak and Barteau [13] which predicted "increased" binding energies for adsorbed species derived from ethylene glycol on the surface monolayer Ni-Pt (111) as compared to Pt (111). We conclude that the increased binding energies of oxygenate intermediate lead to longer residence times on the metal and result in increased dehydrogenation activity. It would be useful to estimate the energetics for the two routes (dehydrogenation *vs.* isomerization) on Pt and Pt-Ni bimetallic surfaces by theory, but that is beyond the scope of the current study. In addition, the dissociation of the O-H bond is suggested to be the rate-limiting step in the conversion of ethylene glycol [13]. The higher dehydrogenation activity of the Pt-Ni catalyst results in faster dehydrogenation of the O-H groups and hence a higher overall reforming rate. This is in agreement with earlier studies [16] and our own results (Chapter 3) where Pt-Ni/Al_2O_3 catalysts showed higher conversions for the reforming of ethylene glycol than Pt/Al_2O_3.

4.3.2 APR of model compounds

Aqueous phase reforming experiments with liquid products formed during the APR of EG was carried out using individual components (Figure 4.2). Reforming experiments (with acetic acid, methanol, or ethanol) were conducted at 275 ºC and 200 bar in the presence of Pt/Al_2O_3 or $Pt\text{-}Ni/Al_2O_3$. Feed concentrations of 1 wt% were used so as to work in the same concentration range as the liquid by-products formed during EG reforming experiments. For example, a total conversion of 15% to methanol, ethanol and acetic acid was observed during the reforming of 20 wt% EG (Table 4.2), resulting in a total concentration of 3 wt% liquid by-products. As the three were in the same range, concentration of each was fixed for further experiments at 1 wt%.

Blank reforming experiments (275 °C and 200 bar) with methanol, ethanol and acetic acid without catalysts showed conversions below 5%. In the presence of Pt/Al_2O_3 and $Pt\text{-}Ni/Al_2O_3$ catalysts, conversions were in the range of 50-80% (Figure 4.2). For methanol the conversion was around 60% (Fig. 4.2A) and for ethanol higher, ±80% (Fig. 4.2B). The higher reforming activity of ethanol on both catalysts may be related to the reforming sequences that take place. The initial step in the reforming of aliphatic alcohols involves the dissociation of the O-H bond resulting in adsorbed methoxy or ethoxy species on the Pt surface [17, 18]. Similar dissociation energies are reported [19] for breaking the O-H bond in these alcohols and can therefore not be responsible for the difference in reforming activity. During reforming of alcohols, hydrogen formation requires the formation of adsorbed carbon monoxide which can undergo WGS to form H_2 and CO_2. In the case of methanol to form CO, it is necessary for the adsorbed methoxy species to undergo three C-H bond cleavages. For ethanol, the adsorbed ethoxy species must undergo two C-H and one C-C bond cleavage. Further it is suggested that the cleavage of the C-C bond in ethanol leads to an adsorbed methyl species [18]. We speculate that the different routes to decompose the alcohols may be the reason for the difference in reactivity. For the reforming of acetic acid (Figure 4.2C), initial conversion levels of ±50% were obtained. However, the conversion decreased rapidly with time for both the Pt and Pt-Ni catalysts, this will be discussed later on in the manuscript.

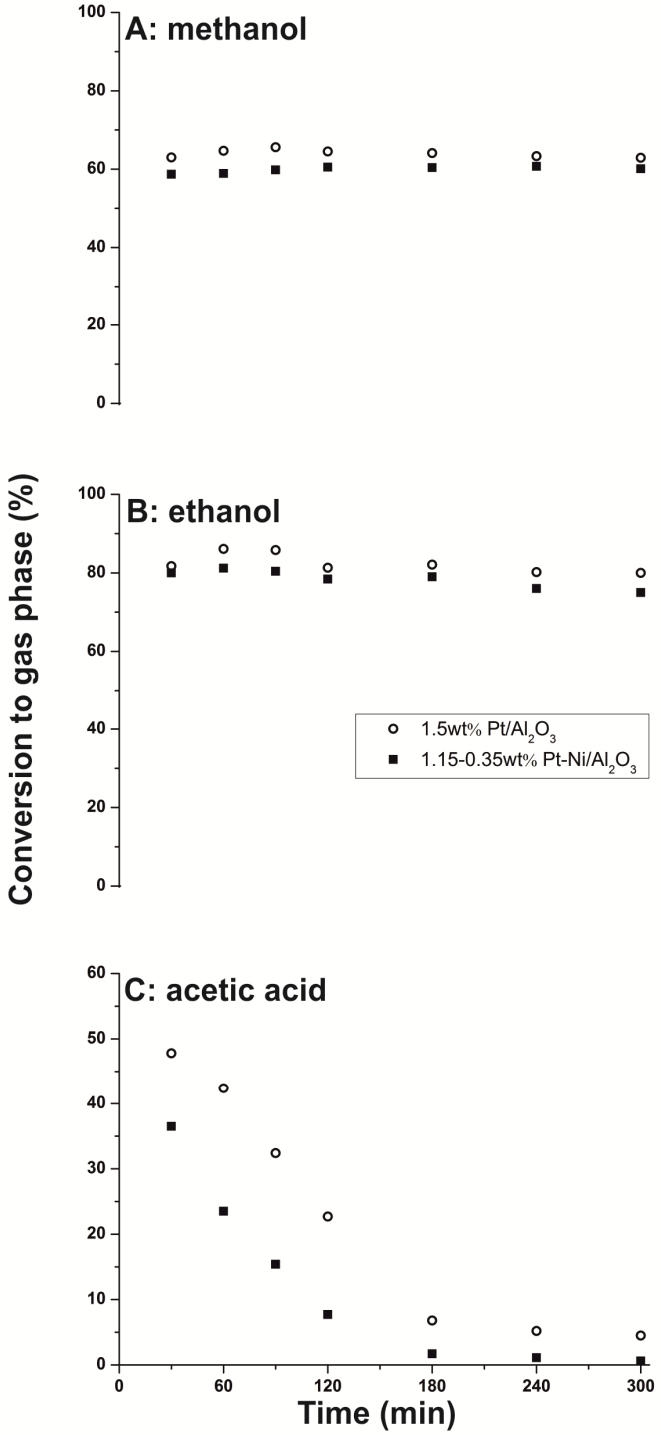

Figure 4.2: Conversion to gas phase for reforming (275 °C and 200 bar) of 1 wt% methanol (A), ethanol (B) or acetic acid (C) using 1.5 wt% Pt/Al_2O_3 (o) and 1.15-0.35 wt% $Pt\text{-}Ni/Al_2O_3$ (▪) catalysts.

4.3.3 Alkane formation during APR

The formation of alkanes during the catalytic reforming of acetic acid, methanol and ethanol are shown in Figure 4.3. The selectivity towards alkanes (mainly methane) was found to be the highest (±47%) during acetic acid reforming. For the reforming of methanol a selectivity of 8% towards CH_4 was observed for the Pt catalyst. In the case of ethanol reforming the Pt catalyst showed a CH_4 selectivity of ±20%. The higher amounts of methane observed during ethanol reforming is attributed probably to the CH_x fragment formed by C-C bond breaking of ethanol [17] on the Pt surface. CH_x fragments can recombine with adsorbed H atoms on the Pt surface to form methane. A similar sequence is also suggested for acetic acid on Pt based catalysts [11, 20]. In the case of methanol, C-O bond breaking is necessary to generate these adsorbed CH_x species that lead to the production of methane. High C-C bond breaking activities for Pt during reforming of ethanol and low activity for C-O bond breaking [5] during reforming of methanol can explain the observed differences for methane formation.

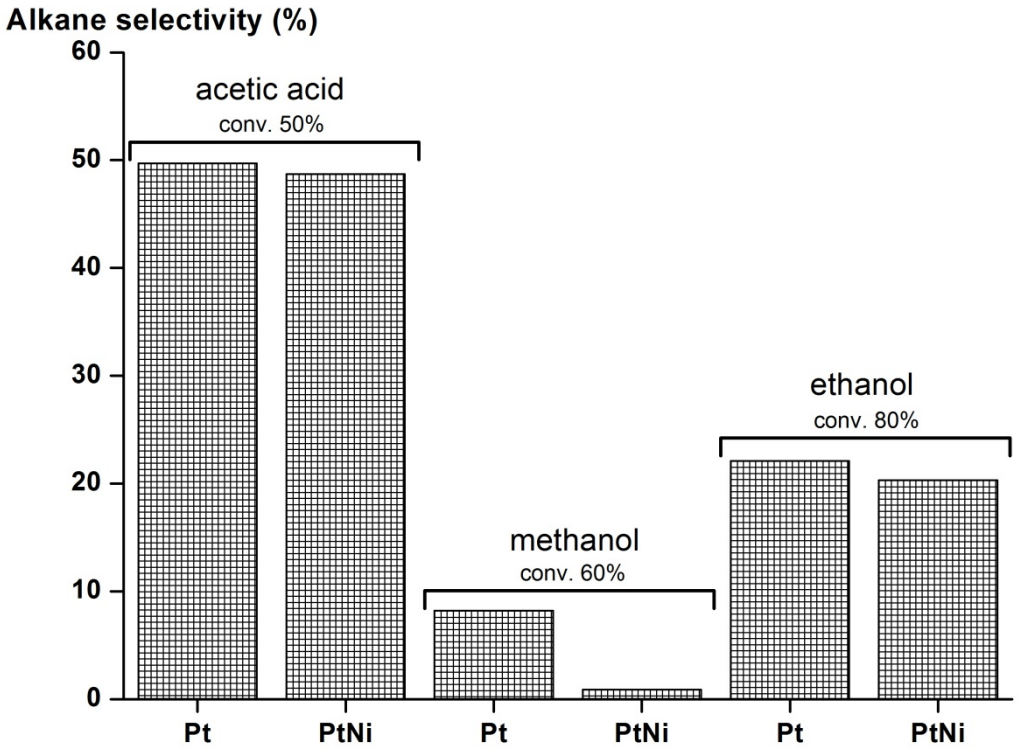

Figure 4.3: Formation of alkane during the catalytic reforming of 1 wt% acetic acid, methanol and ethanol at 275 °C and 200 bar. Conversions to gas phase (conv.) are mentioned in the Figure.

For methanol reforming with the Pt-Ni catalyst almost no methane was formed (Figure 4.3). Methanol was found to be one of the major products during the reforming of EG (Figure 4.1) which explains why Pt-Ni/Al_2O_3 catalyst shows almost no methane formation in agreement with earlier studies [16] and our own results (Chapter 3). The lower methane production observed during methanol reforming in the presence of Pt-Ni can be explained by the enhanced dehydrogenation activity of Pt-Ni catalyst [13], favoring C-H cleavage instead of C-O cleavage in methanol. Promoting the Pt catalyst with Ni did not affect the alkane (methane) selectivity for acetic acid or ethanol reforming as can be expected from the reforming routes. Reforming of these compounds inherently lead to CH_3 species on the catalyst surface, which is a precursor for methane formation. In case of methanol reforming, the intermediate CH_3O must undergo C-O cleavage to form CH_3 (and hence methane). Methane formation during methanol reforming can be prevented by avoiding C-O cleavage.

4.3.4 Catalyst deactivation

Reforming experiments with 1 wt% methanol (Figure 4.2A) and ethanol (Figure 4.2B) solutions showed stable activity levels for both Pt and Pt-Ni catalysts. Catalysts used for acetic acid reforming deactivated during the reaction (Figure 4.2C). Both catalysts showed similar deactivation rates. The catalysts lost all activity after 3 hrs on stream with final conversion levels (~5%) being similar to the reforming experiment without a catalyst.

Deactivation of the catalyst with acetic acid is commonly observed in reforming reactions [11]. The formation of methane resulting from acetic acid decomposition is reported in literature to be a possible cause for deactivation of catalysts [21]. It is suggested that C-H bond breaking in methane further results in CH_x species ($1 \leq x \leq 2$) on the catalytic surface. These fragments can further oligomerize to coke species [11]. However, catalysts used for ethanol reforming were found to be stable while also producing high amounts of methane (20%). It is also known that Pt and Ni catalysts are stable for the reforming of methane. Therefore, it is concluded that methane-induced deactivation is unlikely and the dominant deactivation pathway is due to other causes.

Further, liquid products formed during the APR of acetic acid, methanol and ethanol were determined to find any role for them in catalyst deactivation. During acetic acid reforming, a conversion of 7% to liquid by-products was observed for the Pt catalyst. By-

products were identified as formaldehyde and iso-propanol. For ethanol, a conversion of ±6% to liquid by-products was found for the Pt catalyst. The main product was acetic acid, and the remaining was acetaldehyde (<0.5%). The Cannizzaro reaction (disproportionation of an aldehyde to alcohol and carboxylic acid) could be responsible for some of the acetic acid formed during ethanol reforming. The Pt and Pt-Ni catalysts studied did not influence the amount of acetic acid and acetaldehyde formed during ethanol reforming, while during EG reforming, the amount of acetic acid was strongly dependent on the type of catalyst. This shows that the Cannizzaro-derived reaction is not a dominant contributor to acetic acid formation during EG reforming.

No liquid by-products were observed during methanol reforming. Interestingly, presence of Ni in the Pt-Ni catalyst did not show any significant differences on the type or amount of secondary liquid by-products during reforming of acetic acid, methanol or ethanol compared to the mono-metallic Pt catalyst. No apparent conclusions can thus be derived from these experiments.

In the case of the Pt/Al_2O_3 catalyst that deactivated during acetic acid reforming, CO-chemisorption experiments showed a Pt dispersion of only 0.03% (fresh catalysts 67%), indicating that almost all accessible Pt surface area was lost. Loss of catalytic metal by leaching, metal particle growth by sintering and coke formation are common causes for loss of catalytic surface and hence deactivation of catalysts. XRF elemental analysis of the deactivated Pt/Al_2O_3 catalyst used for acetic acid reforming showed that no Pt was lost by leaching from the catalyst. Sintering is a thermo-physical effect and therefore dictated by the operating conditions (temperate and pressure). Catalyst stability was not affected during reforming of methanol and ethanol when the reaction was performed at the similar operating conditions as for acetic acid reforming, thus excluding sintering as cause of catalyst deactivation. The formation of coke on the surface of Pt based catalysts during steam reforming of acetic acid is often reported [11]. Carbon deposits on the deactivated Pt/Al_2O_3 catalyst which was used for aqueous reforming of acetic acid was studied by TGA-MS up to a temperature of 800 ^{0}C in oxygen (1 v/v% O_2 in N_2). No weight loss attributed to the removal of carbonaceous deposits was observed during the experiment, indicating that carbonaceous deposits were not present on the catalyst. IR and Raman experiments (discussed below) also did not show presence of any carbonaceous species. In addition, regeneration of the deactivated Pt catalyst used for acetic acid reforming was attempted by oxygen treatment (up to 500 ^{0}C) but the treated catalyst did not regain activity for the reforming of EG. Based on

these results, carbonaceous deposits as cause for catalyst deactivation can also be ruled out. Under conventional gas-phase reforming conditions, it is well accepted that steam reforming of acetic acid can lead to coke formation *via* intermediates involving acetone, diacetone alcohol, and mesitylene [11, 22, 23]. Hot compressed water has a high tendency to dissolve organic species, including carbonaceous deposits [24, 25]. Carrying out reforming in hot compressed water therefore plays an important role in keeping the catalytic surface clean of any coke deposits that prevent accessibility of oxygenates to catalytic sites.

Raman spectroscopy was used to study Pt catalysts used for reforming of methanol, acetic acid and water only (blank experiment). Raman spectra were taken at room temperature in air. The obtained spectra are shown in Figure 4.4. The spectra were normalized based on the most pronounced Raman band at 362 cm^{-1} for easy comparison. In all three cases, Raman spectra of the used catalysts showed five sharp adsorption bands in the range of 65-4000 cm^{-1}. These bands are attributed to Boehmite [26, 27], which is formed as a result of the phase change of the γ-Al_2O_3 support in our catalyst when subjected to hot compressed water [see Chapter 3]. The three bands at 362, 494 and 672 cm^{-1} are attributed to vibrational modes of the Boehmite Al-O bond [26]. The two other adsorption bands, located at 3212 and 3076 cm^{-1}, are attributed to stretching vibrations of O-H bonds [26]. A weak band at 3565 cm^{-1} is visible in the spectra of the acetic acid reforming catalyst and this band can be attributed to hydroxyl groups with a higher acidity. Interestingly, the ratio between the normalized bands at 362 cm^{-1} and the OH bands at 3076 and 3212 cm^{-1} show clearly that more hydroxyl species are present on the deactivated Pt catalyst compared to the active catalysts.

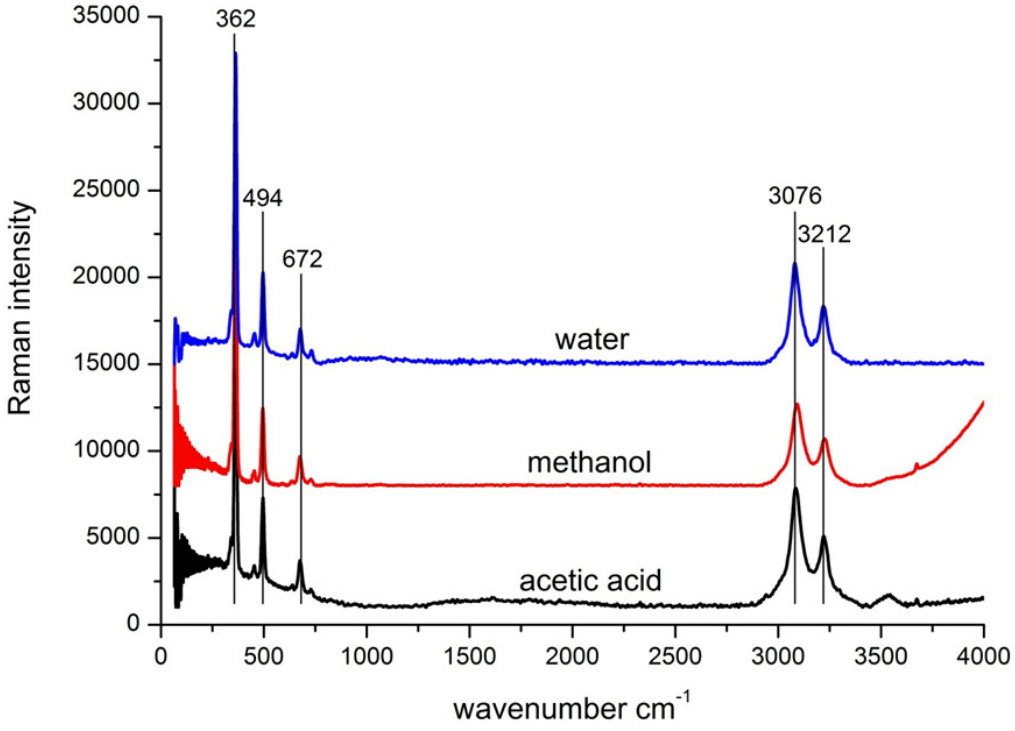

Figure 4.4: Raman spectra of spent 1.5 wt% Pt/Al_2O_3 catalysts used for reforming (275 °C and 200 bar) of acetic acid, methanol and water only.

The differences in hydroxyl groups and the cause for deactivation of the Pt catalyst were further investigated by Fourier-Transformed Infrared spectroscopy (FT-IR). FT-IR spectra of used Pt catalysts were taken at room temperature in air. Spectra were normalized for sample weight and are shown in the frequency range of 2400-1000 cm^{-1} in Figure 4.5A. No information could be derived from the IR spectrum above 2400 cm^{-1} due to the broad and intensive molecular water band that covered the whole range up to the maximum of 4000 cm^{-1}. For all catalysts, a broad band in the frequency region 1000-1200 cm^{-1} was observed which can be assigned to the Al-OH bending vibrations in the Boehmite crystal structure [27]. Multiple weak bands are observed in the region 1300-1900 cm^{-1} and these are attributed to different kinds of adsorbed carbon pollutants (*i.e.* CO_2 adsorption from air leading to surface carbonates) and water adsorption. Two strong bands appeared at 1975 and 2112 cm^{-1} and these have been suggested to originate from complex Al-O-H zigzag structures in Boehmite [27].

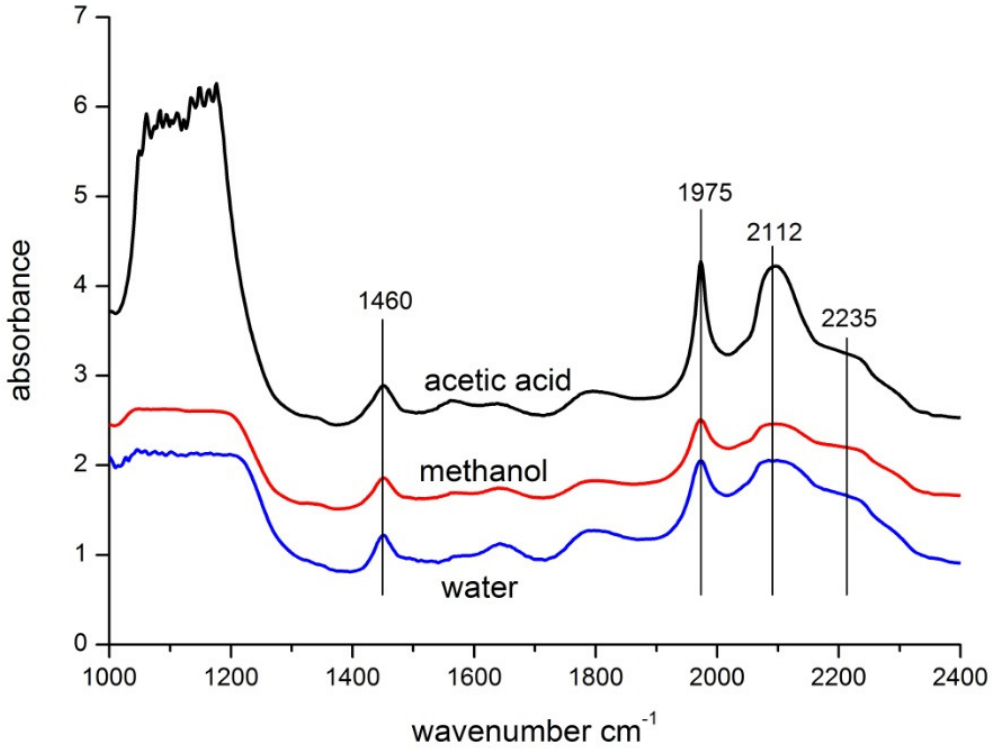

Figure 4.5-A: FT-IR spectra of 1.5 wt% Pt/Al_2O_3 catalysts used for reforming (275 °C and 200 bar) of acetic acid, methanol and water only.

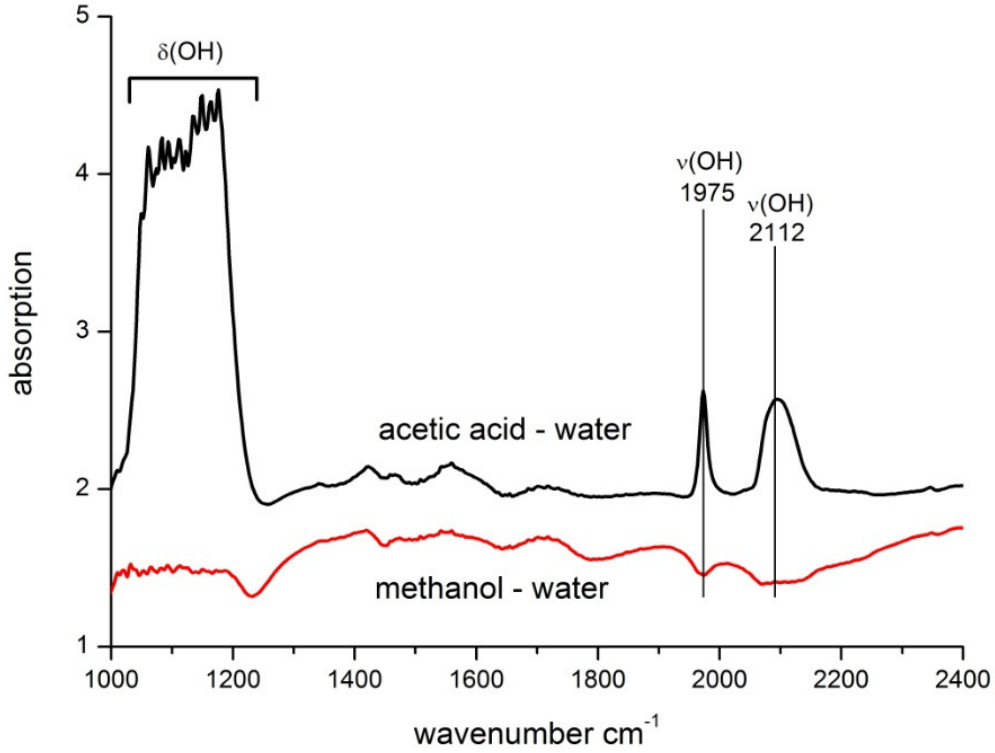

Figure 4.5-B: Differences between FT-IR spectra of 1.5 wt% Pt/Al_2O_3 catalysts used for reforming (275 °C and 200 bar) of acetic acid or methanol and water only.

FT-IR spectra of the used catalysts were subtracted from each other as shown in Figure 4.5B to study differences in chemical groups on the surfaces of the used Pt catalysts. Subtracting the spectrum of the catalyst that was exposed to only water from that of aqueous methanol solution resulted in a more or less flat line, indicating that the surface composition of the active catalysts (used for methanol and water only) are similar. Subtracting the spectrum of the catalyst subjected to only water from the spent deactivated acetic acid catalyst resulted in 3 strong bands; one lattice vibration in the region 1000-1200 cm^{-1} and two sharp OH related bands located at 1975 and 2112 cm^{-1}. Also in the Raman spectra, the acetic acid treated sample showed the highest O-H intensity (Figure 4.4). These results indicate the presence of a highly hydroxylated type of Boehmite in the acetic acid deactivated catalyst compared to the active catalyst used in methanol APR.

A cause for deactivation of the catalyst can be inferred from the increased number of hydroxyl groups. It is known that the stability of the Al_2O_3 surface strongly depends on the pH of the medium [28]. Acids are reported to cause dissolution of Al_2O_3 [29] and this is an important process that can affect catalyst performance. The dissolution rate of metal oxide supports increases at lower pH values and involves protonation of Al-O-Al bonds to form Al-OH. Further protonation and/or rearrangement of oxide ligands are responsible for dissolution of Al_2O_3 [29]. The increase in hydroxyl groups on the surface of the catalysts used for acetic acid reforming indicates that the surface structure of Al_2O_3 is affected by acetic acid. Dissociation constants for acids are much higher in hot compressed water compared to normal water [25], and therefore, we propose that acetic acid behaves as a stronger acid in hot compressed water resulting in protonation and sequential leaching of the alumina surface. In hot compressed water, where solubility of inorganic oxide materials is low, it can be expected that hydroxylated alumina that leached off can be re-deposited on the catalyst. Figure 4.6 shows the TEM image of the Pt deactivated catalyst. The Pt particle and the lattice distances of the Al_2O_3 are clearly visible. The Al_2O_3 lattice distance is measured in the picture to be 0.7nm. The Pt particle is covered by a layer that shows the same lattice distances of 0.7 nm as alumina, indicating that the Pt is covered by alumina. From these results, it is concluded that the cause of deactivation of the Pt catalyst is coverage of catalytic Pt sites by hydroxylated alumina layer.

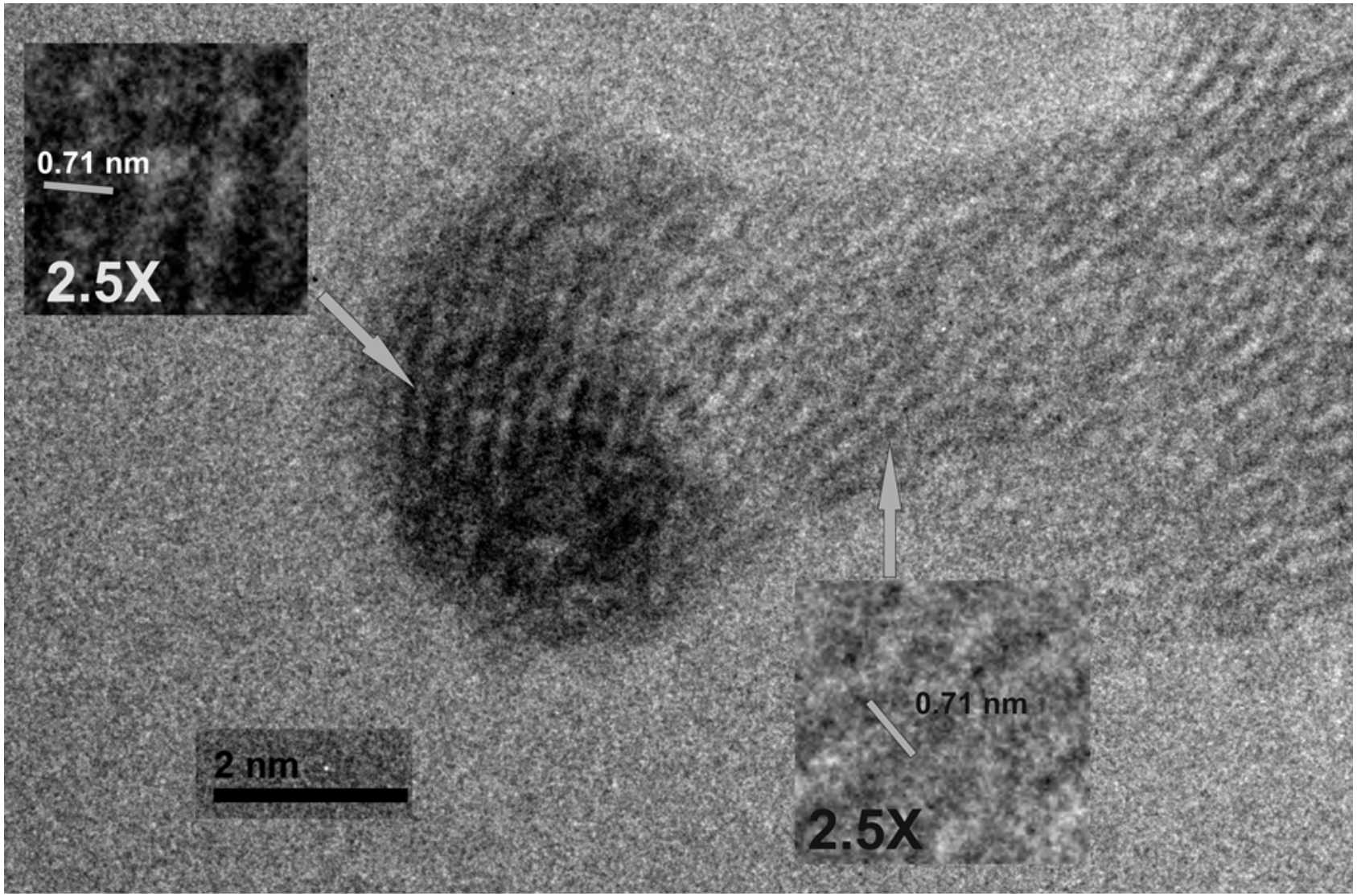

Figure 4.6: TEM image of an alumina covered Pt particle.

Although the exact mechanism responsible for coverage of the Pt particle by alumina is not yet known, we showed here that this mechanism likely involved hydroxylation of the γ-Al_2O_3/Boehmite support and is propagated by a strong acidic environment, resulting from the high proton dissociation of acids in hot compressed water.

4.3.5 Reaction pathways

The reaction pathways involved in the reforming of ethylene glycol proposed by Dumesic et al. [5] have been adapted with the new insights obtained from this study. The resulting extended reaction sequences are proposed in Figure 4.7. Modifications include formation of methanol from ethanol and deactivation by acetic acid. We have identified methanol as an important liquid by-product. Methanol can be formed during the reforming of ethanol as a result of C-C bond cleavage. Reforming of methanol can either lead to methane or to hydrogen and the preferential route is controlled by the dehydrogenation activity of the catalyst. The formation of acetic acid, ethanol and methanol during the reforming of EG is considered undesired because consecutive reactions involving these compounds are responsible for the formation of alkanes (mainly methane). In addition, the presence of acetic acid can cause deactivation of the catalyst. The formation of liquid by-products and alkanes mainly result from C-O bond cleavage, dehydration and hydrogenation reactions. The pathway to high hydrogen yields involves dehydrogenation of ethylene glycol. Competition between dehydrogenation and isomerization of the adsorbed intermediate to acetic acid determines the selectivity toward alkanes (and hence H_2 yields). Addition of Ni to alumina supported Pt catalysts increased the dehydrogenation activity. As a consequence, a decrease in the formation of alkanes and improved stability was accomplished by suppressing acetic acid formation.

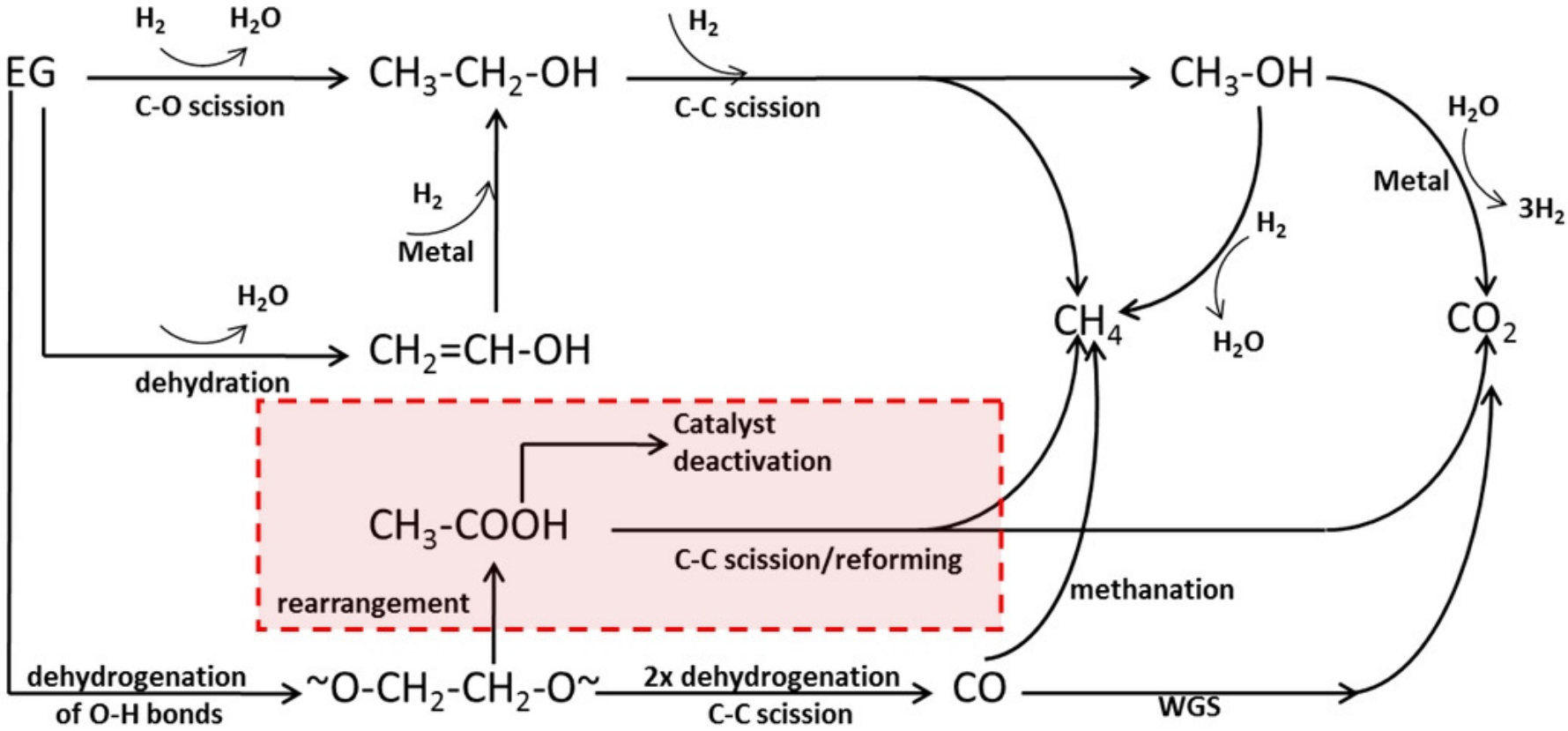

Figure 4.7: Schematical representation of reaction pathways during reforming of ethylene glycol.

4.4 Conclusions

We identified methanol, ethanol and acetic acid as the main liquid by-products during the reforming of ethylene glycol in hot compressed water in the presence of Al_2O_3 supported Pt and Pt-Ni catalysts. Side-reactions involving these liquid by-products lead to the formation of high amounts of methane. Acetic acid was shown to be responsible for the deactivation of Pt and Pt-Ni catalysts by hydroxylation of the Al_2O_3 surface. Re-deposition of the dissolved alumina on the catalyst leads to the blocking of catalytic Pt sites and hence deactivation of the catalyst. The increased dehydrogenation activity of the Pt-Ni catalyst was found to suppress the formation of acetic acid during ethylene glycol reforming and thereby increasing the H_2 selectivity and catalyst lifetime.

References

[1] J.W. Shabaker, G.W. Huber, J.A. Dumesic, J. Catal. 222 (2004) 180-191.

[2] A.O. Menezes, M.T. Rodrigues, A. Zimmaro, L.E.P. Borges, M.A. Fraga, Renew. Energ. 36 (2011) 595-599.

[3] B. Roy, K. Loganathan, H.N. Pham, A.K. Datye, C.A. Leclerc, Int. J. Hydrogen Energ. 35 (2010) 11700-11708.

[4] A. Wawrzetz, B. Peng, A. Hrabar, A. Jentys, A.A. Lemonidou, J.A. Lercher, J. Catal. 269 (2010) 411-420.

[5] R.R. Davda, J.W. Shabaker, G.W. Huber, R.D. Cortright, J.A. Dumesic, Appl. Catal. B 56 (2005) 171-186.

[6] P.D. Vaidya, A.E. Rodrigues, Chem. Eng. J. 117 (2006) 39-49.

[7] A.L. Alberton, M.M.V.M. Souza, M. Schmal, Catal. Today 123 (2007) 257-264.

[8] D.L. Trimm, Catal. Today 37 (1997) 233-238.

[9] F. Frusteri, S. Freni, V. Chiodo, L. Sparado, G. Bonura, S. Cavallaro, J. Power Sources 132 (2004) 139-144.

[10] V. Klouz, V. Fierro, P. Denton, H. Katz, J.P. Lisse, S. Bouvot-Mauduit, C. Mirodatos, J. Power Sources 105 (2002) 26-34.

[11] K. Takanabe, K. Aika, K. Seshan, L. Lefferts, Chem. Eng. J. 120 (2006) 133-137.

[12] K.O. Christensen, D. Chen, R. Lodeng, A. Holmen, Appl. Catal. A 314 (2006) 9-22.

[13] O. Skoplyak, M.A. Barteau, J.G. Chen, Surf. Sci. 602 (2008) 3578-3587.

[14] M. Osada, M. Watanabe, K. Sue, T. Adschiri, K. Arai, J. Supercrit. Fluids 28 (2004) 219.

[15] J. An, L. Bagnell, T. Cablewski, C.R. Strauss, R.W. Trainor, J. Org. Chem. 62 (1997) 2505.

[16] G.W. Huber, J. W. Shabaker, S.T. Evans, J.A. Dumesic, Appl. Catal. B 62 (2006) 226-235.

[17] A. Erdohelyi, J. Rasko, T. Kecskes, M. Toth, M. Dömök, K. Baan, Catal. Today 116 (2006) 367-376.

[18] S. Sa, H. Silva, L. Brandao, J.M. Sousa, A. Mendes, Appl. Catal. B 99 (2010) 43-57.

[19] S.J. Blanksby, G.B. Ellison, Acc. Chem. Res. 36 (2003) 255-263.

[20] B. Matas Guell, I. Babich, K. Seshan, L. Lefferts, J. Catal. 257 (2008) 229-231.

[21] M.M.V.M. Souza, M. Schmal, Appl. Catal. A 281 (2005) 19-24.

[22] X. Hu, G. Lu, Appl. Catal. B 99 (2010) 289-297.

[23] A.C. Basagiannis, X.E. Verykios, Appl. Catal. B 82 (2008) 77-88.

[24] Y. Guo, S.Z. Wang, D.H. Xu, Y.M. Gong, H.H. Ma, X.Y. Tang
Renew. Sustain. Energy Rev., 14 (2010), p. 334

[25] P.E. Savage, J. Supercrit. Fluid. 47 (2009) 407-414.

[26] H.D. Ruan, R.L. Frost, J.T. Kloprogge, J. Raman. Spectrosc. 32 (2001) 745-750.

[27] A.B. Kiss, G. Keresztury, L. Farkas, Spectrochim. Acta A 36 (1980) 653-658.

[28] J.A. Yopps, D.W. Feurstenau, J. Colloid Sci. 19 (1964) 61-71.

[29] B. Kasprzyk-Hordern, Adv. Colloid. Interfac. 110 (2004) 19-48.

Chapter 5

Carbon nanotubes: a promising catalyst support material for APR of biomass waste in supercritical water

D.J.M. de Vlieger, D.B. Thakur, L. Lefferts and K. Seshan, ChemCatChem, (2012)

Catalytic aqueous phase reforming (APR) under supercritical water (SCW) conditions is very promising for the production of renewable chemicals from biomass. Stability issues of catalyst support materials in SCW are a major setback for these reactions and stall the further development and industrial exploitation of this technique. The development of stable catalytic support materials for reactions in SCW is therefore of much importance. Carbon nanotubes (CNT) are widely recognized for their significant physical and chemical stability, high heat conductivity and open structure. These properties are already explored for different applications. In this work, we show that CNT to be a promising stable catalyst support material for reactions in SCW. The efficiency of Pt/CNT as catalyst for the production of hydrogen by reforming of ethylene glycol and acetic acid in SCW was studied and illustrates the applicability of CNT as catalyst support in SCW.

5.1 Introduction

Aqueous Phase Reforming (APR) under supercritical water (SCW) conditions (>374 ^{0}C and 221 bar) has gained interest as a reaction medium due to the special properties it possesses [1-3]. SCW as reaction medium is especially promising for the production of renewable chemicals from biomass due to (i) its high tendency to dissolve bio-organic materials and (ii) overcome mass transfer limitations induced by these large molecules [4-7].

Catalysts are mandatory in the APR process to achieve commercially relevant yields of the desired products (*e.g.* H_2). The majority of APR studies reported [2, 6, 8, 9] were performed with metal oxide (*e.g.* Al_2O_3, TiO_2, and MgO) supports on which a noble metal (*e.g.* Pt, Pd and Ru) was deposited. For example, it was shown in chapter 3 and 4 that Pt/Al_2O_3 is a promising catalyst for the production of "green" hydrogen by sub- and supercritical water reforming of ethylene glycol (>80% water).

However, catalyst stability issues related to the alumina support are common during APR. The first problem involves a phase change of γ-Al_2O_3 to Boehmite (Al(OOH)) due to hydration by the hot compressed water as discussed in Chapter 3 and 4. Boehmite has a much lower surface area (± 20 m^2/g) compared to γ-alumina (200 m^2/g) and this is due to the collapse of mesopores (pore diameters of 50-200 Å) during the phase transition. Metal particles deposited inside these pores can be encapsulated during the collapse, making these catalytic sites inaccessible for reaction. In addition, this phase transition also propagates sintering of the metal particles due to the lower surface area of the support. However, since this transition is rapid, only an initial activity drop is observed and Pt/Boehmite is stable for APR of non-acidic oxygenates as discussed in Chapter 3 and 4. In the case of APR of acidic oxygenates, *e.g.* acetic acid, we have shown in Chapter 4 that further hydroxylation of the alumina surface occurs and migration of these species resulted in the coverage of the Pt metal particles. This makes the metal particles inaccessible and results in loss of activity. It should be taken into account that acidic by-products can be formed during APR of non-acidic oxygenates (*e.g.* acetic acid formation during APR of ethylene glycol (EG)) and thus catalyst deactivation induced by the presence of organic acids is a real issue. There are two options to overcome this; (i) suppress acid formation or (ii) design supports which are stable. We have shown in Chapter 4 that promotion of Pt/Al_2O_3 with a second metal (Ni) suppressed the formation of acetic acid by a factor of 3 during APR of EG, but acetic acid formation could not be prevented fully. Moreover, a majority of biomass derived aqueous streams contain

acidic components. For instance, acetic acid is a major component (10 to 20 wt%) in the aqueous fraction of pyrolysis oil [10]. The presence of carboxylic acids cannot be avoided and therefore other catalyst support materials, *e.g.* carbon based, are possible alternatives.

Activated (amorphous) carbon (AC) is used frequently for reactions in hot compressed water due to its physical-chemical stability. For instance, Ni or Ru on AC have been studied for gasification of bio-oxygenates such as glucose, phenol, lignin and cellulose [11-14]. However, the micro-porosity which dominates AC, make them susceptible to pore blockage by coke which is unavoidably formed during APR of biomass streams [15]. Further, the micro-porosity can also cause diffusion limitations for the larger biomass molecules [11, 16, 17].

All these stability issues indicate that conventional metal oxides or activated carbon are not suitable as catalytic support materials in APR of biomass derived waste. Thus, the development of stable materials is of great importance for the commercial feasibility of APR.

Carbon Nanomaterials (CNM), either Carbon Nano Fibers (CNF) or Tubes (CNT), have attracted a lot of interest in the past decade due to their physical and chemical properties [18-22]. Especially in the field of heterogeneous catalysis, CNM have exhibited promising performance as structured catalyst support materials for different catalytic reactions [23, 24]. CNM are not only reported to be very stable materials due to their crystalline nature but their open structure (large external geometric surface areas, absence of micro and meso-pores) is very beneficial for mass transfer and it decreases the chance of pore blockage by coke. Taylor *et al.* used Ni decorated CNT for SCW gasification of cellulose in a batch process but the stability of the catalyst was not discussed [25]. Chang *et al.* showed earlier that multiwall carbon nanotubes were oxidized by SCW, leading to thinning of the tube walls and collapse of the tube openings. This phenomenon was much more severe when an oxidizing agent such as oxygen was present [26]. However, destruction of the macro CNT structure was not reported.

In this chapter studied, the stability of Pt decorated CNT (Pt/CNT) in supercritical water is studied and furthermore its applicability as catalyst for SCW reforming of ethylene glycol and acetic acid is illustrated. To the best of our knowledge, this is the first study where the efficiency of Pt/CNT as catalyst for SCW reforming is assessed.

5.2 Experimental

5.2.1 Catalyst preparation and characterization

CNT supported Pt catalysts were prepared according section 2.2.2. Catalysts were characterized by XRF, BET, SEM imaging, XRD, XPS and Raman spectroscopy. Further details regarding catalyst characterization are discussed in section 2.3.

5.2.2 Supercritical water reformer

The experimental setup and applied definitions are described in detail in Chapter 2. Undecorated CNT and Pt/CNT were exposed to supercritical water for 6 hrs (450 ºC and 250 bar) to study the effect of SCW on the structure and morphology of the CNT. The catalytic activity of Pt/CNT was studied for the reforming of either a 5 wt% ethylene glycol (EG) or 1 wt% acetic acid (HOAc) solution. A 2mL. min^{-1} flow of the respective oxygenate feed was first preconditions to supercritical water conditions (450 ºC and 250 bar) before it entered the reactor in which 0.1 gr of Pt/CNT catalyst was placed.

5.3 Results and discussion

5.3.1 Stability of CNT in SCW

CNT were subjected to SCW (450 ^{0}C and 250 bar) for 6 hrs to study the effect on the morphology. The SEM image of the pristine CNT (Figure 5.1A) shows clusters of entangled tubes with open ends. Exposure to SCW did not affect the bulk morphology of CNT (Figure 5.1B). Moreover, collapse of the tube walls is not observed and the openings at the end of tubes are still clearly visible, which is in agreement with Chang *et al*. [26]. No indication of pitting or damage of the CNT walls was observed. The effect of SCW on the structural quality (crystallinity) of CNT was studied with Raman spectroscopy and the spectra of the pristine and SCW exposed CNT are shown in Figure 5.1C. Three peaks were observed in the Raman spectra and were located at 1346, 1574 and 2685 cm^{-1}. The most prominent peak (1574 cm^{-1}) is attributed to the G-band which is characteristic for defect-free sp^2 hybridized carbon systems. The peak located at 1365 cm^{-1} is attributed to the defect induced D-band of sp^2

carbon systems. Quantifying disorder in a graphene monolayer is usually made by analyzing the I_D/I_G intensity ratio between the disorder-induced D-band and the Raman allowed G-band. In this case, the ratio was calculated to be ±0.7 for pristine CNT and did not vary after treating the CNT with SCW. The peak positions were similar for both the pristine and spent CNT, confirming that the high crystallinity of the tubes was not affected after SCW exposure.

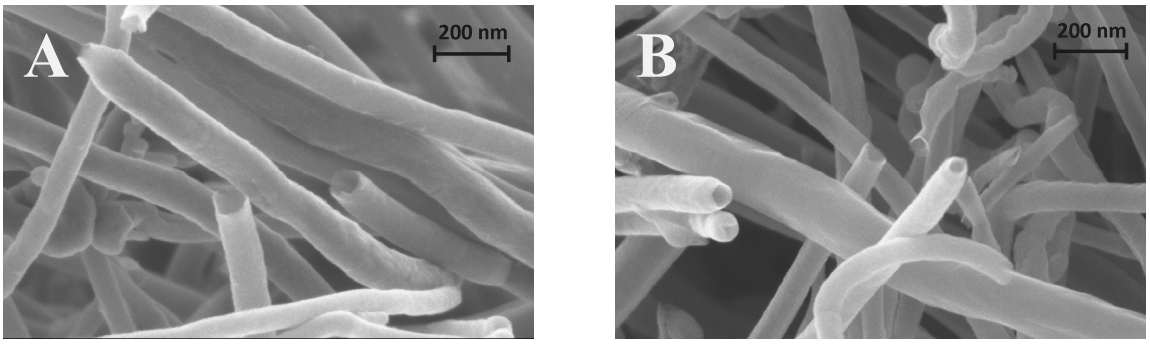

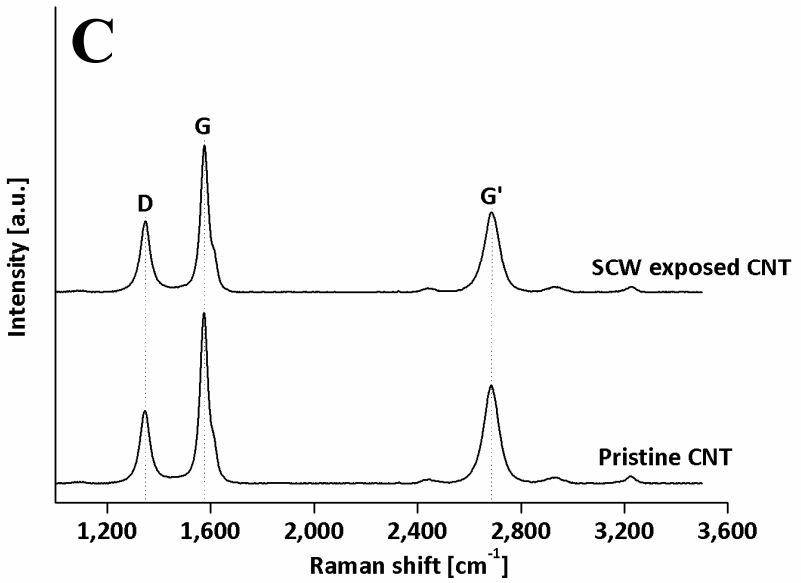

D surface element	CNT pristine	CNT exposed
C (%)	99.3	99.2
O (%)	0.7	0.8

Figure 5.1: High resolution SEM images of CNT before (A) and after exposure (B) to supercritical water (450 °C, 250 bar, 6h). Raman Spectra (C) and XPS derived results (D) of the pristine and SCW exposed CNT.

XPS was further used to study the effect of SCW on the surface of the tubes in more detail. XPS results of pristine as well as SCW exposed CNT are tabulated in Figure 5.1D and shows the atomic distribution of surface species. The surface oxygen concentration of pristine CNT did not vary significantly after exposure to SCW, which shows that the amount of oxygen containing groups did not increase due to exposure to SCW. Extensive functionalization of the carbon support by SCW is therefore excluded. These results indicate that CNT are very stable in SCW.

The chemical inertness of CNM is attributed to the structured graphene sheet, which is the building block of CNM. Graphene sheets have a planar honeycomb structure of a one atom thick layer of sp^2-hybridized carbon atoms, which are considered the strongest among all atomic bonds. CNM are entirely made up of these bonds and this explains their good chemical stability. Surface modifications of CNM have been studied for different applications but very severe conditions have to be used to affect the surface of CNM. For instance subjecting CNM to concentrated nitric acid is used for functionalization of the CNM surface to make it hydrophilic, illustrating the harsh conditions necessary to overcome the chemical inertness of CNM [27]. The hydrophobic nature of CNM is not a problem in SCW as SCW behaves like an organic solvent and hence good wettability of CNM is expected.

5.3.2 Stability of Pt-CNT in SCW

The stability of CNT in SCW was shown in the previous section. For catalytic purposes it is important to decorate the CNM with an active catalytic metal. Metal loss compromises the catalyst efficiency and hence strong bindings between the metal and the CNM supports are vital. In this regard, it is known from literature that Pt-C hybridization is possible between Pt and π orbitals of C-atoms in graphene sheets, resulting in strong Pt-support bonds [28].

The effect of SCW (450 ^{0}C, 250 bar) on stability of Pt decorated CNT was studied. XRF elemental analysis of the synthesized Pt-CNT showed that the Pt loading was 8 wt%. This amount seems high compared to metal loadings (1-3 wt%) of conventional catalysts. However, the low density of CNT is responsible for the seemingly high Pt loading on Pt-CNT. The absolute amount of Pt per volume of Pt-CNT is in the same range as for conventional catalysts. No difference in Pt content of the pristine and SCW exposed Pt-CNT was observed by XRF analysis. In addition, the reactor effluent was analysed by XRF to study

the presence of Pt. The total liquid reactor effluent (800ml) was collected and concentrated to 5 mL by evaporation. The XRF detection limit for Pt in water is 70 $mg.L^{-1}$ and this means that Pt in the concentrated reactor effluent is only detectable when at least 5% of the total amount of deposited Pt (8 mg) leached from the CNT support. XRF analysis of the reactor effluent did not show any Pt, indicating that leaching was below 5%. The XRF results of the SCW exposed Pt-CNT and reactor effluent indicate that leaching of the Pt metal from the CNT support was negligible during the reaction and can be contributed to the strong interaction between Pt and CNT [28].

High resolution SEM images of pristine and SCW exposed Pt-CNT were taken (Figure 5.2A-B) to study the Pt particles. Pt nanoparticles with a size of ±11 nm were visible on both the pristine and exposed Pt-CNT, indicating that Pt particle growth was not significant during SCW exposure. XRD spectra of pristine and exposed Pt-CNT were taken (Figure 5.2C) to study the Pt particles in more detail.

The Scherrer equation was applied to the Pt(111) diffraction line (Figure 5.2C) to calculate average Pt particle sizes. Similar Pt particles sizes of ±11 nm were calculated for both the pristine and SCW exposed Pt-CNT, which are in agreement with SEM observations. Raman spectra of the pristine and exposed Pt-CNT (Figure 5.2D) showed the same absorption bands as undecorated CNT (Figure 5.1C). The relative intensities of the I_D/I_G absorption bands were calculated to be 0.70 and 0.75 for the pristine and SCW exposed Pt-CNT, respectively. The comparable values indicate that the surface structure (crystallinity) of Pt-CNT was not affected by SCW, which was also the case for undecorated CNT (Figure 5.1C). Therefore, it can be concluded that decorating the CNT with Pt does not affect the SCW stability of the material.

XPS results of the pristine and exposed Pt-CNT are tabulated in Figure 5.2E and from this it can be seen that the oxygen content of Pt-CNT increased after exposure to SCW, while an increase was not observed in the case of undecorated CNT (Figure 5.1D). The increase in oxygen might indicate oxidation of Pt by SCW. However, noble metals such as Pt are not able to be oxidized by water under conventional reforming conditions [29]. Also Pt oxidation by SCW is contradicting the work of Crittenden and Parsons, where reduction of a PtO_2 catalyst to Pt^0 was observed in SCW [30].

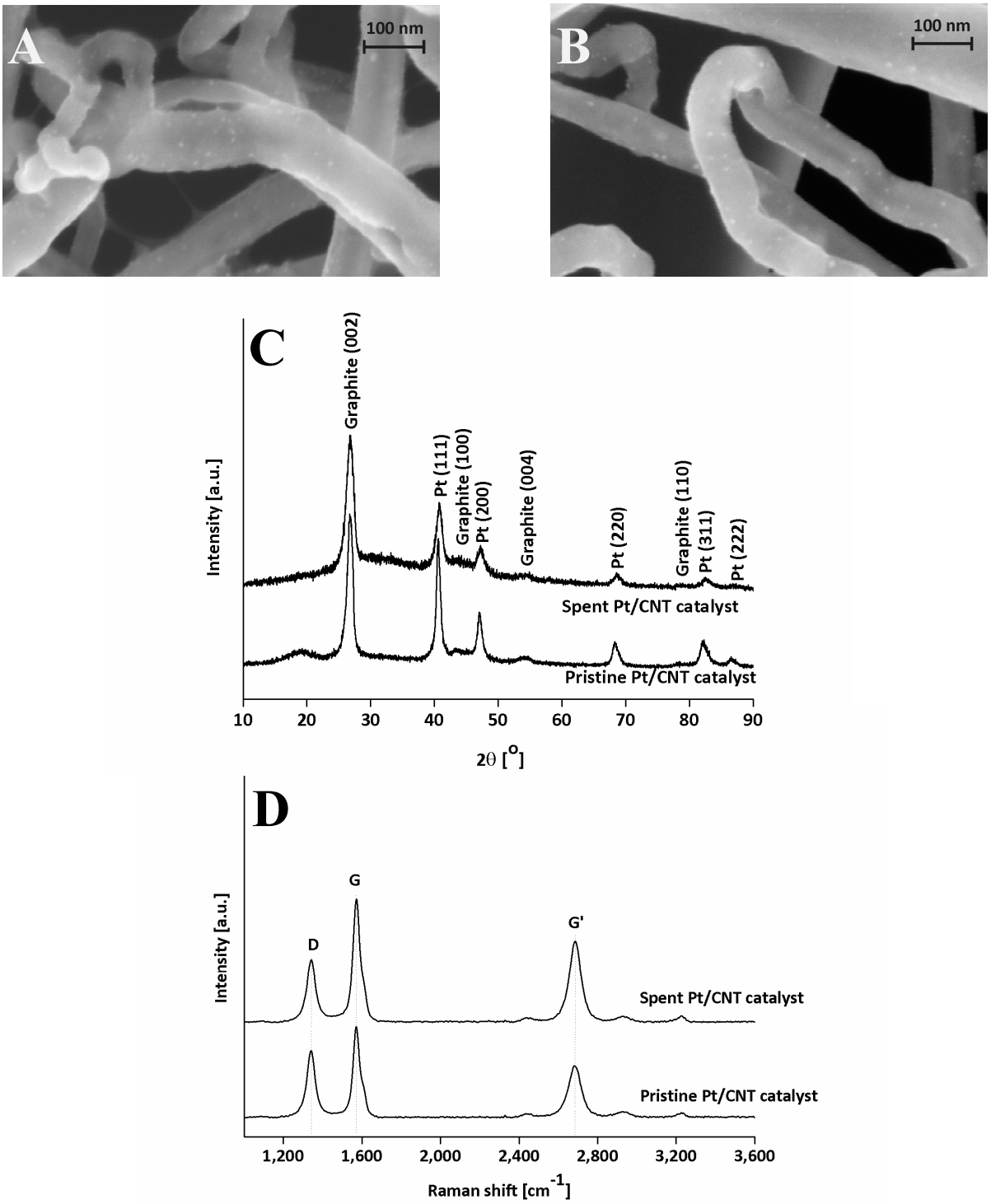

E surface element	CNT pristine	CNT exposed
C (%)	98.0	97.3
O (%)	1.2	2.0
Pt (%)	0.8	0.7

Figure 5.2: High resolution SEM images of Pt-CNT before (A) and after exposure (B) to supercritical water (450 ^{0}C, 250 bar, 6hr); XRD diffractograms (C), Raman spectra (D) and XPS derived results (E) of the pristine and spent Pt-CNT.

The effect of SCW exposure on Pt oxidation state and loading were studied in more detail from the XPS spectra (shown in Figure 5.3). The XPS spectrum for the Pt $4f_{(5/2 \text{ and } 7/2)}$ emission bands of the pristine Pt-CNT are shown in Figure 5.3A. Pt is characterized by the doublet with binding energies (BE) of 71.68 eV ($4f_{7/2}$) and 74.98 eV ($4f_{5/2}$), showing a binding energy difference of 3.3 eV between the maximum intensities of both bands. This corresponds to the characteristics of Pt^0, illustrating that majority of Pt species on pristine Pt-CNT are metallic [31]. The XPS lines of Pt of the SCW exposed catalyst (Figure 5.3B) show the binding energies of Pt $4f_{7/2}$ and Pt $4f_{5/2}$ at 71.67 and 74.97 eV, respectively. These values are similar to the XPS lines of Pt on pristine Pt-CNT (Figure 5.3A), indicating that the electronic properties associated with changes in oxidation state of Pt have not been affected by SCW, confirming the stability of Pt/CNT catalyst. The XPS spectrum of the SCW exposed Pt-CNT revealed a very weak band at 288 eV (not shown), which indicates the presence of C=O groups. The observed increase in oxygen on the SCW exposed Pt-CNT (Figure 5.2E) is therefore related to marginal functionalization of the CNT, which was likely facilitated by Pt under the studied conditions.

In addition to Pt 4f spectra for pristine and SCW exposed Pt-CNT, C 1s spectra were also recorded (not shown here). On the basis of the ratios of area under Pt 4f and C 1s peaks, the amounts of Pt present on CNT before and after SCW exposure can be compared qualitatively. The values of these ratios (*i.e.* Pt/C) were estimated to be 0.0079 and 0.0074 for pristine and used catalyst, respectively. This shows that there is no significant variation in the amount of platinum supported on CNT after SCW exposure. This is also in good agreement with the XRF results, which showed no loss of Pt. Additionally, the Pt size remained unchanged as confirmed by XRD and high resolution SEM analysis. Together with XPS these results indicate that the dispersion of Pt had not been affected due to the exposure of catalyst to SCW conditions and it is substantially stable.

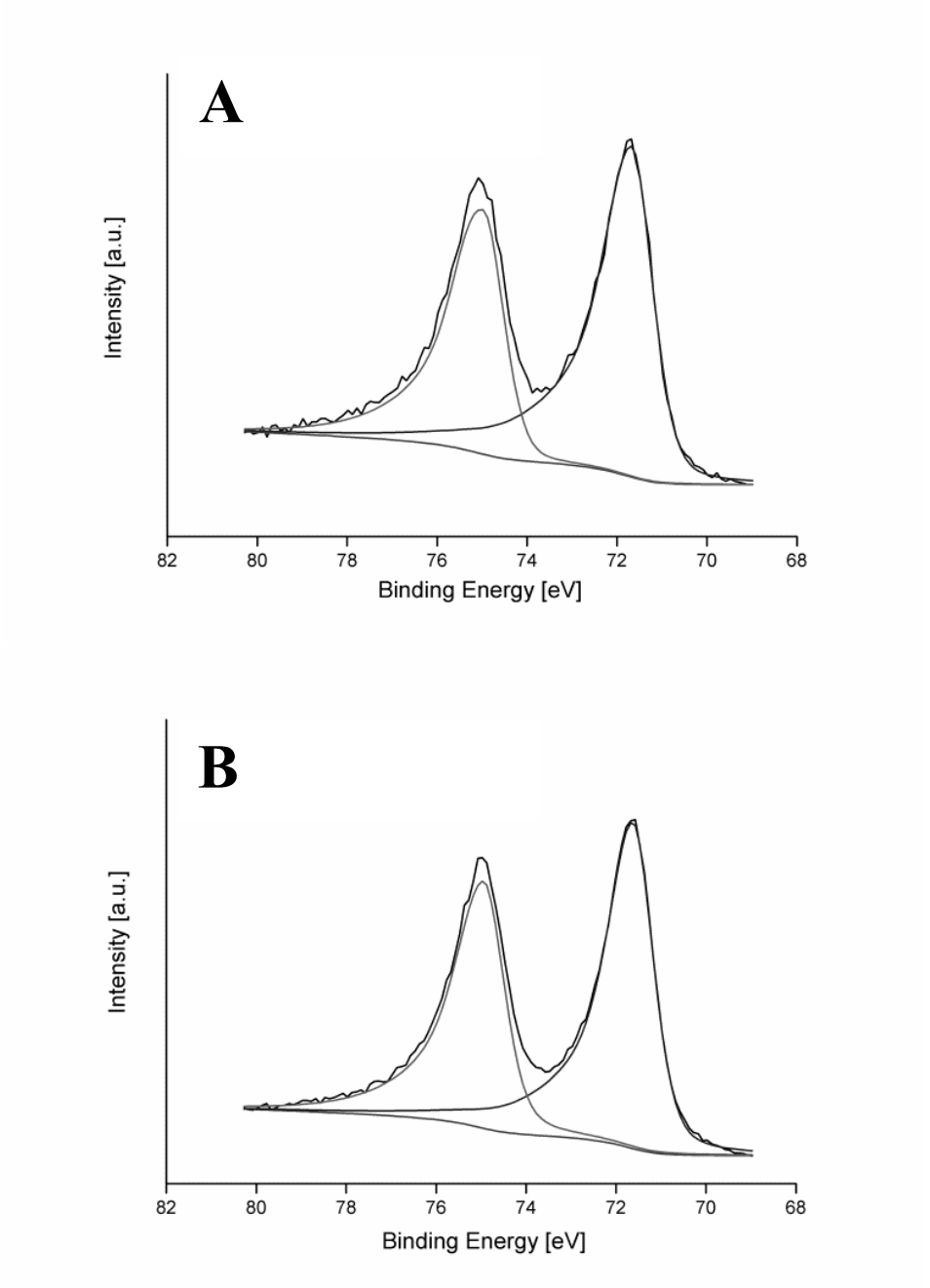

Figure 5.3: XPS spectrum of the Pt 4f photoemission from the PT-CNT catalyst (A) before and (B) after exposure to SCW.

5.3.3 Activity of Pt-CNT for ethylene glycol reforming in SCW

Catalytic reforming of a 5 wt% ethylene glycol (EG) solution was studied at 450 °C under 250 bar pressure. In the absence of a catalyst a conversion of only 5% was observed. A similar conversion was obtained when undecorated CNT were used as catalyst, indicating that undecorated CNT do not show catalytic activity for EG reforming. The catalytic properties of Pt decorated CNT were studied for the EG reforming reaction. The conversion, selectivity towards gas phase products and formation of liquid by-products were followed for 6 hrs and the results are shown in Figure 5.4. A conversion of 85% (Figure 5.4A) was obtained in the presence of Pt-CNT and is remarkably higher compared to the non-catalyzed reaction, illustrating the good catalytic activity of this material. The reforming of EG was highly selective to H_2 and CO_2 in presence of Pt-CNT. Formation of CO was not observed by the GC, indicating that CO levels were below 0.1 v/v%. The low amounts of alkanes formed were mainly CH_4.

HPLC analysis of the reactor effluent (Figure 5.4B) was conducted to identify liquid by-products formed during EG reforming. In addition to EG, six other compounds were observed in the reactor effluent and were identified as formic acid, acetic acid, acetaldehyde, methanol, ethanol and iso-propanol. The sum of carbon in these compounds was in agreement (± 5%) with the TOC value of the liquid reactor effluent, showing that all carbon was accounted for by HPLC analysis.

In chapter 4, we showed that a Pt/Al_2O_3 catalyst deactivated completely within 3 hrs time-on-steam during reforming of a 1 wt% acetic acid solution. No deactivation of the Pt-CNT catalyst was observed during 6 hrs time-on-stream for the EG reforming experiment even though a significant amount of acetic acid (0.2 wt% in reactor effluent) was formed as by-product.

The activity and stability of Pt-CNT during acetic acid reforming was studied in more detail and is discussed in the next section.

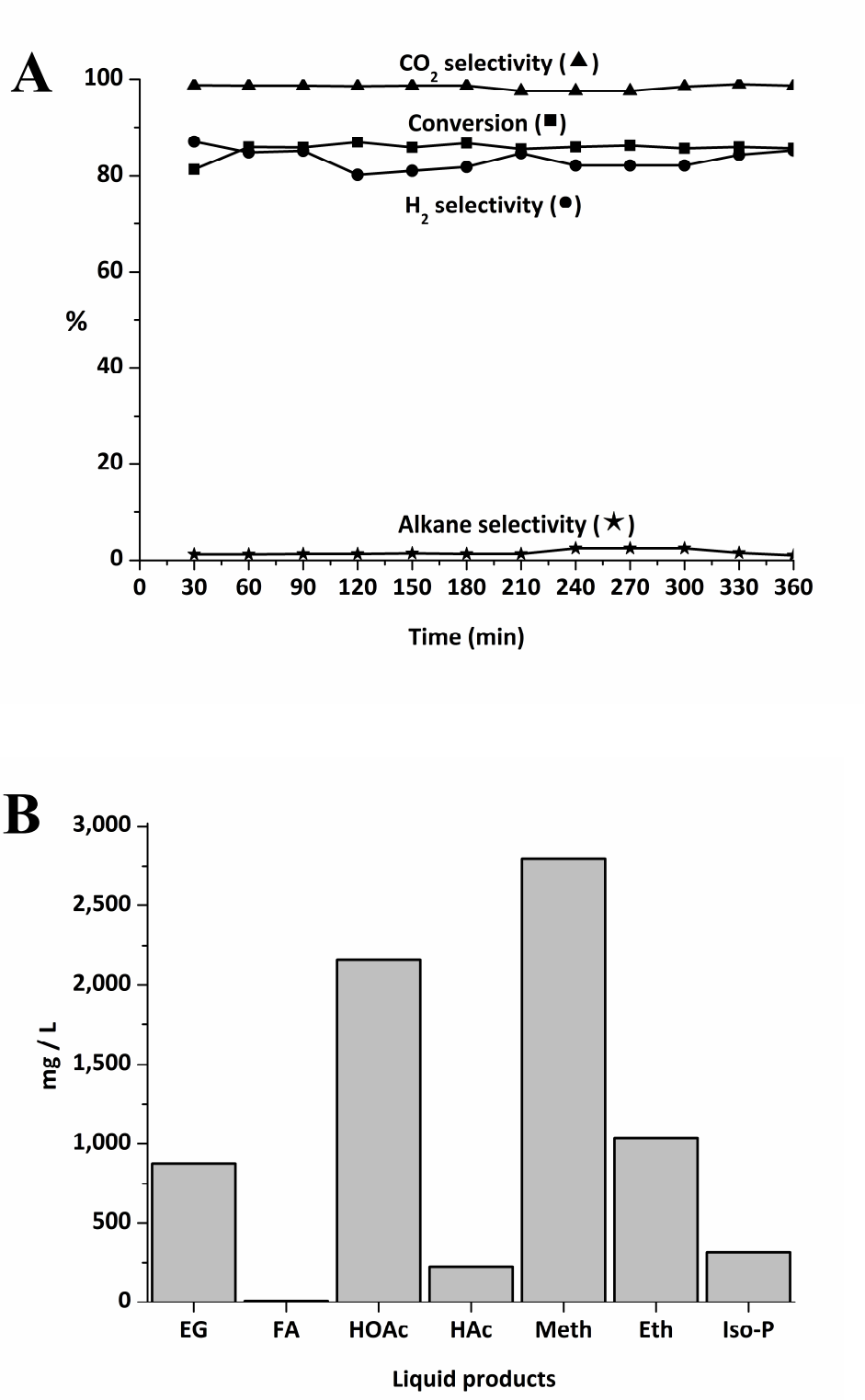

Figure 5.4: Graphical representation of (A) Conversion (■) and selectivity to H_2 (●), CO_2 (▲) and CH_4 (★) (B) Concentration of ethylene glycol (EG), formic acid (FA), acetic acid (HOAc), acetaldehyde (HAc), methanol (Meth) and iso-propanol (Iso-P) in reactor effluent, for the reforming of 5 wt% ethylene glycol in supercritical water (450 ^{0}C and 250 bar) using Pt-CNT catalyst.

5.3.4 Properties of Pt-CNT for SCW reforming of acetic acid

Pt-CNT were studied for the reforming of 1 wt% acetic acid in SCW (450 ^{0}C and 250 bar). This acetic acid concentration was chosen because it was found earlier (Chapter 4) that this concentration induces deactivation of conventional catalysts. A conversion of 3% was observed when no catalyst or only the undecorated CNT were used. Conversion and gas phase selectivities were monitored for 6 hrs during the reforming of the acetic acid solution over Pt-CNT and the results are shown in Figure 5.5A. Gasification conversion of acetic acid was around 58% and is rather low compared to the EG experiment. The acetic acid reforming mechanism is different than for EG, which is the likely reason for the difference in activity. The low acetic acid gasification activity of Pt-CNT indicates that Pt is a poor choice for reforming of acetic acid. Optimizing the metal for acetic acid reforming is discussed in the next chapter. The stoichiometry of acetic acid reforming (CH_3-COOH → CH_4 + CO_2) predicts a CH_4 and CO_2 selectivity of 50%. The selectivity towards alkanes was found to be slightly lower, while a higher CO_2 selectivity of 55% was observed (Figure 5.5A). Furthermore, hydrogen was formed during the reaction. These observations indicate that other reactions (*e.g.* methane reforming) also occurred. No components other than acetic acid were observed in the liquid reactor effluent.

Conversions and selectivities were stable during the entire experiment (Figure 5.5A), indicating that the catalyst did not deactivate under the tested reforming conditions. XRF analysis of the used Pt-CNT catalyst showed similar Pt loadings compared to fresh Pt-CNT, confirming that Pt leaching did not occur. Furthermore, Raman spectroscopy (Figure 5.5B) of the used Pt-CNT showed a similar spectrum with an I_D/I_G intensity ratio of 0.69. As discussed before, the I_D/I_G intensity ratio of pristine Pt-CNT was 0.70. The comparable I_D/I_G ratios of the pristine and used Pt-CNT indicate that the crystallinity of the material was not affected significantly by acetic acid in SCW. XPS analysis of the Pt-CNT catalyst used for acetic acid reforming showed an oxygen concentration of 9%. This value is slightly higher than the 2% that was found for SCW exposed Pt-CNT (Figure 5.2E). These results indicate that acetic acid in SCW caused a marginal amount of oxidation of the CNT support. However, the macro structure and crystallinity of the CNT was not affected as discussed earlier and therefore, it is concluded that Pt decorated CNT are stable catalysts for acetic acid reforming reactions in SCW.

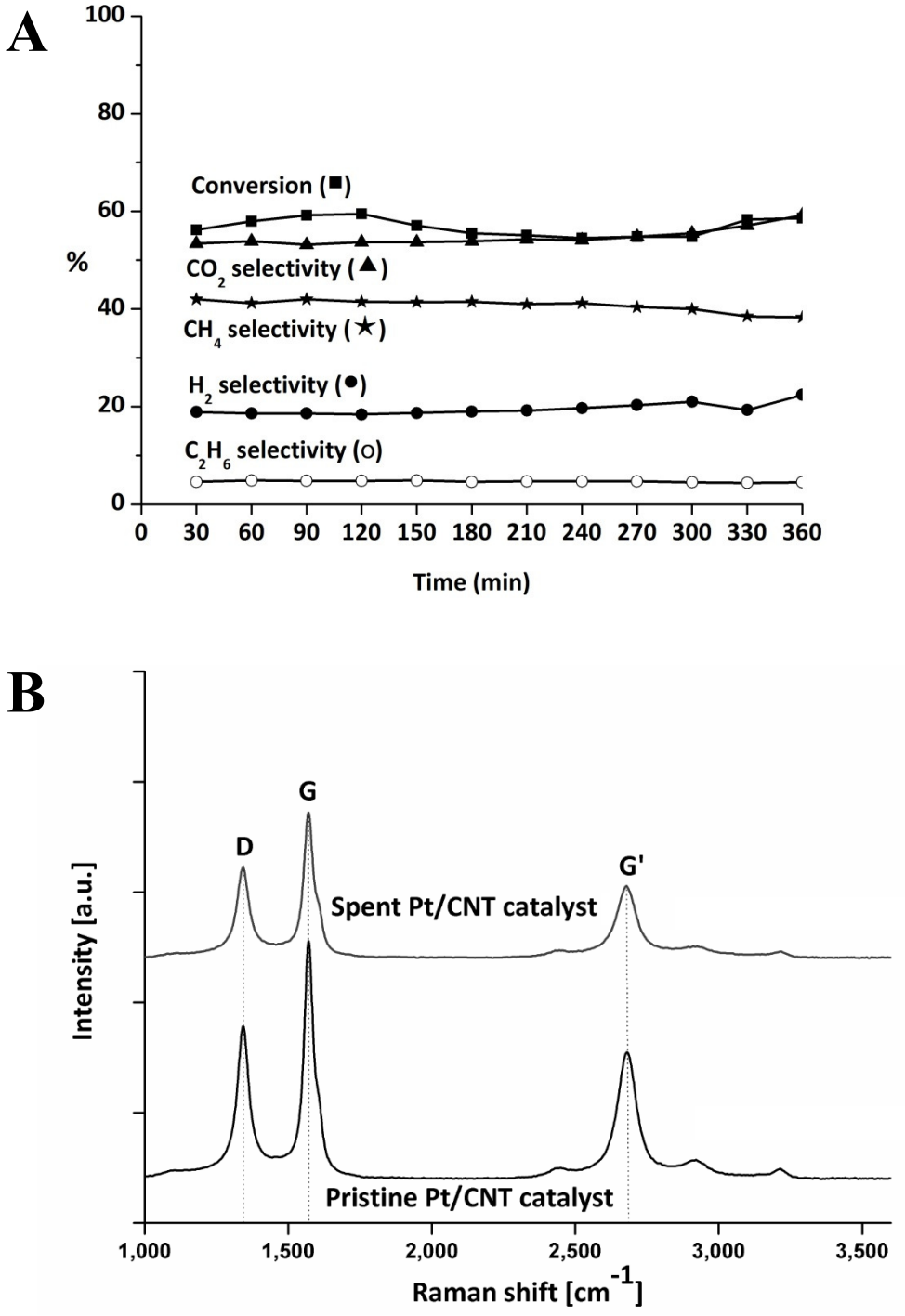

Figure 5.5: Graphical representation of (A) conversion (■) and selectivity to H_2 (●), CO_2 (▲), CH_4 (★) and C_2H_6 (O), for the reforming of 1 wt% acetic acid in supercritical water (450 ^{0}C and 250 bar) using Pt-CNT catalyst. Raman spectra (B) of pristine and spent acetic acid reforming Pt-CNT catalysts.

5.4 Conclusions

It is shown in this chapter that Pt decorated and undecorated carbon nanotubes are very stable in supercritical water. As an illustration of its applicability, the efficiency of Pt/CNT catalyst was demonstrated for the model reforming reactions of ethylene glycol and acetic acid in supercritical water. The physical and chemical stability of CNT offer new possibilities for catalytic reactions in supercritical water

References

[1] P.E. Savage, J. Supercrit. Fluids 47 (2009) 407-414.

[2] Y. Guo, S.Z. Wang, D.H. Xu, Y.M. Gong, H.H. Ma, X.Y. Tang, Renew. Sust. Energ. Rev. 14 (2010) 334-343.

[3] G. Brunner, J. Supercrit. Fluids 47 (2009) 373-381.

[4] J.M.L. Penninger, G.J.J. Maass, M. Rep, Int. J. Hydrogen Energ. 32 (2007) 1472-1476.

[5] R.D. Cortright, R.R. Davda, J.A. Dumesic, Nature 418 (2002) 964-967.

[6] R.R. Davda, J.W. Shabaker, G.W. Huber, R.D. Cortright, J.A. Dumesic, Appl. Catal. B 56 (2005) 171-186.

[7] A. Tanksale, J.N. Beltramini, G.M. Lu, Renew. Sust. Energ. Rev. 14 (2010) 166-182.

[8] A.O. Menezes, M.T. Rodrigues, A. Zimmaro, L.E.P. Borges, M.A. Frago, Renew. Energ. 36 (2011) 595-599.

[9] P. Azadi, R. Farnood, Int. J. Hydrogen Energ. 36 (2011) 9529-9541.

[10] F.H. Mahfud, F.P. Van Geel, R.H. Venderbosch, H.J. Heeres, Separ. Sci. Technol. 43 (2008) 3056-3074.

[11] I.G. Lee, S.K. Ihm, Ind. Eng. Chem. Res. 48 (2008) 1435-1442.

[12] A. Sharma, I. Saito, H. Nakagawa, K. Miura, Fuel 86 (2007) 915-920.

[13] A. Yamaguchi, N. Hiyoshi, O. Sato, M. Osada, M. Shirai, Energ. Fuel. 22 (2008) 1485-1492.

[14] X. Hao, L. Guo, X. Zhang, Y. Guan, Chem. Eng. J. 110 (2005) 57-65.

[15] N.Z. Muradov, T.N. Veziroglu, Int. J. Hydrogen Energ. 30 (2005) 225-237.

[16] E.E. Iojoiu, M.E. Domine, T. Davidian, N. Guilhaume, C. Mirodatos, Appl. Catal. A 323 (2007) 147-161.

[17] S. Czernik, R. Evans, R. French, Catal. Today 129 (2007) 265-268.

[18] J.F. Silvain, C. Vincent, J.M. Heintz, N. Chandra, Compos. Sci. Technol. 69 (2009) 2474-2484.

[19] S.M. Jang, J. Miyawaki, M. Tsuji, I. Mochida, S.H. Yoon, Carbon 47 (2009) 3383-3391.

[20] R. Ströbel, J. Garche, P.T. Moseley, L. Jörissen, G. Wolf, J. Power Sources 159 (2006) 781-801.

[21] S. Perathoner, M. Gangeri, P. Lanzafame, G. Centi, Kinet. Catal. 48 (2007) 877-883.

[22] A.L.M. Da Silva, L.V. Mattos, J.P. den Breejen, J.H. Bitter, K.P. de Jong, F.B. Noronha, Catal. Today 164 (2011) 262-267.

[23] J.K. Chinthaginjala, J.H. Bitter, L. Lefferts, Appl. Catal. A 383 (2010) 24-32.

[57] D.B. Thakur, R.M. Tiggelaar, Y. Weber, J.G.E. Gardeniers, L. Lefferts. K. Seshan, Appl. Catal. B 102 (2011) 243-250.

[58] A.D. Taylor, G.J. Dileo, K. Sun, Appl. Catal. B 93 (2009) 126-133.

[59] J.Y. Chang, A. Ghule, J.J. Chang, S.H. Tzing, Y.C. Ling, Chem. Phys. Lett. 363 (2002) 583-590.

[60] S.D. Gardner, C.S.K. Singamsetty, G.L. Booth, G.R. He, C.U. Pittman Jr, Carbon 33 (1995) 587-595.

[61] T. Kondo, Y. Iwasaki, Y. Honma, Y. Takagi, S. Okada, J. Nakanmura, Phys. Rev. B. 80 (2009) 233408.

[62] K. Takanabe, K. Aika, K. Seshan, L. Lefferts, J. Catal. 227 (2004) 101-108.

[63] R.C. Crittendon, E.J. Parsons, Organometallics, 13 (1994) 2587-2591.

[64] J. F. Moulder, W. F. Stickle, P. E. Sobol, K. D. Bomben, Handbook of X-ray Photoelectron Spectroscopy, Perkin-Elmer Corporation, Eden Prairie (1992).

Chapter 6

Ru/CNT; a commercially promising catalyst for APR of acetic acid in sub- and supercritical water

Catalytic reforming of biomass derived waste streams in sub- and supercritical water is a promising process for the production of sustainable hydrogen. Acetic acid will be a major component (up to 20 wt%) in many anticipated gasification feed streams (*e.g.* the aqueous fraction of pyrolysis oil). Conventional supported (*e.g.* alumina) catalysts deactivate in presence of acetic acid rapidly due to coking and metal/support leaching and hence other catalytic systems must be developed to make this process industrially feasible. Carbon nanotubes (CNT) are very resistant to deactivation during acetic acid reforming in supercritical water and are therefore very suitable as catalyst support. Ru is anticipated to show very high activity for acetic acid reforming and therefore the catalytic performance of Ru/CNT was studied for acetic acid (1-25 wt%) reforming in sub- (195-340 °C, 225 bar) and supercritical water (400 °C, 250 bar). Ru/CNT showed remarkable stability and high reforming activity in low ionic water (supercritical water and low temperature (≤270 °C) subcritical water). Near complete reforming of a 25 wt% acetic acid solution in supercritical water (400 °C, 250 bar) was achieved during 7 h time-on-stream at commercially relevant conditions. Ru oxidation in high ionic medium (subcritical water ≥300 °C) was responsible for deactivation of the Ru/CNT catalyst and therefore this regime should be avoided for catalytic reforming. The high stability of Ru/CNT for acetic acid reforming in supercritical water has paved the way for studying reforming of real biomass derived waste streams under these conditions.

6.1 Introduction

Catalytic APR of bio/organic aqueous feeds is a promising technique for the production of "green" hydrogen [1]. The development of efficient catalysts is essential for commercial exploitation of this process. Acetic acid is a major component (±10 wt%) in many future bio-gasification feed streams (*e.g.* aqueous fraction of pyrolysis oil) [2] and is therefore a relevant model compound. Catalytic APR of acetic acid is very challenging for catalyst stability due to the reasons discussed in Chapter 5.

In Chapter 5, it was shown that Pt decorated carbon nanotubes (CNT) exhibit stable catalytic performance for APR of acetic acid in supercritical water. CNT were shown promising as catalyst support because of (i) its resistance to acetic acid in supercritical water and (ii) the open structure of the material and lack of meso- and micro-pores suppress deactivation of the catalyst by coke blockage. However, the acetic acid reforming activity of Pt was too low to be commercially interesting and must be improved for industrial use. The study described in this chapter, investigates replacement of Pt with a more catalytically active metal for acetic acid reforming.

Steam reforming of acetic acid is reported to involve initial formation of acetate (1) or acyl (2) species on the metal surface by either C-O or O-H bond cleavage [3]. Further C-C cleavage of the acetate and acyl species is necessary to decompose the molecule to C1 species and achieve complete gasification. Davda *et al.* [4] concluded from information available in the literature that Ru and Ni are very promising metals for C-O, and C-C bond cleavage.

The chemical inertness of CNT makes anchoring of metals on them difficult. Kondo *et al.* [5] reported that hybridization of the empty or filled 5d orbitals with the anti-bonding π orbitals of the CNT can result in strong bonds. From the selected catalyst metals (Ni, Ru) for acetic acid reforming, Ni is susceptible to leaching in acidic APR conditions. In agreement, our own studies showed that all Ni was removed from Ni/CNT catalyst under APR conditions (400 °C, 250 Bar). Ru, a more noble metal, is reported to be more inert under these conditions. Sutter *et al.* [6] reported that graphitic layers on Ru show a distinctive lowering of work function (electron ionisation from the Fermi levels to vacuum) compared to clean Ru or graphene, indicating electron transfer from the metal to the carbon network. The latter causes strong bonding between the Ru metal and carbon support. Therefore Ru is promising with respect to reforming activity and stability and hence Ru decorated CNT (Ru/CNT) catalyst

was studied for acetic acid (HOAc) gasification in sub- and supercritical water. This is essential for developing catalysts for reforming of aqueous waste streams which contain carboxylic acids.

6.2 Experimental

6.2.1 Catalyst preparation and characterization

CNT supported Ru catalysts were prepared as described in section 2.2.2. Catalysts were characterized by XPS, XRF, BET, HR-SEM imaging, and Raman spectroscopy. Detailed information about the applied analysis techniques is discussed in section 2.3.

6.2.2 Catalytic testing

The experimental reforming setup used for this study is described in section 2.1. Glacial acetic acid was purchased from Merck (purity of ≥ 99.9%) and was used to prepare solutions of 1, 5, 15 or 25 wt% acetic acid. The reactor was filled with 0.10 gr of Ru/CNT catalyst. Respective acetic acid solutions were flown at a rate of 2 mL. min^{-1} to the reformer. Weight Hourly Space Velocities (WHSV) were calculated to be 18, 90, 269 and 448 per hour, respectively. The aqueous flow was first preconditioned to the operating conditions (subcritical water max. 340 °C and 225 bar, supercritical water 400 °C and 250 bar) before it entered the reactor. The residence time in the catalytic bed was 12 seconds when the reactor was operated at 340 °C (225 bar, water density ~700 g/L) and 3 seconds when the reaction was carried out at 400 °C (250 bar, water density ~150 g/L). The reforming reactions were run for 7 h and conversion and gas phase selectivity values were determined every 30 minutes.

6.3 Results and discussion

6.3.1 Catalyst preparation and characterization

Figures 6.1 and 6.2 show the HR-SEM images of undecorated CNT and fresh Ru/CNT, respectively. The openings of the tubes are clearly visible in both images. A Ru metal loading of 11.1 wt% was found for the freshly prepared Ru/CNT by XRF analysis. The Ru particles are visible as white spots on the walls of the CNT and the majority of the particles are in the size range of 3-5 nm but few larger particle agglomerates up to 40nm were also observed.

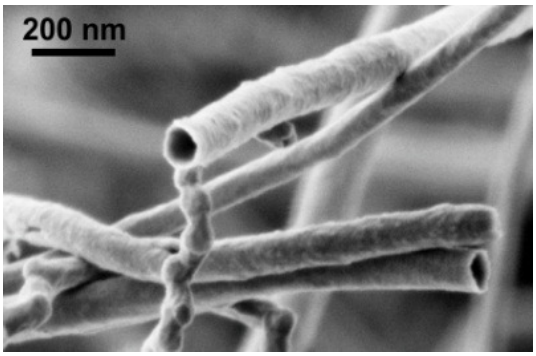

Figure 6.1: HR-SEM image of fresh undecorated CNT

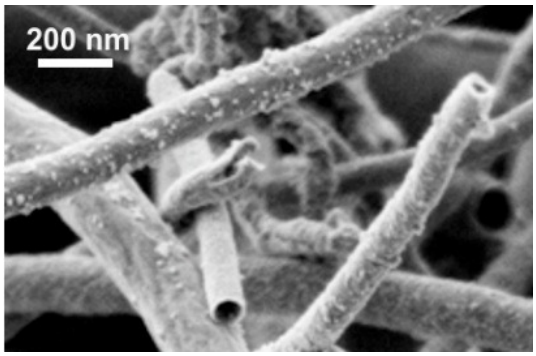

Figure 6.2: HR-SEM image of fresh Ru/CNT

6.3.2 APR of acetic acid over Ru/CNT

Reforming of a 1 wt% acetic acid solution in the absence of a catalyst (blank experiment) in high temperature subcritical water (340 °C and 225 bar) or supercritical water

(400 °C and 250 bar) showed very low carbon to gas conversions, 2% and 4%, respectively. The same conversions were obtained when undecorated CNT were used as catalyst, indicating that CNT do not possess catalytic activity for acetic acid reforming under the studied conditions. Acetic acid reforming reactions over Ru/CNT were followed for 7 h time-on-stream and the conversion as function of time is depicted in Figure 6.3. An initial conversion of ±97 % was obtained for APR of a 25 wt% acetic acid solution in supercritical water (400 °C and 250 bar). The acetic acid reforming activity of Ru/CNT is remarkably high compared to Pt/CNT. For instance, in Chapter 5 we reported that Pt/CNT (8 wt% Pt, 11nm Pt particles) showed a conversion of only 60% for supercritical water reforming (450 °C and 250 bar) of 1 wt% acetic acid, while in this work we were able to obtain near complete conversion of 25 wt% acetic acid reforming at a lower temperature of 400 °C (250 bar) and similar WHSV. Thus choice of Ru allows overcoming the low activity associated with the Pt based catalysts, one of the key objectives of the work described in this chapter.

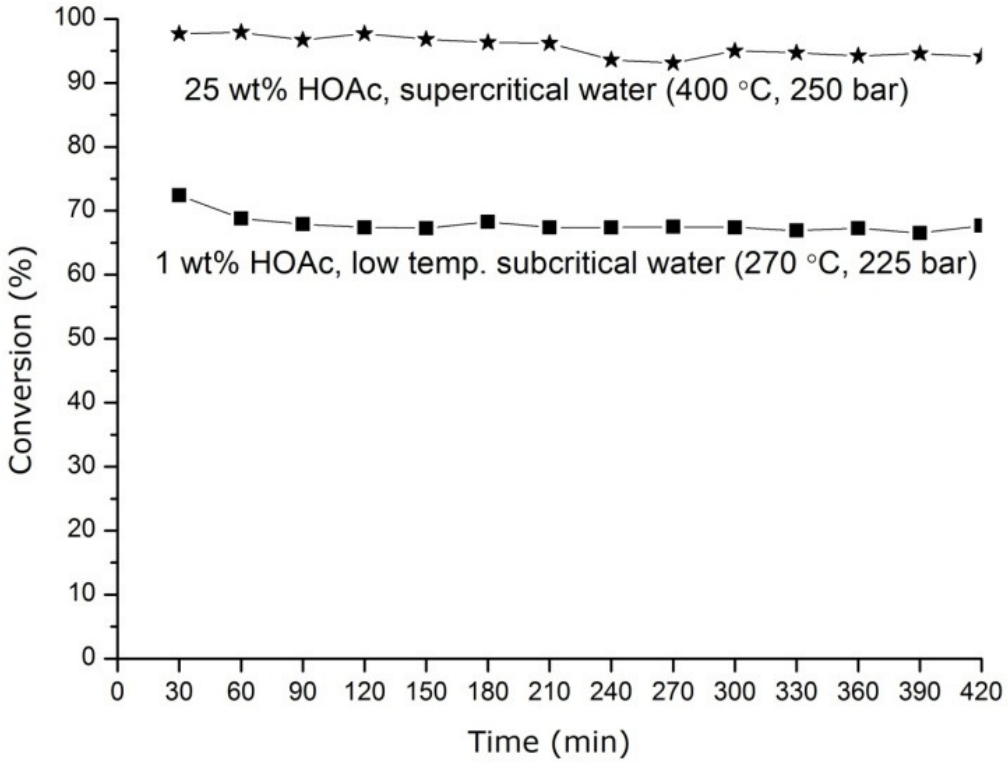

Figure 6.3: Acetic acid reforming in low ionic water over Ru/CNT catalyst. Reforming of 1 wt% HOAc solution in low temperature subcritical water (270 °C and 225 bar) and reforming of 25wt% HOAc solution in supercritical water (400 °C and 250 bar).

The reason for the high acetic acid reforming activity of Ru can be inferred from the (limited) studies on reforming mechanisms in aqueous medium. Hu *et al.* [7] conducted DFT calculations on reforming of formic acid (HCOOH) in gas and aqueous phase over different noble metal surfaces (Pt, Pd, Rh, Au). They showed that the preferred reforming pathway was dependent on the type of reaction medium. In aqueous phase, the formation of aqueous $CHOO^-$ through de-protonation by water is the first step in reforming. The next step is adsorption of the ion on the metal surface, followed by dissociation of the C-H bond to form CO_2. In parallel, the protonated water donates a proton to the catalyst metal surface, where it combines with the hydride subtracted from $HCOO^-$ to form H_2 [7]. If we assume that the mechanism for aqueous reforming of acetic acid, which is a similar type of molecule as formic acid, follows an analogous route as formic acid, we can hypothesize that de-protonated acetic acid (CH_3CHOO^-) adsorbs on the catalyst metal surface, followed by C-C bond breaking to produce CO_2 and adsorbed CH_3^-. The latter can recombine with a proton to form CH_4. This mechanism is basically decarboxylation of acetic acid which is in agreement with Watanabe *et al.* [8]. The rate limiting step during aqueous formic acid reforming is reported [7] to be the recombination of protons and is, dependent of the metal, either limited by proton diffusion or the actual recombination to form molecular H_2. Proton diffusion and H_2 formation rates on Pt are reported to be the fastest of all metals [9]. However, it was shown in this thesis that the acetic acid reforming activity of Ru is much higher than for Pt, implying that diffusion/recombination of protons is not the rate determining step in acetic acid reforming.

The rate determining step in acetic acid reforming is therefore different than during formic acid and must be related to the only mechanistical difference between acetic acid and formic acid reforming. In case of formic acid, the dissociation of the C-H bond of adsorbed H-COO is necessary to achieve complete decomposition and is reported to be facile on Pt and is therefore not rate limiting during formic acid reforming. In case of acetic acid reforming, C-C bond dissociation is required instead of C-H cleavage to achieve decomposition of the respective adsorbed ion (CH_3-COO). From this, we believe that C-C dissociation is rate determining in acetic acid reforming. It is reported [4] that Ru has much higher activity for C-C bond dissociation than Pt and this would explain the observed high APR activity of Ru/CNT for acetic acid. This high activity shown by Ru/CNT makes it a very promising option for commercial applications.

6.3.3 Stability of Ru/CNT

Catalyst stability is a major concern for reforming in sub- and supercritical water. The work described in Chapter 5 shows that Pt/CNT catalyst is stable during supercritical water reforming of acetic acid. Ru/CNT has the advantage of higher activity and at the same time also showed stable APR activity for the conversion of acetic acid under supercritical conditions (400°C, 250 bar, Figure 6.3). However, sub- and supercritical water are considered different reaction regimes due to the extreme differences in water properties [10, 11]. The ionic product in supercritical water is much lower ($Kw=10^{-24}$) than in the supercritical regime. The high ionic product in high temperature subcritical water ($Kw=10^{-11}$) is reported to cause leaching of metals and catalyst stability can be severely affected by this [11]. Carrying out the reaction under the more challenging conditions allows to see if both Ru and CNT remain intact in the catalytic system. Furthermore, reactions at lower temperatures (subcritical water) are favorable for process economics.

First the catalyst was studied for reforming of a 1 wt% acetic acid solution in low temperature subcritical water (270 °C and 225 bar) for 7 h time-on-stream (Figure 6.3). The initial conversion was 72% and decreased marginally to 67 % during the first 30 minutes of the reaction and maintained this conversion for the remainder of the reaction. Under these conditions the ionic product (K_w) is still not very high ($K_w=10^{-13}$).

For practical application, higher oxygenate concentrations are appropriate and in order to get appreciable conversions higher temperatures will be necessary in order to be able to work under industrially relevant residence times (<1 min). However, as the temperatures approach supercritical water conditions the ionic product increases drastically with a maximum around 350 °C ($K_w=10^{-11}$). The good stability of Ru/CNT catalysts in low temperature subcritical water allowed for studying reforming at higher temperatures (still subcritical) to achieve higher activity. Results of such tests are shown in Figure 6.4.

The catalytic reforming of 5 wt% acetic acid (300 °C and 225 bar) showed an initial conversion of 57% but this decreased to 28% after 7 h time-on-stream. The catalyst deactivated and lost more than 50% of its activity. The catalyst was also tested for the reforming of 15 wt% acetic acid in subcritical water at a still higher temperature (340 °C and 225 bar) and the result is shown in Figure 6.4. Almost complete conversion is observed at the beginning of the reaction but decreased to 65% within 4 h time-on-stream.

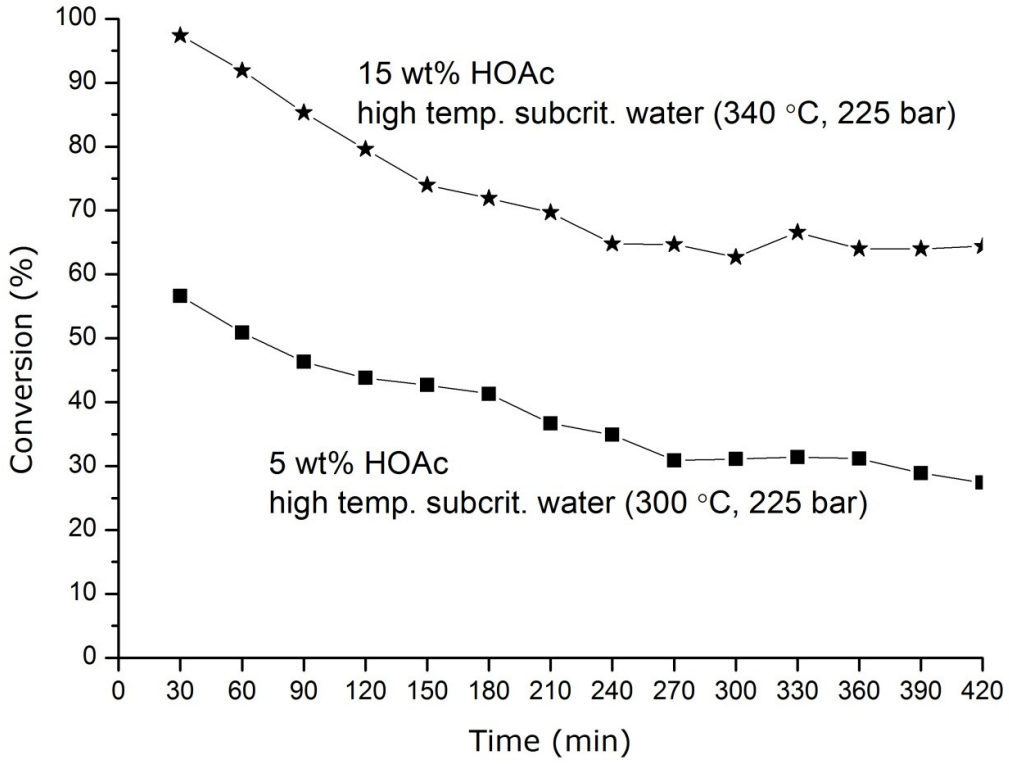

Figure 6.4: Acetic acid reforming in high ionic water over Ru/CNT catalyst. Reforming of 5 wt% HOAc solution in low temperature subcritical water (300 °C and 225 bar) and reforming of 15wt% HOAc solution in supercritical water (340 °C and 225 bar).

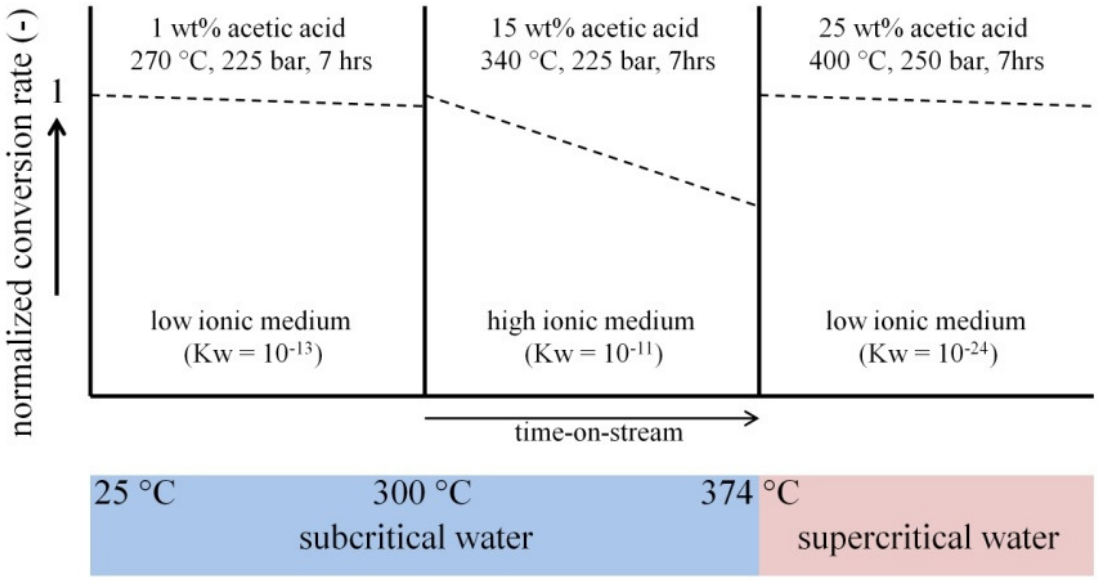

Figure 6.5: Stability of acetic acid reforming (1, 15 and 25 wt%) at different temperatures under 225 bar. The ionic product of water (Kw) under the respective conditions is mentioned in the figure. Activity of the catalyst is normalized with respect to the initial activity.

Deactivation of the Ru/CNT catalyst was observed only during acetic acid (HOAc) reforming in high temperature subcritical water (5wt% HOAc at 300 °C, and 15 wt% HOAc at 340 °C) as summarized in Figure 6.5. This is probably related to the high ion product under those conditions. In general, catalyst deactivation can be related to changes in the support (morphological) and/or active metal (*e.g.* leaching, loss of surface area by sintering or coke deposition, or changes in oxidation state). A detailed analysis of changes in CNT and Ru was taken up and the reasons for deactivation discussed below.

Morphological/structural changes: The obtained BET results of the fresh and used catalysts are shown in Table 6.1. Freshly prepared Ru/CNT showed a comparable surface area as undecorated CNT. Also the used Ru/CNT catalysts showed comparable surface areas as the fresh catalyst, indicating that the surface morphology of CNT was not affected significantly by the reaction environment.

Table 6.1: Surface area of fresh and used Ru/CNT.

Conditions of Ru/CNT catalyst	BET surface area (m^2/g)
Fresh	46.4
Subcritical water reforming (225 bar)	
1 wt% HOAc reforming (270 °C)	40.1
5 wt% HOAc reforming (300 °C)	39.1
15 wt% HOAc reforming (340 °C)	42.3
Supercritical water reforming (250 bar)	
25 wt% HOAc reforming (400 °C)	41.1

HR-SEM images of the fresh and used Ru/CNT catalysts (Figures 6.6-9) were taken to study the effect of the reaction environment on the morphology of the CNT in more detail. The SEM images of the used catalysts do not show any signs of damage to the CNT walls. The openings of the CNT are clearly visible and did not collapse during the reaction and no pitting on the surface of the CNT is observed.

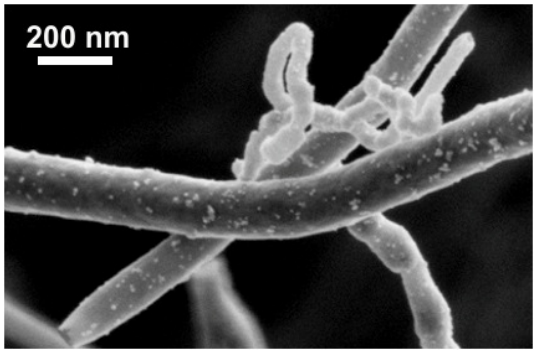

Figure 6.6: HR-SEM image of used Ru/CNT (1 wt% HOAc, 270 °C and 225 bar).

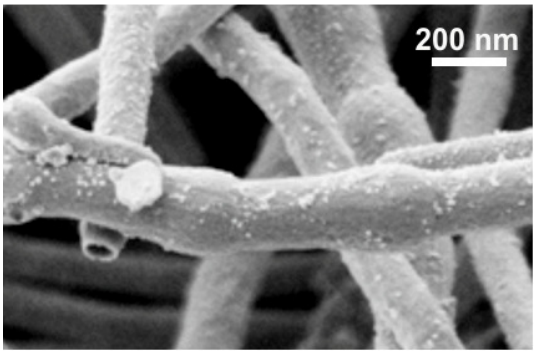

Figure 6.7: HR-SEM image of used Ru/CNT (5 wt% HOAc, 300 °C and 225 bar).

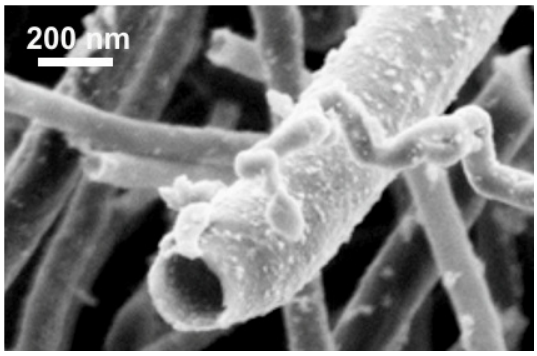

Figure 6.8: HR-SEM image of used Ru/CNT (15 wt% HOAc, 340 °C and 225 bar).

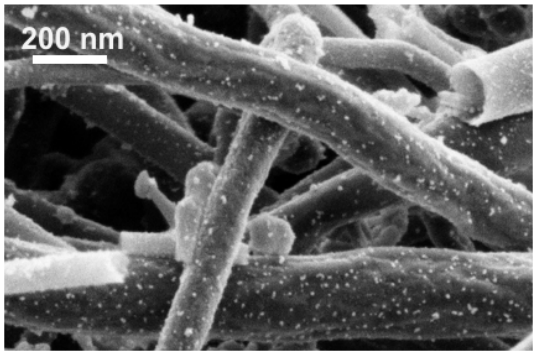

Figure 6.9: HR-SEM image of used Ru/CNT (25 wt% HOAc, 400 °C and 250 bar).

Raman spectroscopy is commonly used to study crystallinity of carbon nano-materials (either fibers or tubes). Raman spectra of the fresh and used CNT are shown in Figure 6.10. No bands were visible below 1000 cm^{-1} and above 3500 cm^{-1} and therefore spectra are only shown in the frequency range of 1000-3500 cm^{-1}. All spectra were normalized to enable a better visual comparison of the peak intensities. Normalization was done based on the most intense band frequency (1556 cm^{-1}) of the fresh Ru/CNT. In the spectra Raman bands observed at 1556 cm^{-1} (G band) and 1340 cm^{-1} (D band) are attributed to defect free and defect induced sp^2 hybridized carbon system, respectively [12]. Intensity ratio of the D, G bands (I_D/I_G) is typically used to assess changes in the crystallinity of graphitic carbon materials. G' band in the spectra (2680 cm^{-1}) is an overtone of D-band [12]. There are four other overtones (2LO, 2G, T+D, D') which are weak and are also not particularly critical for estimating crystallinity of the CNTs and thus are not discussed in detail.

.

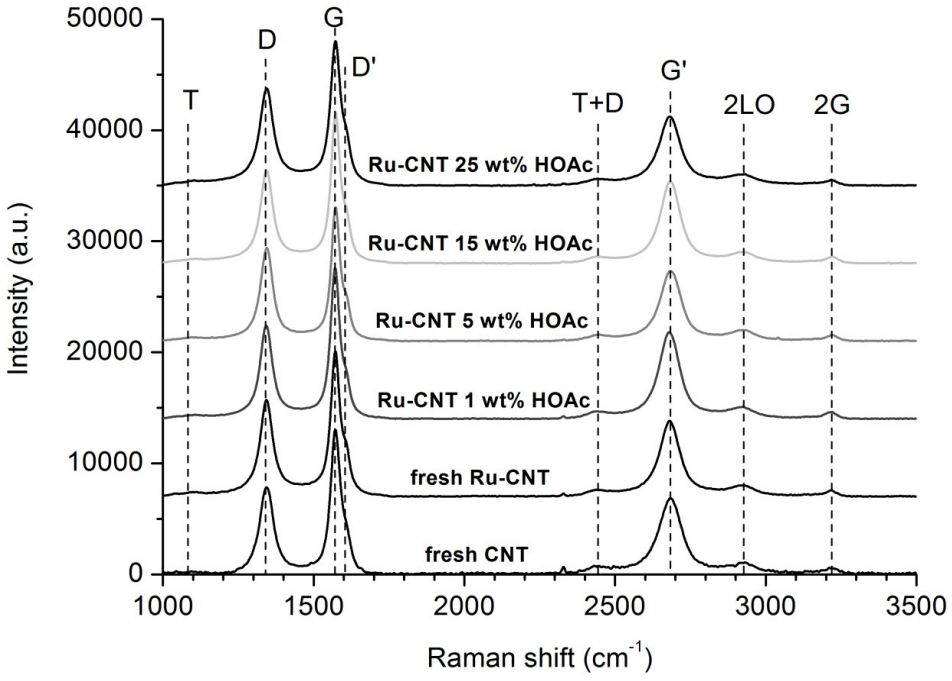

Figure 6.10: Raman spectra of the CNT based catalysts used for acetic acid reforming.

The values of I_D/I_G were determined for the fresh and used CNT based catalysts and are tabulated in Table 6.2. The D/G band intensity ratio is 0.87 for fresh undecorated CNT and a similar number was obtained after decorating the CNT with Ru, indicating that the impregnation method did not induce defects in the CNT structure. The used Ru/CNT catalysts have similar D/G ratios compared to fresh Ru/CNT, showing that exposure of Ru/CNT to acetic acid in sub- or supercritical water did not cause a significant increase in defects in the CNT structure.

Table 6.2: Disorder in the carbon system (Raman spectr. ratio I_d/I_g) and crystallinity (XRD FWHM CNT(002)) of fresh and used Ru/CNT catalysts.

Catalyst	I_D/I_G	FWHM CNT(002)
Fresh CNT	0.87	1.13
Fresh Ru/CNT	0.89	1.15
Ru/CNT in subcritical water reforming (225 bar)		
1wt% HOAc, 270 °C	0.88	1.14
5wt% HOAc, 300 °C	0.89	1.14
15wt% HOAc, 340 °C	0.85	1.16
Ru/CNT in supercritical water reforming (250 bar)		
25wt% HOAc, 400 °C	0.86	1.14

The effect of the reaction on the crystallinity of the CNT was further investigated by X-Ray diffraction (XRD). Figure 6.11 shows the XRD patterns in the 2Θ range of 10-90° for the catalysts. The fresh CNT showed a strong diffraction line at 25° which corresponds to the graphene (002) plane [13, 14]. Further, the strong diffraction line of the CNT (100) plane was observed at 44° in addition to weaker bands above 50°. It can be seen from Figure 6.11 that XRD patterns for the fresh and used CNT based catalysts are similar.

The diffraction line corresponding to the (002) plane originates from the hexagonal sp^2 hybridized carbon network which is considered the building block of CNT [15]. This line is used to study changes in the crystallinity of the CNT by comparing Full-With at Half Maximum (FWHM). A change in FWHM is indicative of structural changes in the grain size and hence a change in crystallinity (line broadening corresponds to loss in crystallinity). The FWHM values of the fresh and used CNT based catalysts are shown in Table 6.2. Similar FWHM values were found for the fresh and used catalysts, indicating that the crystallinity of

the CNT support was not affected by exposure to hot compressed, acidic (acetic acid) water. The results discussed so far show that CNT is a very stable catalyst support material for the full range of studied reaction conditions. This shows the versatility of the material for application in corrosive and aggressive reaction media.

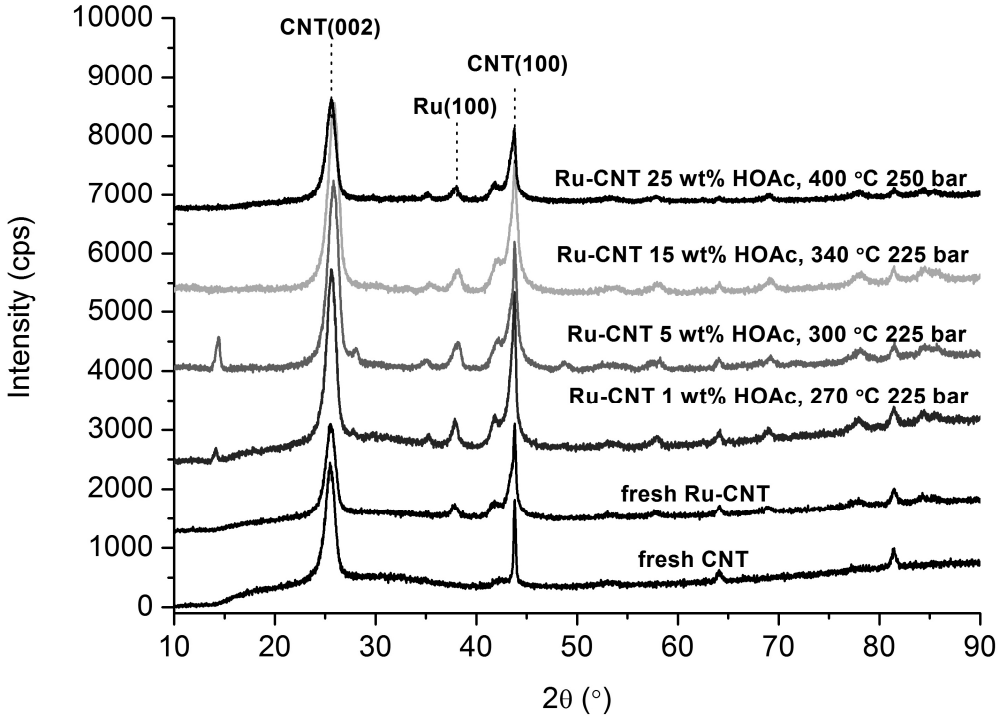

Figure 6.11: XRD patterns of the CNT based catalysts used for acetic acid reforming for 2Θ in the 10-90° range.

Ruthenium leaching: Under the conditions employed in APR, metal leaching can be a common cause for catalyst deactivation. Ru content of the used catalysts was determined by XRF analysis and the results are shown in Table 6.3. It can be seen that the Ru loadings of the used Ru/CNT catalysts were up to 20% lower compared to the fresh catalyst, including the cases where the catalyst performance was stable. These results suggest that Ru leaching took place at the very beginning of the reaction and did not influence catalytic activity.

Typically, Ru loss became more pronounced for the subcritical water experiments at higher temperatures (300 °C, 225 bar). The catalyst deactivation in this case (± 50 % loss in activity during acetic acid reforming, Figure 6.4) cannot be explained fully by the ~10% Ru loss if it is assumed that catalyst activity is proportional to the Ru content. Note that Ru

particle size did not change (Figures 6.2 and 6.7, Table 6.3) during the reaction as discussed in the next section. Furthermore, a 20% Ru loss was observed for the acetic acid reforming experiment in supercritical water, while stable catalytic performances were observed. It is believed that weakly bonded Ru is removed during the startup of the reaction and that the remaining strongly bound Ru is not affected during the reaction itself. Although the initial Ru loss is not seen in the catalytic performance during acetic acid reforming, it probably decreased the starting catalytic activity. Initial Ru leaching can be suppressed by enhancing the anchoring. Functionalization of the CNT support prior Ru impregnation is reported to play an important role in stronger Ru/CNT bonds [16].

Table 6.3: Ru loading of fresh and used Ru/CNT.

Conditions of Ru/CNT catalyst	Ru loading by XRF (wt%)	Ru particle size (nm)
Fresh	11.1	1.8
Subcritical water reforming (225 bar)		
1 wt% HOAc reforming (270 °C)	10.5	1.9
5 wt% HOAc reforming (300 °C)	10.3	1.8
15 wt% HOAc reforming (340 °C)	9.2	1.8
Supercritical water reforming (250 bar)		
25 wt% HOAc reforming (400 °C)	9.3	1.9

Ruthenium sintering: TEM images (Figures 6.2, 6.6-9) showed the stability of the Ru particles during APR. Ru particles ranged from 3-5 nm for fresh catalysts and after use. In the XRD patterns of the catalysts, Ru(100) line at $2\Theta=38°$ [17] was clearly observed (Figure 6.11). Ru particle size calculated based on Scherrer equation (FWHM) showed no appreciable growth of particle size after use. The analysis gave an average Ru particle size of ± 2 nm in all cases, indicating at least that appreciable Ru particle growth did not occur during the reaction in hot compressed, acidic water. Catalyst deactivation by loss of Ru surface area is excluded because sintering/agglomeration of Ru particles was not observed.

Coke formation: Further, coke formation is another problem that is often reported to be the cause of catalyst deactivation, especially during acetic acid steam reforming [18, 19]. The changes in the ratio of Raman spectral bands intensities (I_D/I_G) has been used to follow aromatization (graphitization) when heating poorly organized carbon [20]. Extending this argument, deposition of crystalline or amorphous coke on CNT should change the (I_D/I_G) ratio

of fresh CNT catalyst. No difference in (I_D/I_G) was observed for the deactivated catalyst and therefore coke did not contribute to the deactivation of the studied catalysts. This is not surprising as the high solvability of non-polar compounds (*e.g.* coke) in sub- and especially supercritical water helps in keeping the catalyst surface clean of coke and therefore plays an important role in preventing catalyst deactivation by coking [10, 21].

Deactivation analysis: Reasons for deactivation of Ru/CNT catalyst just below supercritical condition (300-340 °C, 225 bar) needs further attention. In this context, XPS analysis results are shown in Table 6.4. Undecorated CNT have an atomic carbon concentration of ± 99% with oxygen being the remaining 1%. The oxygen is most likely related to oxygenate functional groups on the CNT surface. A small increase in oxygen concentration was observed for freshly prepared Ru/CNT in comparison to undecorated CNT. The oxygen concentration on the surface of the catalysts used for reforming is subcritical water increased significantly compared to fresh Ru/CNT. The catalysts used for supercritical water reforming of 25 wt% acetic acid showed a very low oxygen concentration. A maximum oxygen concentration was found for the experiment conducted at 300 °C with 5 wt% acetic acid. To recall, this is the case where the Ru/CNT showed pronounced deactivation.

The Ru $3d_{5/2}$ peak position in the XPS spectra of fresh and used Ru/CNT catalysts were studied in more detail to determine the oxidation state of Ru. All catalysts showed the presence of Ru^0 (280.5 eV) and Ru^{4+} (281.3 eV). No other Ru oxidation states were observed. The ratio between metallic Ru and Ru^{4+} (Ru^0/Ru^{4+}) was calculated and the values are shown in Table 6.4. It can be seen that the relative amount of metallic Ru decreased for the experiments where the catalyst showed deactivation (300-340 °C, 225 bar) and indicates an increase in oxidized Ru species under those conditions. The experiment conducted in supercritical water (catalyst stable) showed that the oxidation state of Ru on the used Ru/CNT catalyst was more towards the metallic state.

Table 6.4: XPS results of fresh and used Ru/CNT catalysts, showing the atomic surface concentrations (C, O) and oxidation level of Ru.

	Atomic concentration (%)		
	C	O	Ru^0/Ru^{4+}
Fresh CNT	98.95 ±0.14	1.05 ±0.14	-
Fresh Ru/CNT	96.01 ±0.59	3.24 ±0.46	4.0
Ru/CNT in subcritical water reforming (225 bar)			
1 wt% HOAc, 270 °C	92.96 ±1.75	6.23 ±1.79	4.5
5 wt% HOAc, 300 °C	89.64 ±1.29	9.73 ±1.40	3.7
15 wt% HOAc, 340 °C	93.50 ±1.04	5.83 ±0.98	3.3
Ru/CNT in supercritical water reforming (250 bar)			
25 wt% HOAc, 400 °C	96.71 ±0.18	2.87 ±0.16	4.3

Assmann *et al.* reported that catalytically active Ru particles consist of a metallic Ru^0 core which is surrounded by a thin shell of RuO_2 [22]. Deactivation of Ru catalysts is frequently reported under strong oxidizing reaction conditions [23, 24] and is reported to be caused by Ru over-oxidation [24, 25]. Reduction of the deactivated Ru catalyst was conducted to attempt reactivation of the catalyst. The deactivated catalyst was taken out of the reactor and reduced in H_2 (400 °C) and tested again for the reforming of 5% acetic acid. It was found that most of the activity was regained after the reduction treatment (Figure 6.12). This result supports the conclusion that deactivation of Ru/CNT was caused by Ru over-oxidation.

It is not surprising that the Ru/CNT catalyst is more stable in supercritical water than in high temperature subcritical water. The high ion product in high temperature subcritical water causes Ru oxidation of the catalyst by the water. Supercritical water is a milder environment for catalysts due to the lower ion product and also higher coke solubility properties [10, 11]. The low ion product of supercritical water plays a very important role in preventing Ru oxidation of the Ru/CNT catalyst during reforming of very high concentrated acetic acid solutions.

Ru/CNT catalyst showed stable and active catalytic performance for acetic acid reforming in supercritical water and low temperature (≤270 °C) subcritical water. In the next section, catalyst performance of Ru/CNT was studied in more detail for the reforming of acetic acid under those stable regimes.

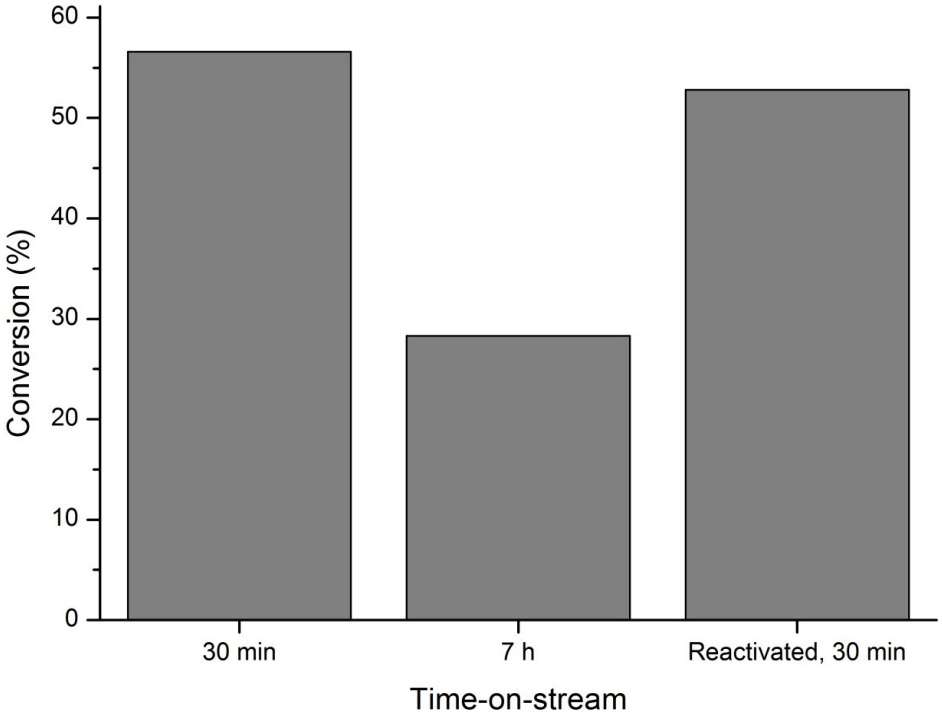

Figure 6.12: Reactivation of the used catalyst by reduction.

6.3.4 Promise of Ru/CNT for APR of acetic acid under commercially relevant conditions

Conditions under which Ru/CNT showed stable catalytic performance, low temperature subcritical water (<270 °C, 225 bar) and supercritical water (400 °C, 250 bar), is interesting in terms of practical applications. Product yields during APR of acetic acid were evaluated for these regimes. Corresponding values for conversions and selectivities are tabulated in Table 6.5. Componental analysis of the liquid reactor effluent by HPLC showed only the presence of unconverted acetic acid. Carbon balances of the reforming experiments were closed within a 5% margin.

During APR, the formation of hydrogen involves reforming and water-gas-shift (WGS). Alkanes on the other hand are formed both *via* decomposition/dehydration of acetic acid as well as methanation of CO_x. It can be seen from Table 6.5 that alkane formation is lower at higher temperatures. This is as expected because reforming is endothermic while WGS and methanation are exothermic reactions.

Table 6.5: Results for the reforming of 1 and 25 wt% acetic acid over Ru/CNT in low temperature subcritical water (195-270 °C, 225 bar) and supercritical water (400 °C, 250 bar), respectively.

Temperature / Pressure (°C / bar)	Gasification Conversion (wt %)	Selectivity (%)			
		H_2	CO_2	CH_4	C_{2+}
195 / 225	3.0	10.9	22.7	77.2	0.1
210 / 225	8.1	5.1	31.9	67.9	0.2
225 / 225	19.1	4.7	38.5	61.3	0.2
240 / 225	33.8	4.8	42.9	56.9	0.2
255 / 225	49.4	5.4	48.4	51.4	0.2
270 / 225	67.5	6.8	48.9	50.9	0.2
400 / 250●	95.4	18.9	62.3	35.8	1.9

● Reforming was performed on 25 wt% acetic acid solution. All other experiments were conducted with 1wt% acetic acid solution.

N.B. Carbon balances of the reforming experiments were complete within a margin of 5%.

Watanabe *et al.* [8] reported that acetic acid reforming in water involves a decarboxylation mechanism in which the alkyl species (CH_x) formed undergoes subsequent reforming / WGS to give hydrogen. From decarboxylation stoichiometry, a CH_4:CO_2 ratio of 1:1 is expected from acetic acid when other reactions are excluded. The formation of higher amounts of methane during reforming indicate that methanation of CO_x occurred (Table 6.5). An increase in CO_2 formation at the expense of CH_4 was observed with increasing temperatures. The selectivities towards CO_2 and CH_4 stabilized around the stoichiometric value expected (50%), indicating that the endothermic reforming became more dominant at higher temperatures.

Figure 6.13 shows the Arrhenius plot which is based on the 1 wt% reforming experiments shown in Table 6.5. Two separate trend lines could be drawn through the data points, indicating separate kinetic regimes. The slope of the linear fit of the data points in the range 240-270 °C is 0.5 times the slope of the fit of the low temperature (195-225 °C) data points. This value is characteristic for catalytic reactions that are affected by internal diffusion limitations. However, the used catalyst CNT support has an open structure and does not have micro or mesopores and therefore internal mass transfer limitations cannot be relevant for this type of support. The observed change is due to a change in kinetics/reactions during the reforming of acetic acid.

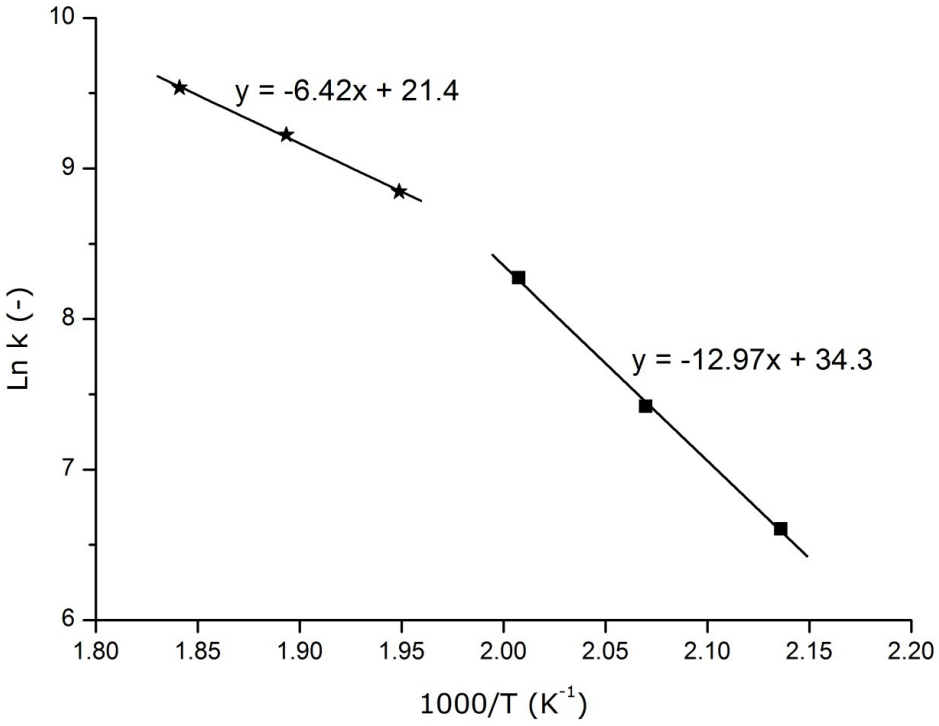

Figure 6.13: Arrhenius plot of catalytic reforming of 1 wt% acetic acid over Ru/CNT catalyst in the temperature range of 195-270 °C and under 225 bar pressure.

An activation energy of 108 KJ mol^{-1} is calculated for the temperature region of 195 – 225 °C. At the lower temperatures, methane formation was also dominant as seen from selectivities (Table 6.5). Reported activation energies in the range of 94 – 224KJ mol^{-1} for CO_2 methanation on Ru-based catalysts shows a large spread [26].

A lower activation energy of 53 KJ mol^{-1} was found for the reforming at higher temperatures. A lower range of activation energies of 55 – 171 KJ mol^{-1} were reported for acetic acid reforming [27] over Ru based catalysts. At the higher temperatures, selectivities approached the expected stoichiometric values of CH_4 and CO_2 for acetic acid reforming by decarboxylation. This shows that methanation of CO_2 species was suppressed at higher temperatures and that acetic acid reforming through decarboxylation was dominant. We suggest that preferences for certain reaction pathways (methanation *vs* reforming) are temperature dependent and the reason for different activation energies at different temperatures.

A CO_2 and CH_4 selectivity of 62 and 36 % was found for supercritical water reforming of 25 wt% acetic acid, respectively. The supercritical water reforming of the high concentrated 25 wt% acetic acid showed a much higher H_2 and CO_2 selectivity compared to the stoichiometric expectance while the CH_4 selectivity was remarkably lower (Table 6.5). These results indicate that methane reforming to produce H_2 and CO_2 took place and is in line with the aforementioned kinetic observations. Based on the acetic acid reforming stoichiometry (50%) and taking into account the production of C_2+ (1.9%), it was calculated that 12.3% of methane was converted to other carbon containing molecules. Complete methane reforming (incl. water gas shift) involves the production of one CO_2 molecule per molecule of CH_4 ($CH_4 + 2H_2O \rightarrow CO_2 + 4\ H_2$). The observed decrease in methane is proportional to the increase in CO_2 and therefore it is possible that methane reforming was a parallel reaction during the supercritical water reforming of acetic acid over Ru/CNT catalyst.

Table 6.6: Comparison of catalytic performance of Pt- and Ru decorated CNT for acetic acid reforming in supercritical water.

	Conversion (%)	**Selectivity (%)**				
		H_2	**CO_2**	**CO**	**CH_4**	**C2+**
Pt/CNT[Chapter 5] 1wt% HOAc, 450 °C and 250 bar	± 58%	18	54	0	42	4
Ru/CNT 25wt% HOAc, 400 °C and 250 bar	± 95%	19	62	0	36	2

The catalytic performance of Pt/CNT for reforming of 1wt% acetic acid in supercritical water (450 °C, 250 bar) was studied in Chapter 5. These results are compared with the performance of Ru/CNT here (Table 6.6). As discussed earlier, the conversion obtained with Ru/CNT is much higher compared to Pt/CNT, while the reaction temperature is 50 °C lower. Alkane selectivities were similar / even marginally lower for a much higher acetic acid concentration (1 *vs* 25 wt%) and at a lower temperature. These observations are remarkable because (i) alkane formation is reported to increase with feed concentrations (Chapter 3 and [28]) and (ii) lower temperatures usually favor methanation. The final aim is to obtain high yields of H_2 but the decarboxylation mechanism of acetic acid reforming, produces alkanes inherently. An integrated or separate methane reforming step is necessary to upgrade hydrogen yields. The Ru/CNT catalyst shows significant methane reforming activity

as described earlier and forms a promising basis for further optimization of the hydrogen yields.

6.4 Conclusions

Catalytic Aqueous Phase Reforming (APR) is an attractive process for reforming of industrially relevant aqueous feeds (up to 20 wt% organics), which typically contain large amounts of acetic acid. In this work, Ru/CNT catalyst was studied for APR of acetic acid and showed promising results. The high ion product of subcritical water in the temperature range 300-340 °C was found to be responsible for deactivation of the Ru/CNT catalyst by over-oxidation of Ru. Deactivation of the catalyst was prevented by performing the reaction in low ionic supercritical water. Stable catalytic properties of Ru/CNT were observed for reforming of acetic acid in supercritical water (400 °C and 250 bar). Under those conditions, Ru/CNT showed very high reaction rates that enabled the conversion of high concentration acetic acid solutions at commercially relevant residence times. The catalytic properties of Ru/CNT are very promising for supercritical water reforming of industrial feeds, such as the aqueous phase of flash pyrolysis oil.

References

[1] R.D. Cortright, R.R. Davda, J.A. Dumesic, Nature 418 (2002) 964-967.

[2] K. Sipila, E. Kuoppala, L. Fagernas, A. Oasmaa, Biomass Bioenerg. 14 (1998) 103-113.

[3] K.I. Gursahani, R. Alcala, R.D. Cortright, J.A. Dumesic, Appl. Catal. A 222 (2001) 369-392.

[4] R.R. Davda, J.W. Shabaker, G. W. Huber, R. D. Cortright, J. A. Dumesic, Appl. Catal. B 43 (2003) 13-26.

[5] T. Kondo, Y. Iwasaki, Y. Honma, Y. Takagi, S. Okada, J. Nakamura, Phys. Rev. B 80 (2009) 233408.

[6] P.W. Sutter, J.I. Flege, E.A. Sutter, Nature 7 (2008) 1485-1492.

[7] C. Hu, S-W. Ting, K-Y. Chan, W. Huang, Int. J. Hydrog. (2012) In Press, DOI: 1016/j.ijhydene.2012.08.035

[8] M. Watanabe, H. Inomata, R.L. Smith jr., K. Arai, Appl. Catal. A 219 (2001) 149-156.

[9] L. Kristinsdottir, E. Skulason, Surf. Sci. 606 (2012) 1400-1404.

[10] J. Kritzer, E. Dinjus, Chem. Eng. J. 83 (2001) 207-214.

[11] J. Kritzer, J. Supercrit. Fluid. 29 (2004) 1-29.

[12] M.S. Dresselhaus, G. Dresselhaus, R. Saito, A. Jorio, Phys. Rep. 409 (2005) 47-99.

[13] S. Collins, R. Brydson, B. Rand, Carbon 40 (2002) 1089-1100.

[14] K. Ishimaru, T. Hata, P. Bronsveld, T. Nishizawa, Y. Imamura, J. Wood. Sci. 53 (2007) 442-448.

[15] A. Aqel. K.M.M.A. El-Nour, R.A.A. Ammar, A. Al-Warthan, Arab. J. Chem. 5 (2012) 1-23.

[16] P. Serp, M. Corrias, P. Kalck, Appl. Catal. A 253 (2003) 337-358.

[17] T.K. Lin, S.J. Chang, B.R. Huang, K.T. Lam, Y.S. Sun, M. Fujita, Y. Horikoshi, J. Electrochem. Soc. 153 (2006) G677-G680.

[18] K. Takanabe, K. Aika, K. Seshan, L. Lefferts, Chem. Eng. J. 120 (2006) 133-137.

[19] D. Wang, D. Montane, E. Chornet, Appl. Catal. A 143 (1996) 245-270.

[20] D. Espinat, H. Dexpert, E. Freund, G. Martino, M. Couzi, P. Lespase, F. Cruege, Appl. Catal. 16 (1985)

[21] J.B. Muller, F. Vogel, J. Supercrit. Fluid. 70 (2012) 126-136.

[22] J. Assmann, D. Crihan, M. Knapp, E. Lundgren, E. Loffler, M. Muhler, V. Narkhede, H. Over, M. Schmid, A.P. Seitsonen, P. VArga, Angew. Chem. Int. Ed. 44 (2005) 917-916.

[23] N.W. Cant, P.C. Hicks, B.S. Lennon, J. Catal. 54 (1978) 372-383.

[24] K. Villani, C.E.A. Kirschhock, D. Liang, G. van Tendeloo, J.A. Martens, Angew. Chem. Int. Ed. 45 (2006) 3106-3109.

[25] J. Assman, V. Narkhede, N.A. Breuer, M. Muhler, A.P. Seitsonen, M. Knapp, D. Crihan, A. Farkas, G. Mellau, H. Over, J. Phys. Condens. Matter 20 (2008) 184017.

[26] P. Panagiotopoulou, D.I. Kondarides, X.E. Verykios, Appl. Catal. B 88 (2009) 470-478.

[27] A.C. Basagiannis, X.E. Verykios, Int. J. Hydrogen Energ. 32 (2007) 3343-3355.

[28] R.R. Davda, J.A. Dumesic, Angew. Chem. Int. Edit. 42 (2003) 4068-4071.

Chapter 7

APR of real aqueous phase of flash pyrolysis oil over Ru/CNT catalyst

In this chapter, supercritical water reforming (400 °C and 250 bar) of a diluted feed stream of the aqueous phase of flash pyrolysis oil is studied over Ru/CNT catalyst. It was found that the reaction conditions caused significant coke/char formation in the preheater. Formation of such carbonaceous material was likely catalyzed by the high ionic product of the subcritical water regime in the preheater. Highly diluted feeds were necessary to prevent blockage of the preheater by coke, but coke formation was still significant under these conditions and prevented the assessment of the Ru/CNT catalyst. Coke formation is a non-catalytic challenge and should first be solved before this process can be studied further.

7.1 Introduction

Catalytic APR of the aqueous phase of flash pyrolysis oil is an interesting route for the production of renewable hydrogen [1]. A major concern for the feasibility of this process is the availability of stable catalysts with commercially relevant activities [2]. Performing the APR reaction in supercritical water is necessary to achieve commercially relevant reaction rates (Chapter 3 and 6) by providing the necessary thermal energy and allowing fast mass transfer rates [2]. Furthermore, the stability of catalysts benefits from the low ionic product (Chapter 6) and the coke solvability properties of supercritical water.

Conventional metal oxide catalyst supports are studied frequently for APR because they enable high reforming rates by providing hydroxyl groups which are required for the bi-functional reforming mechanism. For instance, it was shown in this thesis that reforming rates for ethylene glycol were much higher for Pt supported on Al_2O_3 (Chapter 3) compared to carbon (Chapter 5). Alumina is considered one of the most stable metal oxide catalyst supports but Al_2O_3-supported APR catalysts were found to deactivate in presence of acetic acid (Chapter 4). Many commercially interesting feeds contain large amounts of acetic acid. For instance, acetic acid is a major component of pyrolysis oil with concentration above 10 wt% [3, 4]. Therefore conventional alumina supported catalysts are not suitable for APR of such feeds. High surface area carbon is a more stable catalyst support in the presence of acetic acid. However, the micro- and mesoporous structure of this type of carbon support is very susceptible to deactivation by pore blockage by coke [5]. Coke formation during acetic acid reforming is reported frequently [6, 7] and therefore this type of support is also not suitable for reforming of the aqueous phase of pyrolysis oil.

It was demonstrated in Chapter 5 and 6 that carbon nanotubes (CNT) are very stable in supercritical water, even in the presence of high concentrations of acetic acid. Furthermore, the open structure of CNT helps to (i) prevent catalyst deactivation by coke pore blockage and (ii) enables high mass transfer rates. CNT supported Ni, Pt and Ru catalysts were studied for APR of acetic acid (Chapter 5 and 6) in supercritical water. It was found that only Pt and Ru decorated CNT were stable for this reaction. Pt showed a lower activity towards acetic acid reforming (Chapter 5). However, Ru/CNT catalyst showed commercially interesting acetic acid reforming rates (Chapter 6). The properties of the developed Ru/CNT catalyst paved the way for APR of commercially applicable bio/organic feeds. APR of the aqueous phase of

flash pyrolysis oil was studied in supercritical water over Ru/CNT catalyst and the results are described in this chapter.

7.2 Experimental

7.2.1 Catalyst preparation and characterization

CNT supported Ru catalysts were prepared according section 2.2.2. The Ru/CNT catalyst used for the study in this Chapter was taken from the same batch as used in Chapter 6. Therefore, catalyst characterization details (XRF, BET, SEM imaging, XRD, XPS and Raman spectroscopy) can be seen in chapter 6. Further details regarding catalyst characterization are discussed in section 2.3, Chapter 2.

7.2.2 Supercritical water reformer

The experimental setup and applied definitions are described in detail in Chapter 2. A 2mL. min^{-1} flow of the respective feed was first preconditioned to operating conditions (400 ºC and 250 bar) before it entered the reactor in which 0.1 gr of Ru/CNT catalyst was placed.

7.2.3 Fractionating flash pyrolysis oil

Pyrolysis oil was obtained from the TCCB group (University of Twente, The Netherlands) and was produced by VTT Technical Research Centre of Finland. Figure 7.1 shows the fractionation process of the pyrolysis oil. The pyrolysis oil was extracted with water (volume ratio water:oil = 10 : 1) to remove the water soluble fraction of the oil. The obtained water fraction is referred to as aqueous phase. The aqueous phase was filtered until a clear liquid was obtained. Brown particles were formed in the following days (probably by agglomeration of very small particles that were not removed during filtration) and therefore the liquid was again filtered after two weeks. The liquid phase stayed clear after this second filtration but as a precaution was filtered again before it was used for the reforming reaction. The carbon content of the water phase was determined by TOC analysis just before the

reforming experiment and was found to be 26.0 g / L. The pH of the aqueous solution was 2.8, indicating the presence of large amounts of carboxylic acids.

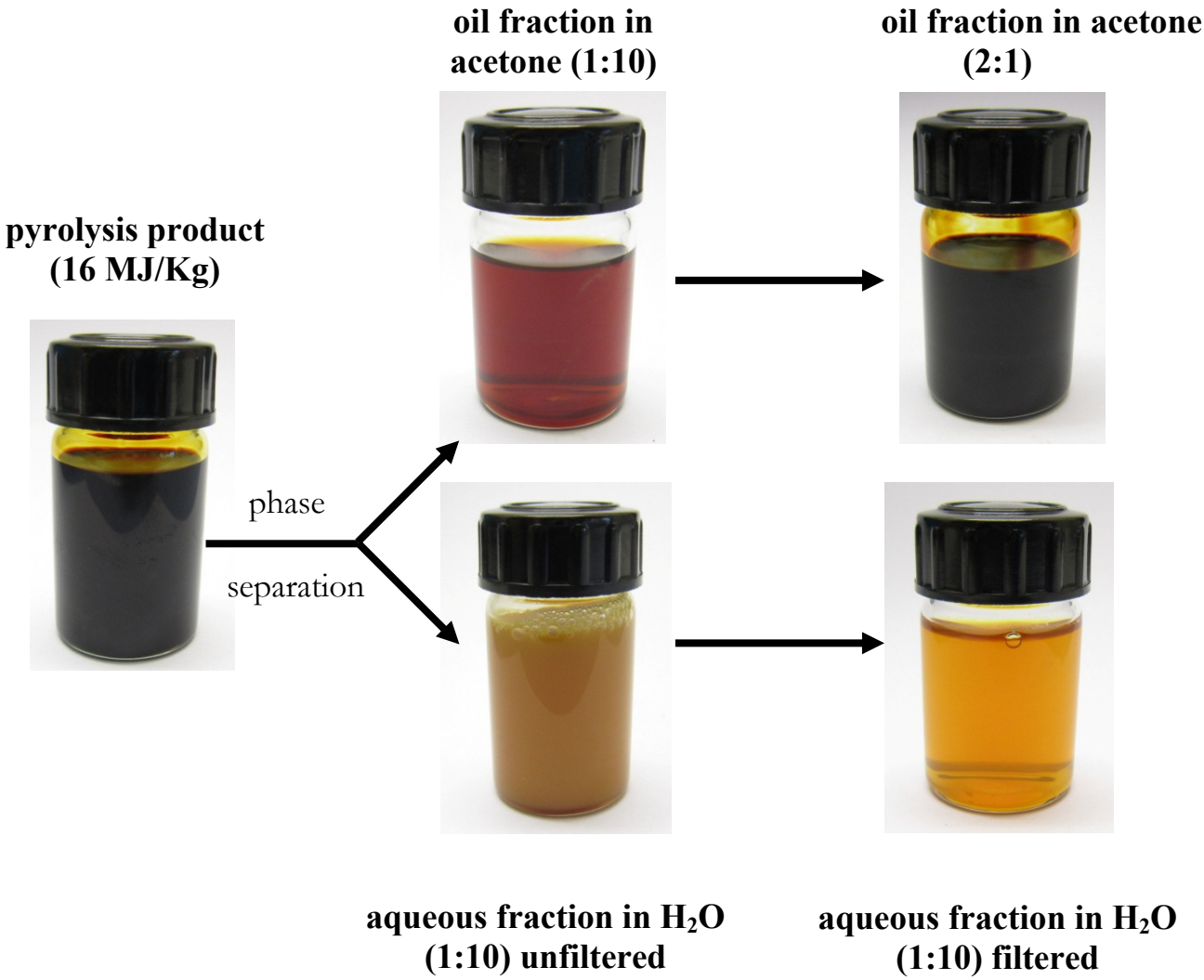

Figure 7.1: Fractionating of pyrolysis oil in aqueous and organic phase.

The organic phase was very sticky and had a very high viscosity. Acetone was used to dilute the organic phase to decrease the viscosity to enable handling of the material for further characterization. The energy content of the pyrolysis product (incl. the aqueous phase) was determined by bomb calorimetry to be 18 MJ. Kg^{-1}. After fractionation, the energy content of the organic phase showed to be 28 MJ. Kg^{-1} (this value is minus the acetone dilution). The energy value of the organic phase is still much lower than crude oil and shows the need for

further upgrading, for instance by hydrogenation. Hydro-deoxygenation, where the oxygen content of the oil is reduced by hydrotreating, helps to improve the qualities of the organic phase, *viz*., (i) decrease acidity by removing acidic components, (ii) improve stability by minimizing aldehydes and ketones, which have the tendency to polymerize during storage, and (iii) improve hydrogen content (H/C ratio) of the organic phase and improve its energy content. This is the background purpose of the current study where it is attempted to generate hydrogen required for the hydrotreating from the aqueous waste, *via* aqueous phase reforming.

7.3 Results and discussion

Supercritical water reforming (400 ºC and 250 bar) of the aqueous phase (water:oil=10 : 1) was first studied in the absence of a catalyst. But the experiment had to be stopped after 1 h due to a large pressure drop between the pump and the inlet of the reactor. Inspection of the setup showed that the preheater was blocked by coke. Coke was also observed on the walls of the reactor but was much less than the amounts present in the preheater. The compounds in the aqueous phase of pyrolysis oil were highly functionalized [8] and it is believed that the conditions in the preheater propagated polymerization reactions leading to coke formation. Gas phase analysis showed the formation of large amounts of CO_x (70% CO_2 and 10% CO in gas product), indicating that coke formation involved decarboxylation and/or decarbonylation [9, 10].

Carbonaceous material can be formed (i) thermally, or (ii) catalytically by the metal of the preheater wall, or (iii) catalytically by the high ion product of the subcritical water in the preheater. The fact that coke was formed in the largest quantity in the preheater indicates that the first two reasons can be excluded and that coke formation was likely initiated by the (subcritical) water properties in the preheater. The preheater brings the feed to supercritical water conditions (> 374 °C and 221 bar) and has to go through the subcritical regime to reach the supercritical state. The ionic product of subcritical water increases with temperature and reaches a maximum of $K_w=10^{-11}$ around 300-350 °C [11]. The high ionic product of subcritical water is reported to catalyze many reactions, including acid/base catalyzed decarboxylation [12, 13] and coupling/polymerization reactions [13], and might be the reason for the high amounts of coke formed in the preheater. Supercritical water has a low ionic

product ($Kw=10^{-24}$) and is a good solvent for non-polar compounds such as coke [11]. Therefore, coke formation in parts of the setup that operate under supercritical water conditions is expected to be lower and this is in agreement with the experimental observations. Coke formation was not observed during reforming of ethylene glycol and acetic acid (Chapter 3 - 6), indicating that other molecules in the aqueous phase are likely more susceptible to form coke.

The aqueous phase was diluted even more (water:oil=30 : 1) to suppress the formation of coke to prevent coke blockage of the preheater. This feed was again used for reforming in supercritical water (400 ºC and 250 bar). A blank experiment (without catalyst) was first conducted to study coke formation and gasification activities. No significant pressure drop was observed during 6 h reaction time. The results of the blank reforming experiment are shown in Table 7.1. The gas formed was again very high in CO_x (Table 7.1). Analysis of the reactor effluent showed that 49% of the carbon in the feed remained in the liquid phase after the reforming reaction. Carbon in gas phase accounted for 11% of removed carbon from the feed, resulting in a carbon balance closure of only 60%. The missing 40% of carbon was transformed to coke. Inspection of the setup after the reaction revealed that coke deposition took place during the experiment on the walls of the preheater and the reactor. However, the quantity of coke was not near enough to cause blockage. Not all coke formed accumulated in the setup. The liquid reactor effluent showed the presence of many black particles which sank to the bottom of the glass vessel. These particles were likely coke that was dissolved initially in the supercritical water and came out of the solution when the conditions were relieved.

Table 7.1: Reforming of aqueous phase of bio oil (water:oil=30) at 400 °C and 250 bar over Ru-CNT catalyst.

Reaction	Carbon removed from liquid (%)	Selectivity gas phase (%)				
		H_2	CH_4	C_2+	CO_2	CO
Blank	51% (11% gas, 40% coke)	12.7	8.5	0.9	67.5	23.1
Ru-CNT 30 min	54% (28% gas, 26% coke)	5.4	9.7	0.7	69.8	19.8
Ru-CNT 6 hr	50% (26% gas, 25% coke)	5.6	11.1	0.7	67.8	20.5

Catalytic reforming over Ru/CNT catalyst was studied next under the same reaction conditions and the results are shown in Table 7.1. A similar amount of carbon was removed from the liquid feed during the catalytic reaction compared to the blank experiment. However, the use of Ru/CNT catalyst increased the amount of gas produced and reduced the amount of coke formed. The composition of gas formed were stable during 6 h time-on-stream. It is difficult to assess catalyst performance when coke is formed in such large quantities. These results indicate that a great engineering challenge exists in preventing coke formation in the preheater and reactor. This problem should first be overcome before the catalytic performance of the Ru/CNT catalyst can be tested reliably.

After the reaction, an attempt was made to remove the catalyst from the reactor for analysis. Both the preheater and the reactor showed the presence of significant amounts of coke. No visible distinction could be made between the coke and the carbon-based catalyst after removal of these solids and post mortum analysis of the catalyst was therefore not possible.

7.4 Conclusions

The catalytic performance of Ru/CNT for supercritical water reforming (400 °C and 250 bar) of the aqueous phase of flash pyrolysis oil was studied. Coke was formed during the reaction and caused blockage of the preheater when mildly diluted feeds were used. Coke formation was likely catalyzed by the high ionic product of the subcritical water regime in the preheater and involved decarboxylation and decarbonylation reactions. Highly diluted feeds were necessary to prevent coke blockage of the preheater during a 6 h experiment. However, even under those conditions, coke formation was significant and prevented an assessment of the catalytic performance of Ru/CNT. Coke formation outside the catalyst zone is a challenge for reactor design and should first be solved before a catalytic process can be applied further.

References

[1] R.D. Cortright, R.R. Davda, J.A. Dumesic, Nature 418 (2002) 964-967.

[2] Y. Guo, S.Z. Wang, D.H. Xu, Y.M. Gong, H.H. Ma, X.Y. Tang, Renew. Sust. Energ. Rev. 14 (2010) 334-343.

[3] K. Sipila, E. Kuoppala, L. Fagernas, A. Oasmaa, Biomass Bioenerg. 14 (1998) 103-113.

[4] A. Demirbas, Fuel Process. Technol. 88 (2007) 591-597.

[5] N.Z. Muradov, T.N. Veziroglu, Int. J. Hydrogen Energ. 30 (2005) 225-237.

[6] K. Takanabe, K. Aika, K. Seshan, L. Lefferts, Chem. Eng. J. 120 (2006) 133-137.

[7] D. Wang, D. Montane, E. Chornet, Appl. Catal. A 143 (1996) 245-270.

[8] D. Mohan, C.U. Pittman, P.H. Steele, Energ. Fuels 20 (2006) 848-889.

[9] M. Watanabe, H. Inomata, R.L. Smith Jr., K. Arai, Appl. Catal. A 219 (2001) 149-156.

[10] J. Gornay, L. Coniglio, F. Billaud, G. Wild, J. Anal. Appl. Pyrolysis 87 (2010) 78-84.

[11] J. Kritzer, J. Supercrit. Fluid. 29 (2004) 1-29.

[12] S. E. Hunter, P.E. Savage, Chem. Eng. Sci. 59 (2004) 4903-4909.

[13] N. S. Kus, Tetrahedron 68 (2012) 949-958.

Chapter 8

Evaluation and concluding remarks.

The thesis is concluded in this chapter. The first part of this chapter evaluates the developed catalytic aqueous phase reforming (APR) technique. APR is compared with conventional steam reforming (SR) in terms of energetics, thermodynamics, catalysis and material considerations. APR of bio/organic feeds in supercritical water showed to be favored above SR. Furthermore, the conceptual integration of the APR process in a bio-refinery is assessed with respect to hydrogen economics. The main achievements of the work described in this thesis are assessed in the second part of this chapter with respect to commercial relevance and future challenges. The developed Ru/CNT catalyst shows commercially attractive properties for APR of bio/organic feeds in supercritical water. However, current non-catalytic challenges with APR of the aqueous fraction of pyrolysis oil prevent feasible exploitation of this process. It is projected that the APR technology developed in this thesis is applicable for reforming of other bio/organic aqueous waste streams that are produced in large quantities in the paper and food industry.

8.1 Evaluation of aqueous phase *vs* steam reforming

Steam Reforming (SR) [1-3] and Aqueous Phase Reforming (APR) [4-6] are two processes that are studied frequently for gasification of the aqueous fraction of bio-oil. SR is the more conventional process which is already being applied in industry for decades (*e.g.* steam reforming of natural gas) [7-8]. SR of aqueous feeds (>80 wt% water) is subjected to a few issues that led to the development of the APR process [4, 9]. For instance, SR of aqueous feeds is reported to be economically unfeasible because of their high water contents and the energy required to carry out the reforming in gas phase [9]. This problem is overcome in APR by keeping the water in the liquid phase by applying elevated pressures.

Furthermore, SR and APR conditions have very different thermo-physical properties that affect catalysis differently. For instance, the phase of the reaction medium can affect mass transfer rates and catalyst stability [10-11]. In this section, SR and the developed catalytic APR techniques are compared and evaluated in terms of energetics, thermodynamics, catalysis and technological challenges.

Energetics: Commercially interesting bio-feeds typically have water contents typically > 80 wt% [12]. SR of suchs streams is commonly performed at temperatures of 700 °C and 30 bar pressure [13]. It was shown in Chapter 6 that near complete conversion of such streams can be accomplished in APR at a temperature of 400 °C and 250 bars pressure. Steam tables [14] were used to determine system enthalpies for SR and APR at those relevant reaction conditions (SR: 700 °C and 30 bar, and APR: 400 °C and 250 bar) to compare energetics of both processes.

It was calculated, that an energy of 3.7 MJ is required to condition 1 kg of water from ambient (25 °C, 1 bar) to gas phase SR conditions (700 °C and 30 bar), while only 2.6 MJ is required to bring 1 kg of water to APR conditions (400 °C and 250 bar). It should be taken into account that these calculations were based on water only and that conditioning of oxygenates in the feed should also be considered. The majority of typical oxygenates (*e.g.* ethanol, glycerol, acetic acid) found in commercially interesting feeds have Enthalpies of Vaporation that are similar to water [15] and therefore the energetic calculations performed for pure water do not have to be adjusted for this parameter. Another parameter involved in these calculation are the specific heat capacities, which for oxygenates are typically half the value of that for water. Based on the aforementioned considerations, it was calculated that a

20 wt% oxygenate feed would require an energy of 3.3 MJ/Kg to bring it to SR conditions and 2.3 MJ/Kg in case of APR. These calculations show that energetics favor APR conditions above that for SR. Furthermore, produced hydrogen is sometimes used for applications that require pressurized hydrogen [16-17]. Hydrogen produced during APR is already pressurized and this eliminates some of the energy required for the compression of the hydrogen for the respective application.

Thermodynamics: The different reaction conditions of SR (700 °C) and APR (400 °C) cause that different products are thermodynamically favored per technique. Reforming of oxygenates results in the production of CO, which consequently can undergo (i) methanation or (ii) water gas shift (WGS). The aim of this process is to produce H_2 and therefore methanation (hydrogen consumption) is undesired, while WGS is desired.

Luo *et al.* [18] calculated thermodynamics for APR of different oxygenates, taking into account reforming, (reversed) water gas shift ((R)-WGS) and methanation reactions. They calculated that low temperature (227 °C) APR favors the formation of undesired methane by methanation of CO. An increase in temperature makes the exothermic methanation reaction less favorable, favoring the formation of H_2 and CO. In addition, CO formation at higher temperatures becomes even more favored due to the endothermic reforming and R-WGS reaction.

The slightly exothermic WGS reaction plays an important role in achieving maximum hydrogen yields but becomes less favorable to form hydrogen at higher temperatures. The methanation reaction (H= -206.2 KJ/mol) is more exothermic in nature than WGS (H= -41.1 KJ/mol) and therefore an increase in temperature has a larger influence on methanation equilibrium than WGS. Maximum hydrogen yields are favored in the situation where the reaction temperature is high enough to suppress methane formation but on the other hand is low enough to favor hydrogen formation by WGS. It was shown by Lu *et al.* [19] that H_2 and CO_2 formation was favored around 500 °C during supercritical water reforming of glycerol. The APR studies described in this thesis were performed in a similar temperature range and hence in a thermodynamically favored environment for hydrogen production.

The high temperatures typically applied in SR suppress (i) methane formation by COx methanation and (ii) hydrogen formation by WGS. Hence, conditions used for SR favor the formation of H_2 and CO [20-21].

Mass transfer rates and residence times: Diffusion rates are very important for catalysts as they control the amount of reactants supplied to the catalytic sites. Slow diffusion rates might result in low reforming rates, while the full catalytic potential of the catalyst is not used. SR is performed in gas phase and diffusion rates in gas are much higher than in water. No reports were found that SR of aqueous feed stocks was limited by mass transfer.

However, it was reported by Shabaker *et al.* [22] that reforming of a 10 wt% ethylene glycol feed under APR conditions (225 °C and 30 bar) was subjected to diffusion limitations. Mass transfer problems were overcome by working in supercritical water (>374 C and 221 bar). The density of supercritical water is much lower than water under ambient conditions and therefore diffusion rates are higher [10-11]. Mass transfer rates were sufficiently high during the supercritical water reforming experiments that are described in this thesis. Near complete gasification was obtained at commercially relevant residence times during supercritical water APR of (i) 15 wt% ethylene glycol (Chapter 3) and (ii) 25 wt% acetic acid feed (Chapter 6). Supercritical water is important to achieve the required diffusion rates that are necessary to obtain high gasification rates at low residence times.

Residence times in the catalytic bed indicate the time that reactants are subjected to catalysts. Long residence times are economically unattractive because they result in either (i) higher amounts of catalysts necessary (and hence the need for a bigger reactor) or (ii) lower feed throughput and hence lower product yields. Commercially attractive residence times for SR of aqueous streams are typically in the order of seconds [23]. It was calculated for APR of a 25 wt% acetic acid feed (Chapter 6) that near complete gasification was obtained at a residence time of 3 seconds when the reaction was carried out at 400 °C (250 bar, water density ~150 g/L). Hence, APR can be performed at similar residence times as SR and APR is therefore very promising in this respect for commercial application.

Catalyst stability: A very important factor in catalysis is the stability of the catalyst. Catalyst instability is a common problem in SR [24-27]. The high temperature (~700 °C) used for SR is frequently reported to induce sintering of the catalytic metal particles and the consequent loss in catalytic surface area causes catalyst deactivation [24-25]. Particle growth does not only result in lower catalytic activities but it can also change product selectivities [28]. Sintering in APR is less of an issue due to the lower reaction temperatures used.

Another serious problem during SR is formation and deposition of carbonaceous species on the catalyst, which causes blockage of catalytic sites and hence deactivation of the

catalyst [26-27]. Coke formation was not observed during APR of ethylene glycol and acetic acid (Chapter 5 and 6) as a result of the solvation properties of hot compressed water, which increase for non-polar compounds with increasing temperature [29]. The solvation properties of supercritical water are comparable to dichloromethane and hence inherent coke solvability in this medium is high [29]. Furthermore, the high diffusion rates in supercritical water ensure that dissolved coke is directed away from the catalyst [10, 29]. Although coke solvability in supercritical water is inherently high, it should be taken into account that the amount of coke that can be dissolved is limited by the low density of supercritical water. These considerations indicate that APR has a big advantage over SR in preventing catalyst deactivation by coke.

On the other hand, problems with catalyst deactivation in APR are also observed and are related to process conditions which are not applicable for SR [Chapter 4 and 6]. Hydroxylation of conventional alumina catalyst support was observed during APR of acetic acid (275 °C and 200 bars) and was attributed to increased acidity of acetic acid under these conditions (high ionic product). The hydroxylated alumina was found to migrate and deposit on catalytic sites, resulting in a total coverage of these sites and thereby making them inaccessible for reactants. The aforementioned mechanism results in deactivation of the catalyst as discussed in Chapter 4. Furthermore, Ru/CNT catalyst deactivated during acetic acid reforming in high temperature subcritical water (300 – 350 °C, 225 bars) as discussed in Chapter 6. It was found that the high ionic product of subcritical water caused over-oxidation of Ru and thereby causing deactivation the catalysts. Performing APR in supercritical water overcame these problems due to the much lower ionic product of this medium. Based on these arguments, it can be concluded that APR in supercritical water is preferred in warranting catalyst stability.

Material considerations: The stability of materials used for the experimental setup is much more challenged under APR conditions than under SR [30]. The high ionic product of subcritical water is known to cause material failure by corrosion/leaching induced cracking [30]. These problems are not observed in supercritical water because the ionic product is much lower in this regime [30]. However, the presence of oxidizing agents (especially, halogen-based inorganic oxidizers) in supercritical water is reported to cause severe corrosion of the majority of materials [30]. However, strong oxidizers are not expected to be present in bio/organic feeds. Furthermore, it was also reported [30] that stable/inert materials exist for every supercritical water application. Due to the reason described above, APR of bio/organic feeds in supercritical water is expected not to be a problem with respect to material stability.

However, it should be noted that supercritical water setups always have parts that operate under subcritical water conditions. Finding materials with long term stability in subcritical water is believed to be one of the challenges of this reaction. Material choice is therefore a very important factor in APR.

The comparison of energetic, thermodynamics, catalysis and material consideration for typical APR and SR conditions were evaluated and showed that APR is preferred for reforming of bio/organic feeds as long as the reaction is carried out in supercritical water.

8.2 Evaluation of APR integration with Bio-refinery

Fractionation of the pyrolysis oil in an organic and aqueous phase is the first step in obtaining high heating value bio-oil. The next step to upgrade the heating value involves de-oxygenation of the organic phase with hydrogen. APR of the aqueous phase of pyrolysis oil is an interesting route to produce the required hydrogen for de-oxygenation of the organic phase. A concept for the integration of APR in a bio-refinery was proposed in Chapter 1 (Figure 1.3). In this section, this concept is evaluated in terms of hydrogen economics. The maximum amount of hydrogen that can be obtained theoretically by APR of the aqueous feed is compared with the amount of hydrogen required to upgrade the bio-oil fraction to commercial relevant heating values. Venderbosch *et al.* [31] published an overview of the composition of a typical bio-oil and these values will be used for the evaluation of this concept. The relevant data is summarized in Table 8.1.

Table 8.1: Composition of a typical bio-oil [31].

component	fraction wt%	average molecular composition (wt%)		
		C	H	O
Water soluble				
Acids, Alcohols	10	36	6	58
Ether-solubles	10	60	6	34
Ether-insolubles	30	46	6	48
H_2O	25	-		
Water insolubles	25	66	7	27

It can be seen from Table 8.1 that 25 wt% of the pyrolysis oil is the desired organic phase that is of interest for the production of liquid bio-fuels. The remaining 75 wt% consists of low heating value and water soluble compounds (oxygenates + H_2O), and is referred to as the aqueous fraction. The oxygenates account for 50 wt% of the pyrolysis oil and these have a weight averaged composition of C=46.8, H= 6.0 and O=47.2 %. The oxygenates in the aqueous phase are of interest for hydrogen production by APR.

First, it is calculated how much hydrogen can be formed during APR of the aforementioned feed. The assumption is made that maximum hydrogen yields are achieved during APR and this implies that (i) all hydrogen atoms in the oxygenate recombine to molecular hydrogen and (ii) carbon undergoes full oxidation by water to form CO_2 and H_2 (water gas shift reaction). The oxygenates (which represent 50 wt% of the pyrolysis oil) contain 6 wt% hydrogen, indicating that 30 gram (or 15 mol) of H_2 can be produced per Kg of initial pyrolysis oil. Furthermore, hydrogen can also be formed by the water gas shift reaction. During WGS, carbon is oxidized by water to form H_2. A single carbon atom can undergo two oxidations by water ($C + H_2O \rightarrow CO + H_2$, and $CO + H_2O \rightarrow CO_2 + H_2$) and therefore, in the optimal case, two hydrogen molecules can be formed per carbon atom. However, the carbon in the oxygenates is already partly oxidized and this should be taken into account when calculating the maximum hydrogen yield potential. It can be calculated for the oxygenates that the molar ratio of oxygen/carbon is 0.77, while fully oxidized carbon has oxygen/carbon ratio of 2. This indicates that 1.23 molecules of hydrogen can be formed per carbon atom in case of optimal hydrogen yields. Oxygenates are for 46.8 wt% composed out of carbon, indicating that the water-soluble oxygenate fraction (50 wt% of pyrolysis oil) contains ~19 moles of carbon per kg of pyrolysis oil. This indicates that another 23 moles of H_2 can be produced by complete oxidation of the already partly oxidized carbon. The above considerations show that a total of 48 moles of H_2 can be produced maximally from the aqueous fraction of 1 Kg of pyrolysis oil.

Next, the amount of hydrogen required for upgrading of the organic phase of pyrolysis oil is calculated. The pyrolysis oil is composed of 25 wt% organic phase. This phase is of interest for liquid bio-fuel production, but needs to be upgraded first by de-oxygenation to increase the heating value. During this process, oxygen in the organic compounds is hydrogenated and removed from the molecule in the form of water. Two hydrogen atoms are necessary to remove one oxygen atom in the form of water ($O + 2H \rightarrow H_2O$). The oxygen content in the organic phase is 27 wt%, indicating that 68 gram (or 4.2 mol) of atomic oxygen

needs to be removed from the organic phase of 1 Kg of pyrolysis oil. These calculations show that 4.2 moles of molecular hydrogen (H_2) are necessary to accomplish full de-oxygenation of the organic phase. Bridgwater [32] reported similar relative hydrogen amounts for this process (8 moles of hydrogen to fully de-oxygenate 250 grams of organic phase that was composed of 50 wt% oxygen). Competing side-reactions (*e.g.* hydrogenation of unsaturated bonds) during de-oxygenation might increase the required hydrogen amounts to achieve full de-oxygenation. It was calculated earlier in this section that maximum H_2 yields of 48 moles can be produced from the aqueous phase of 1 Kg of pyrolysis oil. These calculations show that the amount of hydrogen obtained from the aqueous phase is enough for full de-oxygenation (ignoring hydrogenation side reactions) of the organic phase, when the hydrogen selectivity for the reforming for the aqueous fraction is at least 10%. The integration of APR to generate hydrogen from the aqueous phase of pyrolysis oil to upgrade the organic phase is graphically presented in Figure 8.1, and shows to be conceptually feasible.

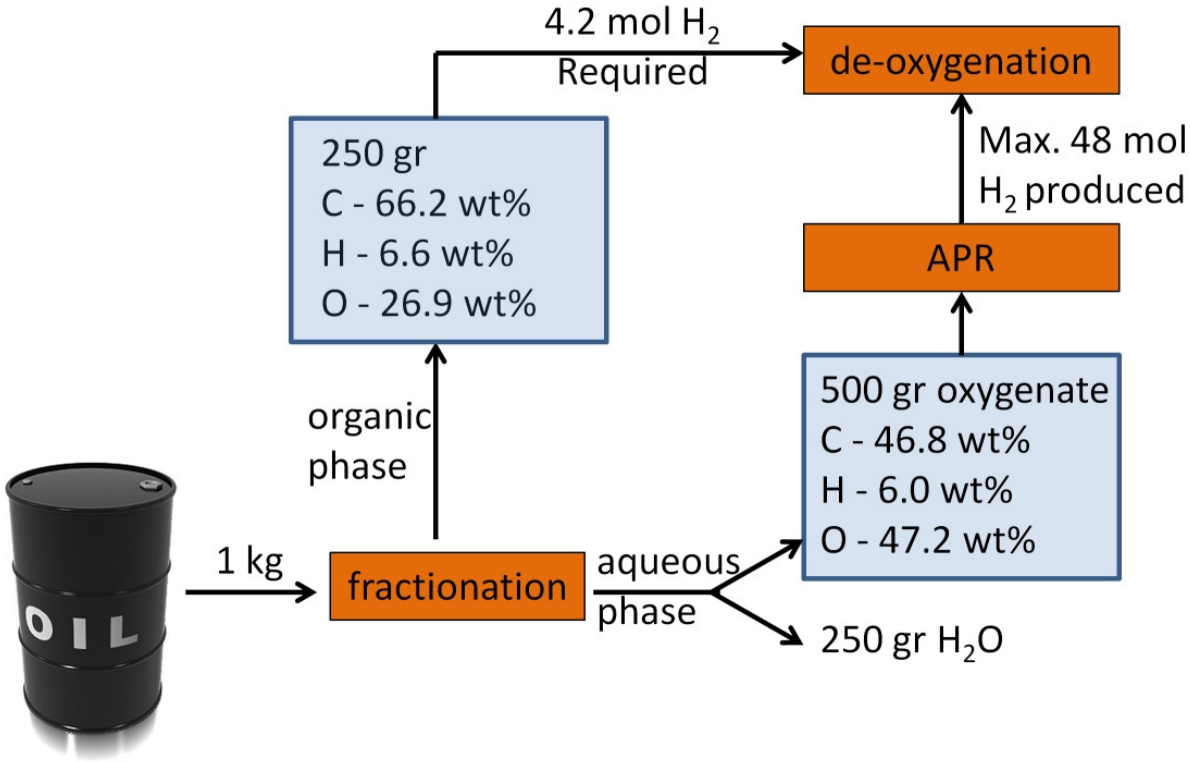

Figure 8.1: Hydrogen economic of APR integration in a bio-refinery.

8.3 Concluding remarks and future challenges

Catalytic Aqueous Phase Reforming (APR) of bio/organic feeds is an interesting route for the production of renewable hydrogen as discussed in detail throughout this thesis. However, the lack of efficient APR catalysts is one of the issues that prevented commercial exploitation of this process. The need for efficient APR catalyst was addressed in this thesis and resulted in the following achievements:

- Development of efficient Pt-Ni/Al_2O_3 catalyst for APR of ethylene glycol in supercritical water at commercially relevant concentrations and reaction rates (Chapter 3).
- Identifying acetic acid as a threat for the stability of alumina-based catalysts (Chapter 4).
- Identifying the role of Ni in Pt-Ni/Al_2O_3 catalysts in enhancing hydrogen yields and extending catalyst lifetime during APR of ethylene glycol (Chapter 4).
- Realizing that metal oxide supports are not suitable for APR of bio/organic feeds that contain carboxylic acids (Chapter 4).
- Development of a stable catalyst (Pt/CNT) for APR of ethylene glycol and acetic acid in supercritical water (Chapter 5). However, reaction rates were too low for commercial purposes.
- Development of a stable catalyst (Ru/CNT) with commercially attractive gasification rates for APR of acetic acid in supercritical water (Chapter 6).
- Realization that APR in subcritical water is very challenging for catalyst and material stability. Therefore, APR in supercritical water is preferred (and also necessary to achieve the required reaction rates) (Chapter 6).
- APR of real aqueous feed (aqueous phase of flash pyrolysis) showed that non-catalytic challenges should be solved first before the developed Ru/CNT can be assessed for this process (Chapter 7).

These achievements are a giant step towards the commercial feasibility of APR of bio/organic feed streams. However, two challenges remain which should first be solved before this process can be commercially employed. The first challenge is related to catalytic performance. The developed Ru/CNT catalyst is very promising for reforming of bio/organic

feeds in supercritical water in terms of stability and gasification rates. However, the desired product is hydrogen and reforming of oxygenates that do not have every carbon atom connected to oxygen (*e.g.* acetic acid), favor alkane formation inherently. Optimization of the hydrogen yields should be performed by either (1) improving the alkane reforming in the reactor by modifying the used catalyst or (2) integrate an alkane reforming step after the gasification reaction.

Coke formation before the APR of bio/organic feeds was found to cause blockage of the experimental setup. This problem is a non-catalytic challenge that should be addressed before APR can be commercially applied for these bio/organic feeds. Pretreatment of the feed might be required to remove the coke-precursors. At this moment, the exact coke-precursors are not identified yet. Acetic acid is a notorious coke-precursor in steam reforming. However, coke formation during APR of highly concentrated acetic acid solutions was not observed. Future studies should be focused first at identifying the pathways/compounds involved in coke formation. Once these are known, solutions to prevent coke formation can be developed. Currently, the food and paper industry produce large amounts of bio/organic waste. These streams might be less susceptible to form coke and might therefore be promising feed streams for gasification by APR. The commercial relevance of gasification of such feeds is not only limited to producing valuable products but it will simultaneously diminish/clean these waste streams.

References

[1] C. Yan, F. Cheng, R. Hu, P. Fu, Int. J. Hydrogen Energ. 35 (2010) 2612-2616.

[2] A. Basagiannis, X. Verykios, Catal. Today 127 (2007) 256-264.

[3] J.A. Medrano, M. Oliva, J. Ruiz, L. Garcia, J. Arauzo, Energy 36 (2011) 2215-2224.

[4] R.D. Cortright, R.R. Davda, J.A. Dumesic, Nature 418 (2002) 964.

[5] J. Xie, D. Su, X. Yin, C. Wu, J. Zhu, Int. J. Hydrogen Energ. 36 (2011) 15561-15572.

[6] Y. Guo, M.U. Azmat, X. Liu, Y. Wang, G. Lu, Appl. Energ. 92 (2012) 218-223.

[7] R. Navarro, M. Pena, J. Fierro, Chem. Rev. 107 (2007) 3952-3991.

[8] S. Adhikir, S. Fernando, A. Haryanto, Energ. Convers. Manage. 50 (2009) 2600-2604.

[9] R.R. Davda, J.W. Shabaker, G.W. Huber, R.D. Cortright, J.A. Dumesic, Appl. Catal. B 56 (2005) 171-186.

[10] Y. Guo, S.Z. Wang, D.H. Xu, Y.M. Gong, H.H. Ma, X.Y. Tang, Renew. Sust. Energ. Rev. 14 (2010) 334-343.

[11] J. Kritzer, J. Supercrit. Fluid. 29 (2004) 1-29.

[12] A. Nakamura, E. Kiyonaga, Y. Yamamura, Y. Shimizu, T. Minowa, Y. Noda, Y. Matsumura, J. Chem. Eng. Jpn. 41 (2008) 1-12.

[13] S. A. Chattanathan, S. Adhikari, N. Abdoulmoumine, Renew. Sust. Energ. Rev. 16 (2012) 2366-2372.

[14] http://enpub.fulton.asu.edu/ece340/pdf/steam_tables.PDF

[15] J.S. Chickos, W.E. Acree Jr. J. Phys. Chem. Ref. Data 32 (2003) 515.

[16] S.P. Cicconardi, A. Perna, G. Spazzafumo, Int. J. Hydrogen Energ. 29 (2004) 457-551.

[17] B. Sun, D. Zhang, S. Liu, Int. J. Hydrogen Energ. 37 (2012) 13088-13091.

[18] N. Luo, F. Cao, X. Zhao, T. Xiao, D. Fang, Fuel 86 (2007) 1727-1736.

[19] Q. Yan, L. Guo, Y. Lu, Energ. Convers. Manage. 47 (2006) 1515-1528.

[20] N. Wang, N. Perret, A. Foster, Int. J. Hydrogen Energ. 36 (2011) 5932-5940.

[21] H. Chen, Y. Ding, N. T. Cog, B. Dou, V. Dupont, M. Ghadin, P.T. Williams, Renew. Energ. 36 (2011) 779-788.

[22] J.W. Shabaker, R.R. Davda, G.W. Huber, R.D. Cortright, J.A. Dumesic, J. Catal. 215 (2003) 344-352.

[23] J. Nisamameenate, D. Atong, V. Sricharoenchaikul, Adv. Sci. Lett. 12 (2012) 872-876.

[24] J. Sehested, J. Catal. 217 (2003) 417-426.

[25] H. Devianto, Z.L. Li, S.P. Yoon, J. Han, S.W. Nam, T.H. Lim, H. Lee, Int. J. Hydrogen Energ. 35 (2010) 2591-2596.

[26] K. Takanabe, K. Aika, K. Seshan, L. Lefferts, Chem. Eng. J. 120 (2006) 133-137.

[27] D.L. Trimm, Catal. Today 37 (1997) 233-238.

[28] K. Lehnert, P. Claus, Catal. Commun. 9 (2008) 2543-2546.

[29] P. Kritzer, E. Dinjus, Chem. Eng. J. 83 (2001) 207-214.

[30] P. Kritzer, J. Superc. Fluid. 29 (2004) 1-29.

[31] R.H. Venderbosch, A.R. Ardiyanti, J. Wildschut, A. Oasmaa, H.J. Heeres, J. Chem. Tech. Biotech. 85 (2010) 674-686.

[32] A.V. Bridgwater, Catal. Today 29 (1996) 285-295.

Publications

Journal Papers

- D.J.M. de Vlieger, A.G. Chakinala, L. Lefferts, S.R.A. Kersten, K. Seshan and D.W.F. Brilman. *Hydrogen from ethylene glycol by supercritical water reforming using alumina supported noble and base metal catalysts*. Applied Catalysis B: Environmental 111 – 112 (2012) 536 – 544

- D.J.M. de Vlieger, B.L. Mojet, L. Leffert and K. Seshan. *Aqueous phase reforming of ethylene glycol – Role of intermediates in catalyst performance.* Journal of Catalysis 292 (2012) 239 – 245

- D.J.M. de Vlieger, D.B. Thakur, L. Lefferts and K. Seshan; *Carbon nanotubes: A promising catalyst support material for supercritical water gasification of biomass waste.* ChemCatChem 4 (20120) 2068 – 2074

- D.J.M. de Vlieger, L. Lefferts and K. Seshan; *Ru decorated carbon nanotubes; a commercially promising catalyst for reforming bio-based acetic acid in sub- and supercritical water.* Submitted to Journal of Catalysis

Oral Proceedings

- *Carbon nanotubes: the promising solution to catalytic problems in supercritical water.* 15th International Catalysis Congress, 1 – 6 July 2012, Munich-Germany
- *Carbon nanotubes as catalyst support material for reactions in supercritical water.* Carbocat-V, 28 – 30 June 2012, Brixen-Italy.
- *Carbon nanotubes: Promising support material for catalytic reactions in supercritical water.* Netherlands Catalysis and Chemistry Conference, 5 – 7 March 2012, Noordwijkerhout – The Netherlands
- *Renewable hydrogen from aqueous organic wastes – Risk of intermediates on catalyst performance for aqueous phase reforming of ethylene glycol.* TransACTS, 31 January – 1 February 2012, Lunteren – The Netherlands
- *The Effect of Liquid By-Products on the performance of Alumina Supported Pt and Pt-Ni catalysts during Ethylene Glycol reforming.* Netherlands Process Technology Symposium, 24-26 October 2011, Papendal – The Netherlands
- *Hydrogen from supercritical water reforming of ethylene glycol using alumina supported metal catalysts,* Netherlands Catalysis and Chemistry Conference, 28 February – 2 March 2011, Noordwijkerhout – The Netherlands
- *Hydrogen from supercritical water reforming of ethylene glycol using alumina supported metal catalysts.* COST Congress, 20 – 21 January 2011, Utrecht – The Netherlands
- *Hydrogen from supercritical water reforming of ethylene glycol using alumina supported metal catalysts,* TransACTS, 12 January - 13 January 2011, *Lunteren* – The Netherlands

Acknowledgements

After 4 years of hard work, my scientific journey reached a new apogeum by completing the PhD thesis that you are now holding in your hands. I learned a lot in those years and was guided and directed by the many discussions and collaboration that I had with supervisors, colleagues and even with people outside the field of expertise. This section is therefore dedicated to the people that shared their time, enthusiasm and expertise with me so I could make biased decisions regarding directions and steps to bring this scientific journey to a good end.

Seshan, a sincere gratitude goes to you, my daily supervisor. The door of your office was always open for scientific discussions as well as informal chitchat. Your relaxed character and pragmatic way of working always took away any worries that I had concerning my project. Seshan, you gave me guidance during my project and moreover I learned a lot from you, especially regarding technical writing. Dear Seshan, thank you again, I learned from the best!

Leon, I would like to thank you for offering me the opportunity to do my PhD at CPM and furthermore for the many scientific discussions that we had, which helped me to decide the right directions of my project. Your yearly BBQs were always a pleasure to attend.

Barbara, thank you for the many scientific discussions. You taught me a lot, especially to be very critical about the interpretation of results (remember the wrongly identified coke in the Raman Spectra!). Your cheering and motivating character brings life to CPM.

I also want to express my gratitude to Anand Chakinala, Wim Brilman and Sascha Kersten for the fruitful collaborations and discussions that led to a publication in Applied Catalysis.

My gratitude also goes to Benno Knaken and Karst van Bree for building (and repairing) my setup. Furthermore, Bert Geerdink, I would like to thank you for the technical support in the lab and for your help with computer/multi-media related issues. It was always a pleasure to work with you.

A special thanks goes to my room-mates Masoud, Marijana and Hrudya. Masoud, I always found your stories about Iran interesting and I hope that the Iranese future will be bright and without troubles. I'm sure that you and Fatimeh will be able to go to the place that you desire! Marijana and Hrudya, it was never boring with you in the room. I wish you guys all the best with finishing your PhD.

Louise, thank you for all the XRF and BET measurements. I am glad that you reached a new high score with the number of yearly measurements. That shows how important your job is and how much we rely on your expertise. I always enjoyed talking to you. I wish you all the best and I'm sure that you will enjoy the time after your retirement. In the near future, I do expect to read in the newspapers that you became national Bridge champion.

Karin, thank you for all the help in the lab and for all the chemisorptions and BET measurement that you performed for me. I always enjoyed talking to you and still regret that we missed each other in the Monastry in Seeon. All the best for the future.

I would also like to thank Gerard Kip, Rico Keim, and Mark Smithers for performing XPS, TEM and SEM experiments.

I supervised three student during my PhD and I want to thank them for their contributions to my project. Yasmin, Ifeanyi and Kaisa, Thank you! Kaisa I wish you all the best with the PhD position that you accepted in the CPM group. Yasmin and Ifeanyi, I wish you all the best with your scientific careers.

Bart, Thank you for the scientific discussions that we had regarding my work. I wish you all the best in your career with Johnson Mathhey.

Digvijay, thank you for all the interesting stories about the Indian social and political system. Furthermore, I want to thank you for the fruitful scientific collaboration. After a few wines during one of the conferences, we decided to undertake a very interesting interdisciplinary project which resulted in novel results which were published in ChemCatChem. I wish you, Aabha and Yashwardhan a happy and bright future.

Patrick, I started my career in CPM under your supervision and soon I followed your footsteps and accepted a PhD position in the same group. Thank you for your guidance during my master project and showing me the fun of doing research.

Ruben, thank you for being my friend and paranimph. You were ready to help everybody, anywhere, anytime! I really appreciate your friendliness and your active character. Your sporting skills always amazed me…from cycling, running, and darts… to hitting the bulls-eye two times!

Mr. Reed, You bold buddy! Thank you for being my friend and paranimph. I highly appreciate it. You always amazed me with your retarded stories and your English humor. Also bear in mind that your furry vermin friends can't have a better keeper than you!

Furthermore, I want to thank all my (former) colleagues Arie, Son, Sergio, Lianne, Maaike, Raman, Songbo, Cristina, Chau, Shilpa, Rao, Yingyang, Tom, Arturo, Joline, Lidy, Sabine, Roger, Kamilla, José, Yejun. Zeljko, Igor, Martine, Inga, Gacia, Kumar, Davide and Berta, for the enjoyable time in CPM.

At last, I would like to thank my family for their support and given confidence. A special thanks goes to my mother Wilma for developing and drawing the Mandala that is presented on the cover of this thesis. The meaning of the Mandala is described on the inside of the cover. Wilma, I know that you struggled a lot with the geometry of the leafs but you did a great job! It is an honor to use your drawing on the front cover. At last I want to show my deepest gratitude to my girl Astrid who was always standing on my side. You have been a great support and motivator and you are the reason that I was never stressed out because you always knew how to comfort me with your love! Thank you!